Miguel Hernandez University

Bioengineering Institute
And
Department of Materials Science, Optics and Electronic Technology

PhD Thesis

DEVELOPMENT OF NEW CONDUCTIVE POLYMERS AND MICROSCOPIC STUDIES FOR IMPROVING NEURAL INTERFACES

Author

SAEID MOHAMED ABDELHAMID ELKATLAWY

(M.Sc. in Condensed Matter Physics and B.Sc. in Physics)

Advisors

PROF. EDUARDO FERNANDEZ JOVER

PROF. ANTONIO FIMIA GIL

Elche (Alicante), SPAIN

July 2013

Miguel Hernandez University at Elche

Bioengineering Institute
Biomedical Neuroengineering Group (Nbio)
Unit of Neuroprosthesis and Visual Rehabilitation (UNRV)

And

Department of Materials Science, Optics and Electronic Technology
Area of Optics

PhD Thesis (Major: Experimental Biophysics)

DEVELOPMENT OF NEW CONDUCTIVE POLYMERS AND MICROSCOPIC STUDIES FOR IMPROVING NEURAL INTERFACES

Thesis Submitted for the Degree Doctor of Philosophy (PhD) in Bioengineering at the
Miguel Hernandez University

Author

Saeid Mohamed Abdelhamid Elkatlawy

(M.Sc. Degree in Condensed Matter Physics and B.Sc. Degree in Physics)

Advisors

Prof. Eduardo Fernandez Jover   Prof. Antonio Fimia Gil

July 2013

Elche (Alicante), SPAIN

Don Eduardo Fernández Jover, Director del Grupo de Investigación "*Unidad de Neuroprótesis y Rehabilitación Visual*" del Instituto de Bioingeniería y Don Antonio Fimia Gil, Catedrático de Óptica del Departamento de Ciencia de Materiales, Óptica y Tecnología Electrónica de la Universidad Miguel Hernández de Elche,

Informan:

Que Don **SAEID MOHAMED ABDELHAMID ELKATLAWY**, FÍSICO, **ha realizado bajo su dirección el trabajo** experimental que recoge en su tesis Doctoral titulada "**DEVELOPMENT OF NEW CONDUCTIVE POLYMERS AND MICROSCOPIC STUDIES FOR IMPROVING NEURAL INTERFACES**".

Que han revisado los contenidos científicos y los aspectos formales del trabajo y dan su conformidad para su presentación y defensa públicas.

Y para que así conste y a los efectos oportunos, firman el presente en Elche a veintinueve de julio de dos mil trece.

Fdo.: Eduardo Fernández Jover   Fdo.: Antonio Fimia Gil

Universidad Miguel Hernández

A quien corresponda:

Eugenio Vilanova Gisbert, Catedrático de Toxicología y Director del Instituto de Bioingeniería,

HACE CONSTAR

Que da su conformidad a la lectura de la tesis doctoral presentada por D. Saeid Mohamed Abdelhamid Elkatlawy, titulada **"Development of new conductive polymers and microscopic studies for improving neural interfaces"**, que se ha desarrollado dentro del Programa de Doctorado de Bioingeniería de este Departamento, bajo la dirección del Prof. Eduardo Fernández Jover y el Prof. Antonio Fimia Gil.

Lo que firmo en Elche, a instancias del interesado y a los efectos oportunos, a veintinueve de julio de dos mil trece.

Eugenio Vilanova Gisbert
Catedrático de Toxicología
Director del Instituto de Bioingeniería

Universidad Miguel Hernández

"Science is a wonderful thing if one does not have to earn one's living at it."

-Albert Einstein (1879 – 1955)

To my Parents;

One of whom didn't live to see it accomplished.

Preface

Looking at a problem from a view point of an individual academic discipline can quite often develop a "tunnel vision". On the other hand, interdisciplinary research involves the combination of two or more academic disciplines into one research project. Interdisciplinarity aims at solving a specific problem in a specific research field by creating something new that crosses the boundaries and opens the way to "think outside the box".

As a physicist, I thought it was quite hard to do anything other than pure physics. However, after I gained my M.Sc. degree in condensed matter physics, I decided to learn to "think outside the box" and to make a change in my scientific career. So I made a career shift to employ interdisciplinary approaches to solve problems in biological sciences. I believe that was a great decision and doing interdisciplinary research was a major step forward in my scientific career.

The present dissertation is an interdisciplinary based work aims at solving some challenging and demanding problems in neuroscience by employing other academic disciplines. During the development of this thesis I gained tremendous amount of knowledge in several fields such as neuroscience, neuroengineering, electrophysiology, electrochemistry and microscopy. Most importantly, I learnt how to "think outside the box". I must confess that this thesis has tremendously increased my knowledge and has enriched my appreciation and understanding of several research disciplines. I hope that the work presented in this thesis is a valuable addition to the scientific database.

Saeid Elkatlawy

Acknowledgments

Scientific research is not an individual's recipe; at least three ingredients need to be brought together: *Opportunity*, *Direction* and *Teamwork*. So when it comes to acknowledgements, one needs to acknowledge all these ingredients, altogether. Hence, I would like to take this opportunity to acknowledge several persons and institutions. First, I would like to express my profound gratitude to the 'Gobierno Español' represented by the 'Ministerio de Ciencia e Innovación' and the 'Subprograma de Becas FPI' for giving me the *Opportunity*.

I would also like to take this opportunity to express my profound gratitude to my thesis advisors: Prof. Eduardo Fernandez Jover and Prof. Antonio Fimia Gil. I thank them for their tireless guidance, timely encouragement and inspiration during my thesis work. I have gained tremendous amount of knowledge from their expertise and I highly admire their contribution to my research career. Their *Direction* has boosted my expertise and was a major step in my scientific career. I really thank Eduardo for giving me the *Opportunity* to join his group and to use all the lab's installations. I also thank Antonio for giving me the *Opportunity* to work on the digital holographic microscope in his laboratory and for the useful discussions that we had.

I would also like to express my profound gratitude to Prof. Toribio F. Otero (Catedrático de Química-Física de la Universidad Politécnica de Cartagena). I really acknowledge all the help and guidance that he has provided me. I thank Toribio for all the electrochemistry expertise that I gained and I thank him for being always accessible via phone or email when I needed his advice.

Last, but not least, I would like to take this opportunity to acknowledge my family. Especially, I express my profound gratitude to my mother, the greatest woman I've ever known. I thank her for being always there and for her unconditional and unlimited support and love. I express my profound gratitude to my late father; he was my very first tutor and he always supported me. Even after his death, I always felt his support and encouragements. I would also like to thank my sisters and brothers. Especially I thank my brother Abdelhamid for his support and advice and for being always there whenever I needed him. I thank Dalia, my beloved wife, and I dedicate this thesis to her; I really appreciate her positive attitude and her existence in my life.

Finally, I would like to take this opportunity to acknowledge my friends and colleagues in Egypt and to wish them all the Best.

Saeid M. A. Elkatlawy

Elche (Alicante), SPAIN

July 2013

Table of Contents

List of Figures

Figure (8-9): Representation for a magnified cellular body of a neuron of developmental age of 15 days   156

List of Tables

Glossary of Abbreviations

CPs   Conducting Polymers

Py   Pyrrole monomer

pPy   Polypyrrole

PSS   Poly Sodium 4-Styrenesulfonate

pPy/PSS   Polypyrrole conducting polymer doped with PSS molecule

LUMO   Lowest Unoccupied Molecular Orbital

HOMO   Highest Occupied Molecular Orbital

PDL   Poly-D-lysine Hydrobromide

PBS   Phosphate Buffered Saline

DMEM   Dulbecco's Modified Eagle Medium

HBSS   Hank's Balanced Salt Solution

PFA   Paraformaldehyde

GFAP   Glial Fibrillary Acidic Protein

GPES   General Purpose Electrochemical System

MEA   Multielectrode Array

SEM   Scanning Electron Microscope

CV   Cyclic Voltammetry

WE   Working Electrode

RE   Reference Electrode

CE   Counter Electrode

ITO   Indium Tin Oxide

TiN   Titanium Nitride

BSA   Bovine Serum Albumin

DM   Digital Microscope

EIS   Electrochemical Impedance Spectroscopy

DIV   Days *in vitro*

NB   Neuroblastoma

CCD   Charge-Coupled Device

MO   Microscope Objective

DHM   Digital Holographic Microscopy

BS   Beam Splitter

OPL   Optical Path-Length Difference

Chapter One

Chapter I

Introduction and Thesis Overview

1.1 Rationale and Research Motive

Neurodegenerative diseases and neural dysfunctions, due to environmental causes, can have dramatic consequences on the quality of life of individuals. Neurodegeneration shows up as a loose of nerve functions or disconnections in neuromuscular paths (Przedborski *et al* 2003, Rich 2001, Crumrine 2001). This can result in behavioral and psychological disturbances, like the case of Alzheimer's disease; or in motor problems and postural instability, like the case of Parkinson's disease. On the other hand, excited tissues, such as neural and muscular tissues, are meant to be activated electrically. This activation can be either intrinsically (naturally) by means of ionic signaling and action potentials; or extrinsically (artificially) by means of electrical stimulation electrodes (Rutten 2002). These artificial electrodes, or neural interfaces, are employed to interface with the nerve, or muscle, tissue and are meant to evoke potential differences that can result in the activation of neural or muscular pathways (Kandel *et al* 2000). Neural interfaces are also meant to sense and record bioelectric signals, or nerve activity, from neural populations. Neural interfaces are to be implanted into nerve cell's membrane or in close proximity to cellular populations. Traditionally, neural interfaces are metal based microelectrodes. The use of these metal based microelectrodes for therapeutic rehabilitation was initially deemed promising by restoring activities to afflicted areas (Cohen 2007, Normann 2007, Li and Mogul 2007). However, it was soon appreciated that metal based neural interfaces have their disadvantages and obstacles. Particularly, the eventual degradation of neural tissue and

interface electrodes and issues of electrode biocompatibility and immune responses (Polikov *et al* 2005, Biran *et al* 2005). These complications present themselves as adverse tissue responses arising from the trauma of the initial insertion of electrodes which can lead to intrinsic foreign body responses, glial inflammation and neuron-electrode connection loss (Polikov *et al* 2005, Szarowski *et al* 2003, Marin and Fernández 2010). Other limiting contributions occur due to the large differences in mechanical characteristics between the stiff metal electrode and the soft biological tissue (Biran *et al* 2005).

On the other hand, there is a need of new tools able to help in the development of these technologies. In this context, this thesis introduces a new imaging technique, called digital holographic microscopy (DHM), and explores its potential usefulness for a better understanding of neural interfaces (Gabor 1948, 1972, Cuche *et al* 1999, Schnars and Jüptner 1994). This technique allows access to three-dimensional networks of neurons and provides quantitative measurements of materials and living cells.

1.2 Hypothesis and Theory

As rationalized in the previous section, improvements have to be made on the electrode site interface with biological tissue. For that purpose, the issue demands a bioactive material with outstanding properties. This material has to be electrical conductor to be able to carry the stimulation charge and it has to be soft enough to manifest mechanical characteristics similar to that of biological tissues. It also must be biologically compatible and needs to last longer in a highly aggressive environment such as the nervous system. Thanks to their, softness, wetness and reasonable electrical conductivity range (Otero 2009, Otero *et al* 2004), conductive polymers (CPs) can be a good candidate for coating electrode surfaces. However, conductive polymers' biocompatibility needs to be assessed with biological tissues and their capacity to record from, and stimulate, neural tissues needs to be studied (Fonner *et al* 2008, Polikov *et al* 2005).

This thesis presents studies on conductive polymer polypyrrole and its potential for improving electrode/tissue site interface for neural probing. Electrochemical behaviour of conductive polymer polypyrrole for neural interfacing is studied. Studies on physical and topographic characteristics of the electrogenerated conductive polymer polypyrrole are presented. *In vitro* assays are performed on the biocompatibility of different polymeric compositions of polypyrrole, for different biological tissues. The potential of polypyrrole conducting polymers for probing nerve tissue and their capacity to record from, and stimulate, neural populations are studied.

On the other hand, the thesis uses a new methodology based on light interferometry and called Digital Holographic Microscopy (DHM), to quantitatively assess the morphology of networks of neurons since it can be used as a noninvasive and label free imaging tool for *in vitro* assays (Gabor 1948, 1972, Cuche *et al* 1999, Schnars and Jüptner 1994). Furthermore we plan to use the DHM to check the effect of applied electrical stimuli on the neural electrodes.

1.3 Thesis Aims

i. Develop new bioactive electrode/tissue interfaces based on conductive polymers that can be useful to overcome issues of conventional metal-based electrodes.

ii. Deposit, electrochemically, coatings of conducting polymer polypyrrole (pPy/PSS) on several types of metal-based electrodes.

iii. Study the physical and electrochemical characteristics of conducting polymer polypyrrole and its potential for new neural interfaces.

iv. Assess the biocompatibility of the developed polypyrrole conducting polymers.

v. Check the potential of conducting polymer polypyrrole to record and stimulate populations of neurons.

vi. Study the effect of applied electrical stimuli on neural electrodes using digital holographic microscopy.

vii. Employ digital holographic microscopy to study morphometric characteristics of neural cells.

1.4 Thesis Structure and Organization

This thesis is composed of ten chapters followed by bibliography. Chapter one presents an introduction on the rationale and research motive, aims of the work and thesis structure. Chapter two introduces background information and literature review of the "state of the art" of the topics related to artificial interfacing to the nervous system. Chapter three presents materials, methods and equipments employed through the development of the thesis. Chapter four presents the electropolymerization and physico-chemical characterization of one of the most studied conducting polymers, polypyrrole. The chapter starts by introducing studies on the electropolymerization of polypyrrole on indium tin oxide coated glass substrates and on titanium nitride microelectrodes. Then, it presents electrochemical and physical characterization of the deposited polymer film. Chapter five presents biocompatibility studies of polypyrrole for human neuroblastoma cells, glial cells and neural cells extracted from mouse brain. Polymer biocompatibility is assessed by means of optical as well as fluorescence microscopy. Biocompatibility assessment of polypyrrole conducting polymer is studied with or without chronically applied electric field, during cellular growth. Microelectrodes coated and uncoated with polypyrrole are then used for recording electrical activity from neural populations. Chapter six presents an introduction to digital holographic microscopy (DHM) as a new "cutting edge technology" for materials science studies and biological imaging. Chapter seven introduces studies, using digital holographic microscopy, on the effect of applied electrical stimuli on microelectrodes, either bare or polypyrrole coated. Chapter eight employs the new imaging technique DHM to study morphometric characteristics of neural cells. It presents *in vitro* studies for live as well as for fixed neural cells. Chapter nine presents thesis conclusions. Chapter ten '*Resumen de la Tesis Doctoral*' presents a

summary of the thesis in Spanish. Each chapter in the thesis starts with a general

overview and ends up with a conclusion for the chapter's contents. Finally, the

bibliography is provided at the end of the thesis.

Chapter Two

Chapter II

Background Information and Literature Review

2.1 Chapter Overview

Neural engineering, also called neuroengineering, is a recently developed interdisciplinary research field that heavily relies on the shoulders of other fields. Examples for fields involved in neuroengineering are neuroscience, bioelectricity, electrophysiology, biophysics, materials science, electrochemistry and microscopy and imaging techniques. Neuroengineering aims, mainly, at neuroprosthetics and neural rehabilitation with the final objective of improving quality of life of individuals suffering from neurodegenerative or neuropathological diseases.

This chapter presents background information on the topics employed during the thesis development. It also reviews the literature and the "state of the art" of the works developed on the same problem treated here or on other related problems. The biological concepts introduced in this chapter, and in the rest of the thesis, are meant to be related to the nervous system of mammals.

2.2 Nerve Cell

More than a hundred years ago a relatively detailed description of the nerve cell was introduced by Camillo Golgi and Santiago Ramon y Cajal. Based on Golgi's method "*la reazione near*" or the black reaction staining technique, Ramon y Cajal initiated a series of discoveries that lead to our understanding and appreciation of the nervous system as a complex network of individual nerve cells (Ramòn y Cajal 1909). The nerve cell (the neuron) is the fundamental constituent of the nervous system and is the milestone of its functions and operations. Mostly, the structure of neurons is similar to that of other biological cells, but unlike other cells, neuron is an electrically excited and highly active cell. The typical morphological structure of a neuron, figure (2-1-A), consists of three main parts: The Cell Body, the Dendritic Arborizations and the Axon. The cell body (also called soma) contains the nucleus that carries all genetic information of the cell, and is the "central processing unit" of the nerve cell. The cell body receives incoming information through dendritic arborizations. Dendritic arborizations, or dendrites, are the "input devices" that collect information through synaptic connections from other neurons and send it directly to the cell body. The axon, a relatively long fiber extending from the cell body, is the "output device" that carries out the processed information, the electrical outgoing (ionic) signals, from the cell body down to the axonal terminals and then to other cells' dendritic arborizations through synaptic connections.

Figure (2-1-B) shows a drawing by Ramón y Cajal for a pyramidal cell from mouse cerebral cortex. The cell had its cell body deep in the cortex and the dendritic arborizations extending towards the cortical surface while the axon travels deep inside (Ramòn y Cajal 1909).
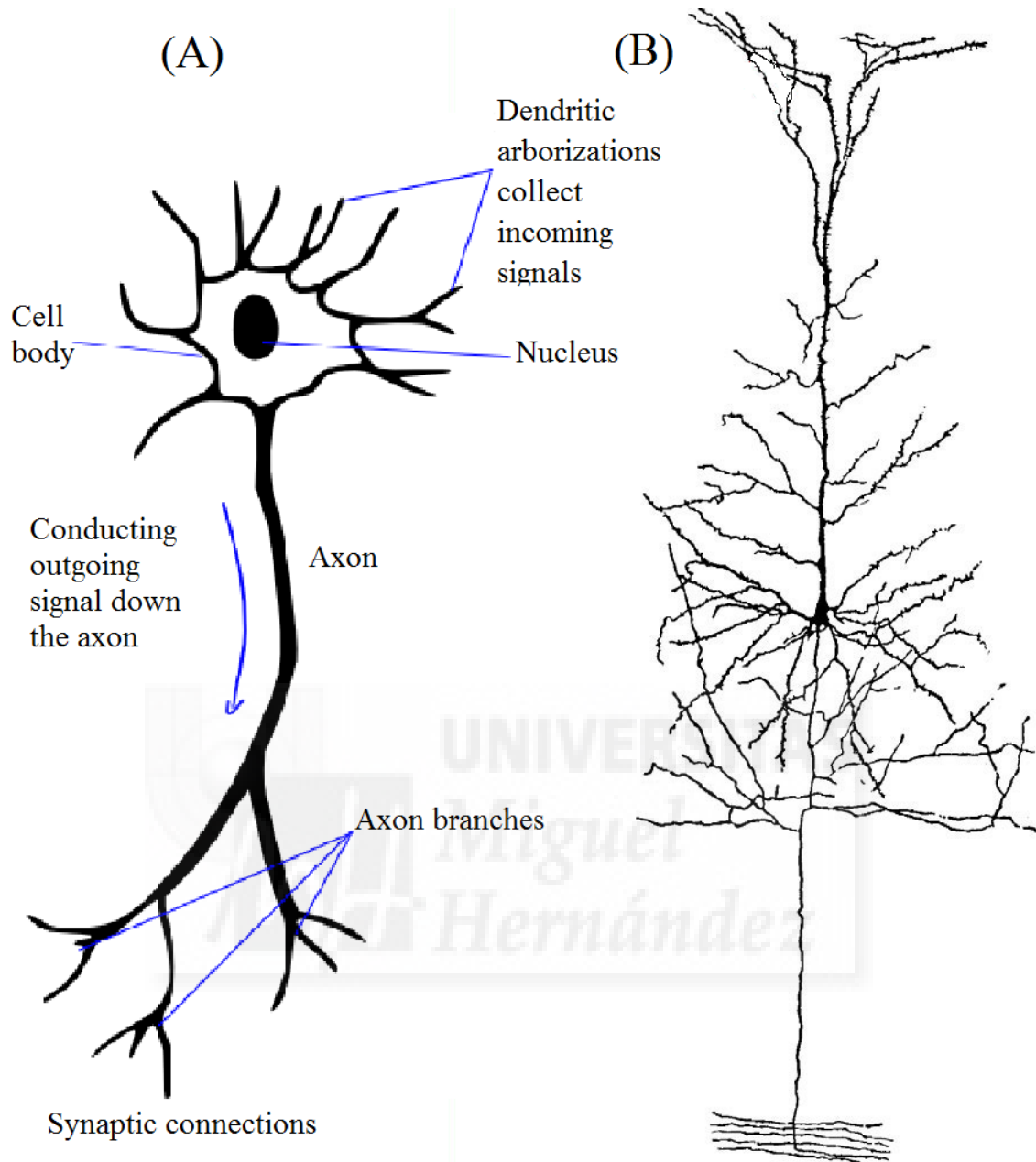
Fig. 2-1: The Nerve cell.

(A) Schematic drawing for typical basic morphological structure of the nerve cell, showing the dendritic arborizations that collect incoming signals to the cell body, then the cell body generates the conducting outgoing signal down the axon to the axonal terminals to release neurotransmitters at synaptic connections.

(B) A hundred years old drawing by Ramón y Cajal for a pyramidal cell from mouse cerebral cortex. The cell had its cell body deep in the cortex and the dendritic arborizations extending towards the cortical surface while the axon travels deep inside. The graph is modified from (Ramòn y Cajal 1909).

In the nervous system of mammals, a neuron fires an action potential in a unidirectional way. That means the dendritic arborizations collect and receive the incoming signals from the surrounding synaptic connections and send them to the cell body. At a threshold point, the cell body generates the outgoing signal and sends it through the axon down to the axonal terminals. Neural networks are responsible for the information processing and transmission through the electrical signals travelling amongst neurons within the nervous system. The conspicuous operations and functions that take place in mammals' body and the extraordinary and highly sophisticated behaviour of humans are based on a huge network of interconnected neurons mastered by the brain (Kandel *et al* 2000).

2.3 Neuroglial Cell

Brain and nervous system cannot be discussed without talking about an important cell type that intensively exists in the nervous system (especially the brain) called glial cells (Greek word for glue). In fact, glial cells do not have a direct role in information processing within the brain. The different types of glial cells have two important functions as support structures to neurons. The astrocytes or astroglias keep the appropriate chemical environment for the nerve cells. The oligodendrocytes or oligodendroglias and Schwann cells form an isolating covering called myelin sheath around axons. This myelin sheath has crucial effects on the speed of action potential propagation down the axon (Kandel *et al* 2000). These supportive glial cells take part in supplying nutrients and oxygen, destroy pathogens and remove apoptotic neurons (caused by intrinsic neuron's suicide) as well as take part in modulating neurotransmission and plasticity (Auld and Robitaille 2003).

2.4 Action Potentials and Ionic Signaling

According to Ramon y Cajal principle of dynamic polarization, a typical neuron has four different types of signals. Input (or incoming) Signal received by dendrites. Trigger Signal at the connection point (called trigger zone) between cell body and the axon. Conducting Signal takes place along the axon fiber down to axonal terminals. Output (or outgoing) Signal that takes place at the axonal terminals (Ramòn y Cajal 1909). However, the communications between neurons take place at a junction called synapse. Synapses are either chemical or electrical and they differ fundamentally in their transmission mechanisms. At electrical synapses, gap junctions between pre- and postsynaptic membranes allow current to flow passively through intercellular channels. This current flow changes the postsynaptic membrane potential, initiating (or in some cases inhibiting) the creation of action potentials. At chemical synapses, there is no intercellular continuity, and thus no direct flow of current from pre- to postsynaptic cell. Synaptic current flows across the postsynaptic membrane only in response to the secretion of neurotransmitters which open or close postsynaptic ion channels after binding to receptor molecules (Kandel *et al* 2000, Purves *et al* 2001). Neurotransmitters are those endogenous chemicals that originate from within the nerve cell and they are stored into special vesicles clustered beneath the membrane of the axonal terminals (Sourkes 2009).

The origin of action potentials is the electrochemical potential differences between outside and inside the cell membrane, or the trans-membrane potentials, of the excited nerve cell. When at rest, meaning that a neuron is not sending signals, the inside of the neural cell membrane has a negative charge relative to the charge outside the membrane. Electrically charged ions maintain the balance of positive and negative

charges. This balance is controlled by specialized gates around the cell membrane called voltage gated ion channels (or ion channels). These voltage gated ion channels open and close allowing certain ions to pass through while preventing or restricting the movement of other ions. In this rest state, sodium or potassium ions cannot easily pass through the membrane, through sodium or potassium ion channels. The negative charge inside the cell cannot be compensated, because the ions are unable to cross the barrier of the voltage gated ion channels. In order for the cell to maintain its polarized state it must actively transport ions. This ionic transportation mechanism is known as the sodium/potassium ionic pump. For every two potassium ions that pass through the membrane, three sodium ions are pumped out. When a conduction signal is sent out from the cell body the sodium channels open attracting positive sodium ions inside the cell membrane, depolarization occur. Once the cell reaches a certain threshold, an action potential will be fired by rushing potassium ions outside the cell and sodium gated ion channels close, repolarization occur. After the neuron has fired, there is a refractory period in which another action potential is not possible. During the time of refractory period, potassium channels reopen and sodium channels close, gradually returning the neuron to its resting potential (Kandel *et al* 2000).

Figure (2-2) represents a schematic drawing to explain the action potential firing and the related ionic signaling stages. Action potentials are short spikes causing the membrane potential to be temporarily positive. They are the natural and intrinsic way to activate and/or stimulate neural cells at the synaptic connections and muscular tissue at the neuromuscular junctions. They evoke the release of neurotransmitters through synaptic connections. The information encoded in the cell body and carried by action potentials through the axon is transferred to other neurons.

Fig. 2-2: Action potential and ionic signaling in case of chemical synapses.

A schematic drawing showing the different stages by which action potential occurs due to ionic channel activities through the cell membrane.

(A) Cellular membrane at rest, inside the membrane there is high concentration of potassium ions. Outside the membrane, there is high concentration of sodium ions.

(B) During action potential, voltage gated ionic channels open allowing sodium ions in and potassium ions out. Action potential propagates from cell body to axonal terminals as sodium ions open.

(C) Schematic representation of an action potential signal. Represents membrane potential in mV vs. time in ms.

2.5 Bioelectricity and Electrophysiology

Research on body electricity, or bioelectricity, and electrophysiology has its bases on the work by the Italian physician and physicist Luigi Galvani in 1791 (Galvani 1791). Galvani, in his famous experiment on the frog, discovered that electrical stimulation of nerve cells can evoke muscular contractions, but he concluded that the electrical signal came from inside the frog nerve. However, one year later, Alessandro Volta recognized that the electrical signal was originated from the combination of two different metals of the surgery tweezers used by Galvani. This combination together with the saline solution, composed by different biological relevant ions, in the biological tissue evoked a potential difference inside the frog body (Volta 1800). This was the discovery of what is called Galvanic cell in electrochemistry. However, these two discoveries were the bases of the research on electrophysiology.

As explained in the previous section, neural and muscular tissues can be stimulated in a natural way by means of intrinsic electrical signals called action potentials. Furthermore, artificial electrical stimulation of neural or muscular tissue is also vital. Thus either natural (intrinsic) or artificial (extrinsic) stimulation of neural tissue can evoke behavioral and/or mechanical responses (Hodgkin and Huxley 1952, Tehovnik 1996). The external excitation of the neural tissue takes place when applying an electric field along the axis between dendrites and the axon, and this electric field reaches a special threshold value. Once the threshold value is reached, and as the intrinsic excitation occurs, the cell fires action potentials evoking the release of neurotransmitters at the synaptic connections. The application of the electric field is achieved by introducing a special electrode, called neural interfaces, in close contact to the neural tissue (Stoney et al 1968).

2.6 Neurodegeneration and Neurodegenerative Diseases

The term neurodegeneration refers to the process of losing neural structure or neural function, and it could be related to either pathological or environmental causes that mainly affect neurons, neural structures or neural paths. Neurodegenerative diseases are those diseases caused by neural disorders or neural dysfunctions (Przedborski *et al* 2003, Rich 2001, Crumrine 2001), and they are estimated to be a few hundreds. Examples for the most famous neurodegenerative diseases are: Alzheimer's disease (De-Paula *et al* 2012), Parkinson's disease (Archibald *et al* 2013, Surmeier and Sulzer 2013), Huntington's disease (Bates 2005, Leavitt *et al* 1999), Epilepsy or epileptic seizures (Fisher *et al* 2005, Chang and Lowenstein 2003), Retinitis Pigmentosa (Busskamp *et al* 2010, Ferrari *et al* 2011), Cognitive disorders and impairments and Age-related diseases (Brown *et al* 2005, Przedborski *et al* 2003). The reason behind neurodegeneration still essentially unknown, however, we surely know that it shortens the life time and it causes individuals to suffer from poor life quality (Przedborski *et al* 2003).

2.7 Neuroprosthesis and Neural Interfaces

For the sake of pain relief and improvement of life quality in patients suffering from neural dysfunctions, attention is caught to pharmacology. However, this goal can be achieved by drugs in only a few percent of those patients (Cruccu *et al* 2007, Finnerup *et al* 2005). On the other hand, thanks to the discovery by Galvani (Galvani 1791) and other subsequent efforts (Hodgkin and Huxley 1952), electrical stimulation of excited tissue for neural rehabilitation has shown much interest and success in several clinical uses (Peckham 1987, Rutten 2002). By inserting metallic or, in general,

conducting electrodes inside the nerve cell's membrane or ensembles of neural populations in close proximity to neurons, it is possible to activate neural pathways to other neurons or to neuromuscular junctions. This electrical stimulation produces an artificial depolarization of the membrane ion channels, evoking the firing of action potentials (Ferreira and Marshall 1985, Ranck 1975). Electrical stimulation was applied to stimulate phrenic nerve for diaphragm pacing and respiration control (Glenn and Phelps 1985). Neuromuscular stimulation was employed to excite the paralyzed muscles due to spinal cord injury (Cybulski et al 1984). Implanted electrodes carrying electrical stimulation was employed for bladder evacuation (Brindley et al 1986). Intra-cochlear bipolar electrodes were used to electrically stimulate auditory nerve (Van den Honert and Stypulkowski 1987). Attempts have been made using electrical stimulation for controlling epileptic seizures (Li and Mogul 2007).

Some of the metal based electrodes have had profound implications on the quality of life of individuals suffering from sensory or motor dysfunctions. In particular it has shown a great success in clinical applications of cochlear implants (Edgerton et al 1982, Maillet et al 1995, Spelman 1999). At the neurosurgery level, metal based electrodes have had profound potential in deep brain nuclei stimulation (DBS) for tremor treatment in Parkinson's disease (Lozano et al 2002, Kringelbach et al 2007, Benabid et al 2011). For visual neuroprosthetics, stimulation electrodes implanted into a blind patient's visual cortex caused the patient to experience light sensations in form of intermittent white spots, called phosphenes (Dobelle and Mladejovsky 1974, Brindley and Lewin 1968, Cha et al 1992). Microelectrodes for cortically based visual neuroprosthetics have been developed (Torab et al 2011, Fernández et al., 2005; Normann et al 2009, 1999b). Electrical stimulation is also used to evoke or control the

aggression behaviour of different species (Delgado 1969, 1966, Siegel *et al* 1999). And the famous 1963 experiment performed by Jose Delgado to control an angry bull by means of electrical stimulation of the aggression region in the brain (Delgado 1969).

However, it was soon appreciated that repeated chronic stimulations necessary for lasting rehabilitation can have their disadvantages. Examples are the eventual degradation of tissue and electrodes, issues of biocompatibility and immune responses. In section 2.8 these issues will be discussed in some details.

2.8 Neural Interfaces: Biocompatibility Issues and Immune Response

As stated in the previous section, electrical stimulation, using metal based electrodes, for therapeutic rehabilitation have been used in treatments of spinal cord injury, stroke, sensory deficits and neurological disorders (Rutten 2002). Initial results were deemed promising with successful restoration of activity to afflicted areas (Navarro *et al* 2005, Schmidt *et al* 1996, Normann *et al* 1999a). However, it was soon appreciated that repeated chronic stimulations necessary for lasting rehabilitation can have their disadvantages. In particular, the eventual degradation of tissue and electrodes, issues of biocompatibility and immune responses (Polikov *et al* 2005, Biran *et al* 2005, Marin and Fernández, 2010). The negative immune response to the implanted electrodes results in the formation of a fibrous cocoon around the electrode that isolates it from the surroundings (Schultz and Willey 1976, Turner *et al* 1999) and affect the electrode stability and drives it off the area of interest (Liu *et al* 1999). These implants also exhibit several problems during chronic implantation. These complications present themselves as adverse tissue responses arising from the trauma of the initial insertion of electrodes which can lead to intrinsic foreign body responses, glial inflammation and neuron/electrode connection loss near the implant (Szarowski *et al* 2003). Other limiting contributions occur due to the large difference in mechanical properties between the stiff electrodes and the soft tissue while others have reported a "kill zone" in which neurons appear to die off approximately up to 200μm away from implants (Biran *et al* 2005, Henze *et al* 2000). Hence, in order to overcome these problems and improve the communication to the nervous system for therapeutic rehabilitation, new communication paradigms have to be introduced.

On the other hand, in electronic devices and metallic electrodes the information is carried by electrons: All the carriers are identical in both charge and chemical nature. In the nervous system of mammals the information carriers in the neuron are chemical ions (such as: Cl^-, Na^+, Ca^{2+}) each of them carries a different charge. Even those carrying the same charge (such as: Na^+, K^+) carry different chemical information. This ionic flow inside and outside the electrically excitable neuronal membrane causes a membrane depolarization. Membrane depolarization results in a functional response called action potential, as explained previously, which stimulates the release of cellular output signals called neurotransmitters (Kandel *et al* 2000). The intensity of the ionic flow through the membrane ion channels is controlled by the channel protein conformational (electromechanical) movement, providing the nervous pulse with conformational (memory) information. By flow of the same charge the information trailed in neuronal systems overcome by several orders of magnitude that transferred in electronic or optical means (Martinez and Otero 2013).

Bearing in mind that nervous system is a highly developed and sophisticated thermodynamically energy conversion machine. In order to better communicate electronic and neural worlds, a transducer (energy converter) is required. This transducer will present itself as a new communication paradigm to the nervous system. This new paradigm will provide improvements at the site interface between neural implant and biological tissue. It also will act as an energy converter that converts electronic energy into ionic energy and vice versa.

Conductive polymers are ideal electroactive material for working with biological systems, and they can improve on interfacing metal electrodes and biological tissue. Hence, several works have reported on the potential of emerging electroactive materials,

which are able to mimic the biological characteristics and functions so they can improve on the previous mentioned issues. Studies to evaluate the influence of conductive polymers on the inflammatory response during wound-healing processes were reported (Lehle *et al* 2004). Biocompatibility of conductive polymers for medical implants was reported (Malmstrom *et al* 1998, Quester *et al* 2003, Fulzele *et al* 2003, Zelikin David M; Farhadi, Jian; Martin, Ivan; Shastri, Venkatram & Langer, Robert 2002).

2.9 Conductive Polymers

Conducting (conductive) polymers (CPs) were discovered and their electrical conductivity was explained in 1977 (Shirakawa *et al* 1977). Even if the electronic conductivity of conducting polymer polypyrrole was first reported in 1963 (Bolto *et al* 1963), but its origin was not explained by that time. The conductivity and its origin were reported later and the discoverers gained the 2000 Nobel Prize in Chemistry (Heeger 2001, Shirakawa 2001, MacDiarmid 2001a).

2.9.1 Origin of Conductivity

Unlike conventional polymeric materials (plastics) which normally thought to be insulating materials, conducting polymers exhibit an electrical conductivity. This electrical conductivity can be either intrinsic or extrinsic. Extrinsic conductivity arises from the introduction of conducting metallic pieces or fragments into the polymer, by which the polymer-metal composite can carry and conduct electrical charges. Intrinsic conductivity is an inherent property that arises in a polymer (Bower 2002). However, if we consider metallic conductors we find that conductivity is due to the electronic band structure. Whence, the valence electrons can travel freely to the conduction band due to the absence of the forbidden gap. In insulators, the forbidden gap, or the band gap, is very wide and electrons cannot travel from valence band to conduction band. However, in semiconductors, the band gap is relatively narrow and the valence electrons can travel to the conduction band if they have enough activation energy to cross the narrow band gap (Harrison 1970), see figure (2-3).
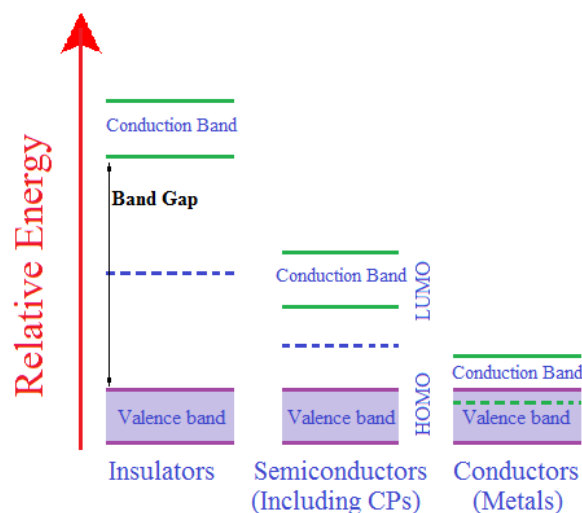
Fig. 2-3: Schematic drawing of band structure in insulators, semiconductors and conductors. It represents the fully occupied valence band, the forbidden energy gap and the conduction band. It also shows the lowest unoccupied molecular orbital (LUMO) in the conduction band and the highest occupied molecular orbital (HOMO) in the valence band. LUMO/HOMO orbital system plays an essential role in the conductivity of conducting polymers.

Metals manifest electronic conductivity due to the free movement of electrons through their structure. Conducting polymers conductivity is similar to that of semiconductors (MacDiarmid 2001b). Moreover, the chemical structure of conductive polymers shows a special distribution of π electrons placed at the carbon-carbon backbone of the polymeric chain. The conjugation (the interaction) between π bonds (covalent chemical bonds) results in delocalized (free) π electrons states. Accordingly, in order for conducting polymers to manifest intrinsic conductivity they must possess not only free charge carriers (electrons) but also a LUMO/HOMO π orbital system that allows the free movement of these charge carriers between valence band and conduction band. LUMO and HOMO are acronyms for lowest unoccupied molecular orbital and highest occupied molecular orbital, respectively. In semiconductors, LUMO defines the lowest unoccupied molecular orbital in the conduction band and HOMO defines the

highest occupied molecular orbital in the valence band. A conducting polymer is synthesized by oxidation of its corresponding monomer. While synthesis, an oxidizing dopant can change band structure either by taking electrons from the valence band to the conduction band (called *p*-doping) or by adding electrons directly to the conduction band (called *n*-doping). This electron addition to the LUMO makes the conduction band to be partially filled and a radical anion, called polaron, is created (Bredas and Street 1985). The creation of this polaron initiates the injection of states from the bottom of the conduction band and the top of the valence band into the (forbidden) band gap, ending up with the polymer being conductor.

2.9.2 Biological Applications

Thanks to their softness, reactivity and ease of synthesis (Otero 2009), conducting polymers have caught much attention for biological applications. Many studies were developed on the interfacing between biological tissues and conducting polymers (Foulds and Lowe 1986, Wong *et al* 1994, Schmidt *et al* 1997, Garner *et al* 1999, Cui *et al* 2001).

2.9.2.1 Polypyrrole

One of the most studied conducting polymers is polypyrrole (pPy) and it has attracted a lot of attention for biomedical applications (Hodgson *et al* 1995, Williams and Doherty 1994). Polypyrrole conducting polymer $[C_4H_5N]_n$, figure (2-4), displays particular characteristics including electronic conductivity. Toxicity test was performed on polypyrrole and it was reported to be within the ISO standards (Wang *et al* 2004).

Polypyrrole is a relatively stable to air and water can easily be synthesized, with low costs, either by chemical or by electrochemical oxidation of pyrrole monomer (Vernitskaya and Efimov 1997). As will be explained later, electrochemical synthesis is an easy method and it is widely used for research purposes. It enables the control of electro- and physico-chemical characteristics of the polymer during polymerization process (Otero *et al* 2010). Additionally, the electronic conductivity of polypyrrole can be increased several-fold by introducing an external dopant anion during electropolymerization (Kumar and Sharma 1998).
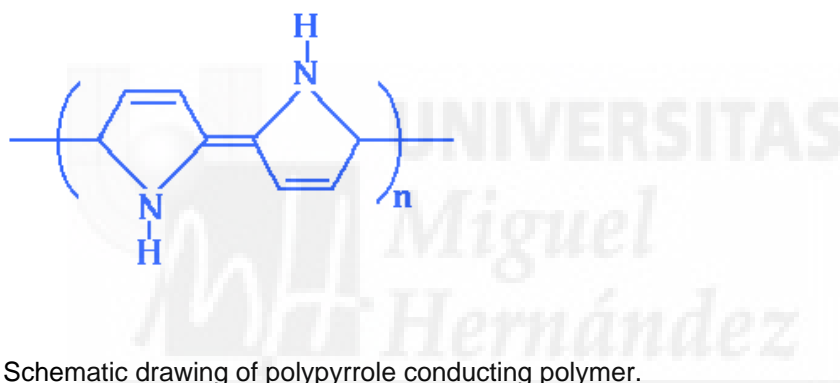
Fig. 2-4: Schematic drawing of polypyrrole conducting polymer.

Finally, and in relation to the topics listed in the previous chapter, this chapter presented the background information to establish the work needed to fulfill the aims of this thesis. Schematically, the issue of neurodegeneration and its possible solution can be presented as shown in figure (2-5).

Lastly, as the topic of digital holographic microscopy is a completely new one, there is a separate chapter (chapter VI) in this thesis to present this new microscopy technique.
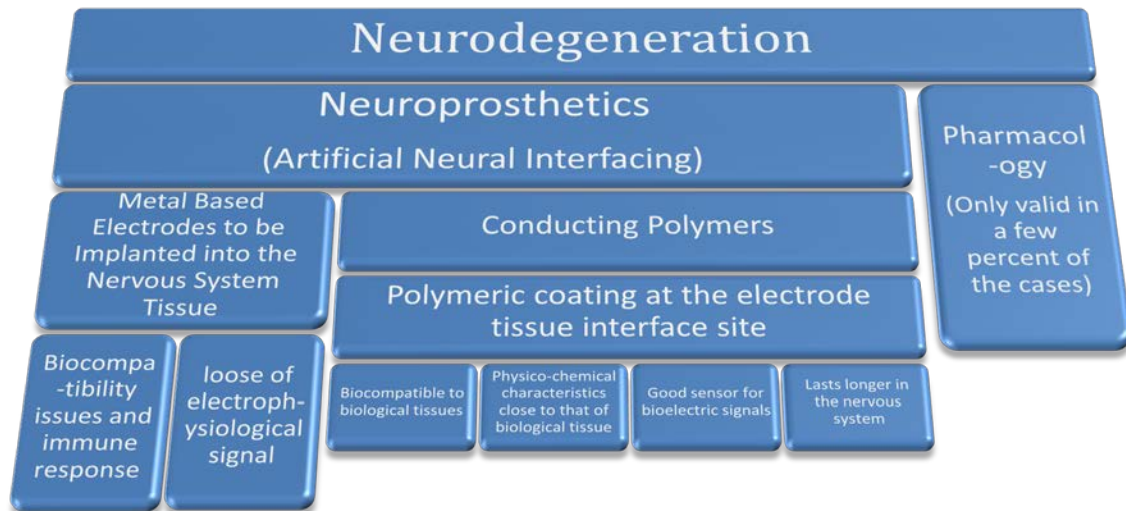
Fig. 2-5: Schematic representation neurodegeneration and its possible solutions.
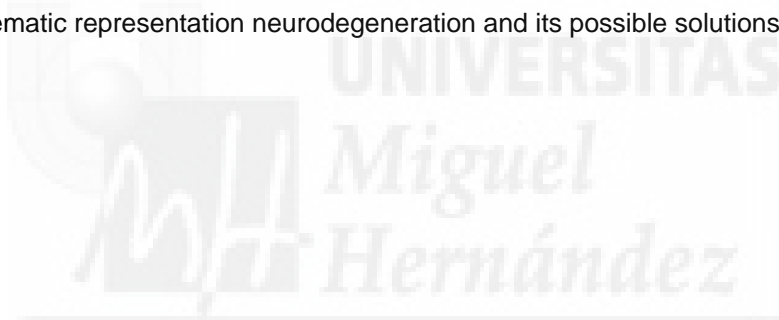
Chapter Three

Chapter III

Materials, Methods and Equipments

3.1 Chapter Overview

This chapter presents the list of materials used in the work, the methods and techniques and the equipments and facilities employed in this thesis. First, it starts by introducing the list of reagents, chemicals, tissue culturing media and antibodies. It also presents the biological tissues and animals used for the study. Then the chapter introduces the list of equipments and facilities, employed in the thesis, with a brief introduction to each of them. It ends up with introducing the methods and procedures used in the development of the thesis work.

3.2 Materials

3.2.1 Reagents and Chemicals

- Pyrrole monomer (Py >98%, Sigma Aldrich) was purified by distillation under vacuum prior to use and kept refrigerated at -20 degree Celsius

- Poly(Sodium 4-styrenesulfonate) (NaPSS) was purchased from Sigma Aldrich and was used as delivered

- Sodium chloride salt (NaCl) min 99.5% from Sigma Aldrich

- Potassium chloride salt (KCl) min 99 % from BDH Prolabo Chemicals

- Methanol 32213-1L from Sigma Aldrich

3.2.2 Media (Tissue Culture and Fixation)

- Poly-D-lysine Hydrobromide PDL P0296-50 mg from Sigma Aldrich

- Dulbecco's Phosphate Buffered Saline (PBS) solution with Ca^{2+} and Mg^{2+} from Biochrom AG

- Laminin L2020-1mg from Sigma Aldrich

- Neuro-Basal B27 (NB/B27) supplement (50X) from Fischer's Life Technologies - Invitrogen (Gibco)

- Neuro-Basal Fetal Bovine Serum (Gold) (NB/FBS) from PAA laboratories GmbH

- Glutamax-100X 35050-038 100 ml from Life Technologies - Invitrogen (Gibco)

- Penicillin Streptomycin (Pen/Strep) from Life Technologies - Invitrogen (Gibco)

- Dulbecco's Modified Eagle Medium (DMEM) 1X from Life Technologies - Invitrogen (Gibco)

- Ham's F12 Nutrient Mixture 1X from Life Technologies - Invitrogen (Gibco)

- Trypsin-Edta: 0.05% Trypsin-EDTA 1X 25300-062 500 ml from Life Technologies - Invitrogen (Gibco)

- Hank's balanced salt solution (HBSS) with sodium bicarbonate, liquid, sterile-filtered, suitable for cell culture from Sigma Aldrich

- PFA Paraformaldehyde (DAC) PRS-Codex Panreac Quimica SAU - España

3.2.3 Antibodies

All antibodies were purchased from Sigma including:

- Microtubule-associated protein MAP2b (mouse 1/100)

- Blue-fluorescent nucleic acid stain DAPI (1/500)

- Neurofilament cytoskeleton marker (rabbit 1/1000)

- Glial fibrillary acidic protein (GFAP) (rabbit 1/500)

- Secondary antibody Anti-488 (rabbit 1/1000)

- Secondary antibody Anti-555 (mouse 1/1000)

3.2.4 Animals and Biological Tissues

- E17.5 pregnant rats (Sprague Dawley) were purchased from Janvier Laboratories.

- Human neuroblastoma cultures: Neuroblastoma SH-SY 5Y Cell line, human Neuroblast from neural tissue, from Sigma Aldrich.

3.3 Equipments and Facilities

3.3.1 Electropolymerization

- Potentiostat/galvanostat controlled by a general purpose electrochemical system (GPES) µAutolab Type III form ECO Chemie.

- Reference electrode: Metro Ohm Ag/AgCl 3M KCl electrode

3.3.2 Electrophysiology setup

Electrophysiology and stimulation setup is composed of three main parts. First part is Multielectrode Arrays (MEA) that is composed of two plates (upper and lower) between them the microelectrode culturing plate containing live cells is stated. These two plates are connected to the pulse generator through electrical threads. The second part is the pulse generator called STG1002 generator. Third part is a powerful computer together with MC Rack software. Microelectrodes array consists of 8 x 8 grids of titanium nitride electrodes of 30µm diameter and inter-electrode spacing of 200µm. Microelectrode culture plates, STG1002 stimulator and MEA setup are bought from Multi Channel Systems, Reutlingen, Germany.

3.3.3 Scanning Electron Microscopy

JEOL Scanning Electron Microscope (SEM) was used to study the surface morphology of both metallic microelectrodes and polymer coatings with a typical voltage of 20 kV at a high vacuum mode.

3.3.4 Imaging

- Confocal Microscopy: Confocal microscope with an oil immersion 40x objective and with 100W illumination model Leica DM2500; supplied by Leica Microsystems.

- Optical Microscopy: Olympus IX51 inverted microscope with external power supply 200 V unit TH4-200

3.3.5 Digital Holographic Microscopy

A reflection configured digital holographic microscope in dual wavelength mode. The microscope model is R2100 series from Lyncée Tec SA. The microscope configuration and working procedure will be explained in some details in chapter VI.

3.3.6 *In vitro* Chronically Applied Stimulation

In vitro chronically applied stimulation was carried out using Stim 100 API 2.0 fully programmable current (voltage) generator from Biomedical Technologies S.L. Spain. The system is based on the software (stimulation manger) and the hardware which is based on main board with one current generator module.

3.3.7 Electrochemical Impedance

Impedance measurements were carried out using a bioimpedance meter μcell*View* from i2m Design. The system is a battery powered bench top based unit controlled by PC through a Bluetooth connection (Guimerà *et al* 2009, Calderón *et al* 2007). The μcell*View* was programmed and calibrated to work in the frequency range from 100 Hz to 100 kHz.

3.3.8 General purpose devices

- UV lamp U.V. Esteril from JP Selecta SA

- Ultrasonic bath 1L mod. 3000512 from JP Selecta SA

- Water bath thermostat Selecta from Tectron Bio

- Water deionizer from Millipore Elix

- Weighing Balance model BP615 (readability 0.0001 g) from Sartorius

- Automatic cell counter ADAM-MC from Digital-Bio

- Tissue culture: hood and incubator HERA Cell from Heraeus Germany

- Stereo zoom microscope Leica zoom 2000 from Leica

- Heating plate and magnetic agitator AGIMAIC-N from P-Selecta

3.4 Electropolymerization of Conducting Polymers

Conducting polymers can be synthesized either chemically or electrochemically. In this thesis electrochemical polymerization is employed using 3-electrode cell configuration. The typical structure of the 3-electrode electrochemical cell, figure (3-1), consists of a working electrode (WE) on which the polymer is oxidized and/or electrochemical studies are performed. The reference electrode (RE) is placed close to the working electrode and its function is to maintain a constant potential across the film surface. The counter electrode (CE) works as the supplier of the electrons that are used to initiate the electropolymerization reaction. The electrochemical cell is connected to an electrical supplier, called potentiostat.

In the present study, the electrical supply was a potentiostat/galvanostat controlled by a general purpose electrochemical system (GPES) μAutolab Type III form ECO Chemie. The potential of the working electrode was measured with respect to a MetroOhm Ag/AgCl 3M KCl electrode. For the working electrode, two different types of substrates were employed. Firstly, a "macro-substrate" was employed for the film synthesis. For that purpose, and in order to be able to optically monitor cellular division and growth, the transparent indium tin oxide coated glass (ITO) substrates were used. Secondly, a "micro-substrate" was employed. For that purpose, and in order to study the potential of conducting polymers for electrophysiological recordings, titanium nitride (TiN) microelectrodes were used.
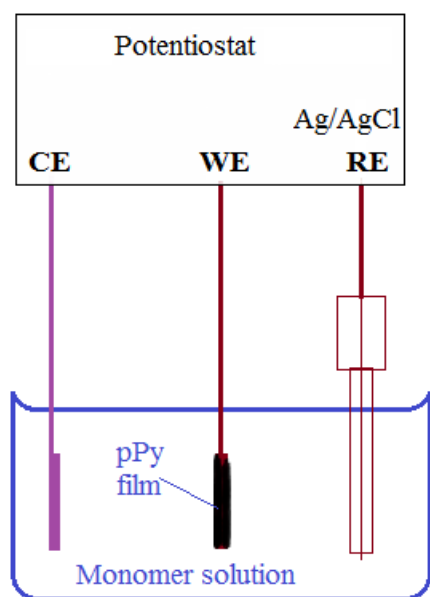
Figure (3-1): Graphical representation of three electrode electrochemical cell used for electropolymerization. Typically, it consists of a potentiostat that provides anodic current, counter-electrode (CE), working electrode (WE) and reference electrode Ag/AgCl (RE). The three electrodes are immersed into the monomeric solution, once the anodic current is initiated, the conducting polymer oxidized on the working electrode.

3.4.1 Electrochemical Deposition of Polypyrrole Films

3.4.1.1 ITO substrates employed as working electrodes

Conducting polymer polypyrrole doped with the negatively charged molecule poly(sodium 4-styrenesulfonate), (pPy/NaPSS or simply pPy/PSS), was chose as explained in chapter II. Films of pPy/PSS were grown potentiostatically on ITO substrates.

- Working electrode: ITO substrates, with physical dimensions (32mm * 32 mm * 1.1mm) were used as the working electrodes.

- Counter electrode: A stainless steel plate with physical dimensions (40mm*20mm*2mm) was used.

3.4.1.2 TiN microelectrodes as working electrodes:

For the aim of studying the polymer as an electrophysiological probe, titanium nitride (TiN) microelectrodes of the size 30 µm were employed. The electrodes are stated in multielectrode array (MEA) plate as a matrix of 8x8 electrodes, with inter-electrode spacing of 200 µm.

- Working electrode: TiN microelectrode, size 30 µm.

- Counter electrode: A platinum plate with physical dimensions (10mm*4mm*1mm)

3.4.2 Electropolymerization Procedure: Chronoamperometry

Prior to use, ITO substrates were accurately cleaned with a degreasing solution made of 20% w/w of ethanolamine deionized water. The substrates were immersed in the solution and heated up to 80 °C under ultrasonic agitation for 15 minutes. Then the substrates were removed from the solution, rinsed several times with deionized water and dried under nitrogen flow. For titanium nitride (TiN) microelectrodes in MEA, prior to polymerization, the MEA plate was cleaned in an ultrasonic bath at room temperature then it was rinsed thoroughly with deionized water.

Either ITO substrates or TiN microelectrodes were connected as working electrode in the 3-electrode cell. The electrogeneration of the polymer films was performed from 0.1M pyrrole and 0.05M NaPSS aqueous solutions. The oxidized (pPy^{n+}/PSS^{n-}) conducting polymer was deposited under potentiostatic conditions by submitting the ITO substrates (as working electrode) at 0.75V for 200 seconds. The chronoamperometric response was recorded in parallel.

3.4.3 Cyclic Voltammetry (CV)

Cyclic voltammetry (CV) is an electrochemical technique employed to provide qualitative information about electrochemical reactions. Cyclic voltammetry is a powerful tool to locate the potentials of the redox (reduction/oxidation) reactions in an electrochemical system, figure (3-2: B). It is able to characterize the electron transfer kinetics and transport properties of electrochemical species. Cyclic voltammetry consists of linearly scanning the potential of a stationary working electrode using a triangular potential waveform, as in figure (3-2: A). For the different electrochemical studies different number of scans is performed. The response of the potential sweeping

versus the current is called cyclic voltammograms. Cyclic voltammograms provide large number of physico-chemical characteristics of the studied material (Wang 2004).

3.4.3.1 CV Procedure:

Once electrogenerated, the electroactivity of the polypyrrole film was checked in the background electrolyte (aqueous solution of NaCl or KCl) by cyclic voltammetry between -0.6 and 0.6 V, vs. Ag/AgCl, at a scan rate of 0.05V/s. Reduced pPy/PSS^{n-} $(Na^+)_n$ and $pPy/PSS^{n-}(K^+)_n$ films were obtained from the electrogenerated oxidized (pPy^{n+}/PSS^{n-}) films by cyclic voltammetry (CV) in 0.1M NaCl or 0.2M KCl solutions respectively, stopping the last sweep at the cathodic potential limit (-0.6 V).
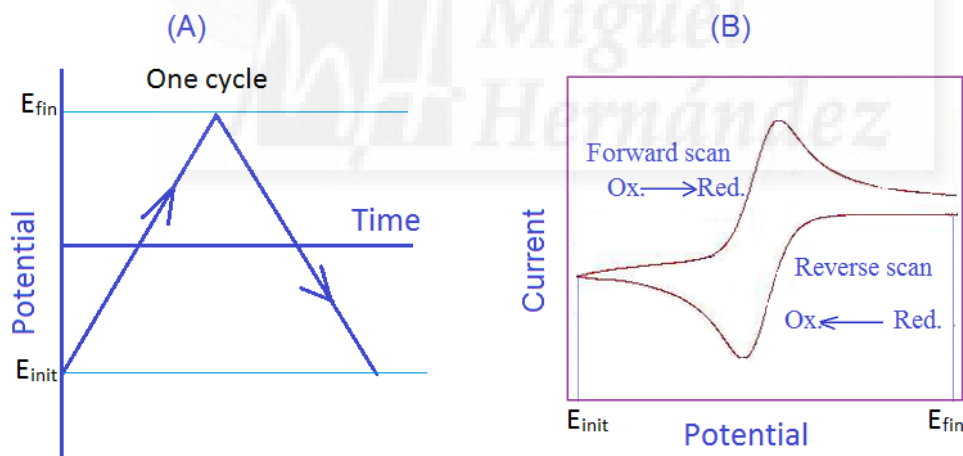
Figure (3-2): Schematic representation of cyclic voltammetry.

(A) Potential vs. time excitation signal during cyclic voltammetry experiment. In one cycle, the potential starts from initial value E_{init} to final value E_{fin} in the forward scan, then from E_{fin} to E_{init} in the reverse scan.

(B) Typical cyclic voltammograms for a reversible redox reaction. Forward scan from negative positive potentials represents oxidation process, and reverse scan from positive to negative potentials represents reduction process.

3.5 Tissue Culture

3.5.1 Primary cultures

Dissociated cultures of hippocampal neurons (Cornu Ammonis areas CA1-CA3) were prepared from E17.5 Sprague Dawley sibling embryos. The tissue was kept in 2 ml of HBSS (Hank's Balanced Salt Solution) then a 10 mg/ml final concentration of trypsin was added to the medium. The system was thermostated at a 37 °C for 13 min to catalyse the action of the enzyme. The tissue was then transferred to a 15 ml falcon tube containing 4ml of Neurobasal (NB) / Fetal bovine serum (FBS), then the tissue was triturated using combination of fine pore fire polished Pasteur pipettes (Volac).

Once the tissue was dissociated the cell density was determined using a haemocytometer. The polymer modified ITO substrates or the microelectrodes plate of MEA arrays were pre-treated by immersion overnight in aqueous solution of Poly-D-lysine (PDL) (50 mg/ml) in order to enhance cell attachment. The PDL was then aspirated away and the substrates were washed with phosphate buffered saline (PBS) twice. A final coating with laminin, a protein found in the extracellular matrix, by immersion in 50μg/ml will further help anchor the dissociated hippocampal cells. The same procedure was performed for microelectrode arrays MEA plates.

The cells were maintained in a mixture of 500 ml NB/B27 supplement (promotes neural growth) and 500 ml NB/FBS (promotes glial growth), each supplemented with Glutamax and Pen/Strep (dilution 1/100). Glutamax improves cells viability and growth while preventing build up of ammonia and Pen/Strep helps to prevent any infections. Cells were kept in an incubator at 37°C in 5% CO_2 atmosphere. Cells were then seeded onto either the coated pPy/PSS-ITO electrode or the

microelectrodes plate in MEA arrays, some of the MEA microelectrodes coated with polymer films some remain uncoated.

Pure glial cultures were grown following the same method described above, excluding of B27 supplement, thus facilitating only glial proliferation.

3.5.2 Neuroblastoma cell cultures

Neuroblastoma SH-SY 5Y Cell line, human Neuroblast from neural tissue, (Sigma) was cultured in a medium of 1:1 mixture of DMEM 4.5 g/l and Ham's F12 medium and 10% FBS. The conductive polymer modified ITO substrates was placed in a Petri dish and was covered by a sufficient quantity of 0.5% Trypsin-Edta. The cells were then seeded on the slide at a density of $1x10^5$ cells per dish, and cell medium was replaced each 4 days. Seeded cells were kept in an incubator at 37˚C in 6% CO_2.

3.5.3 Immunohistochemistry: Fixation and Staining

Cells where fixed in using 4% paraformaldehyde (PFA) for 20 min. Cells were then permeabilized using 0.25% Triton X-100 for 5 min. Cells were then placed in 10% Bovine Serum Albumin (BSA) for 1hr at room temperature to block any non-specific protein interactions. All antibodies were prepared in 3% BSA. Cells were incubated in primary antibodies overnight at 4˚C and then washed three times with PBS. Secondary antibodies were then applied and kept at room temperature for 1hr followed by another 3 washes with PBS. Cover slips were then mounted with Mowiol coverslip mounting solution onto glass cover slides.

3.6 Imaging

A Leica DM 2500 confocal microscope with an oil immersion 40x objective was used to take pictures of the fixed cells. Images were taken using lasers of different wavelength for the different fluorophores: 410 nm, 488 nm and 543 nm. Lasers scans on samples including several fluorophores were performed sequentially, with the corresponding excitation/emission filters, in order to avoid any cross talk between channels. Bleed-through between different channels was assessed whenever a new setting was implemented and found to be negligible for all experiments described here. Image resolution was at 1024 x 1024 pixels. In each case, care was taken to avoid the saturation of any of the fluorophores. The pin-hole size was adjusted automatically by the software to achieve maximal confocality and minimal interference form out-of-focus light. Z-stacks were taken at 0.2μm intervals to image the entire field of view.

3.7 *In vitro* electrophysiological recording with MEA system.

Multielectrode array (MEA) plates together with multichannel setup for *in vitro* electrophysiological studies were supplied from Multi Channel Systems, Reutlingen, Germany. Neural cells were plated directly onto the multielectrode array (MEA) plate which contains the polymer-coated microelectrodes in a MEA that consisted of 8 x 8 grids of titanium nitride (TiN) microelectrodes of 30μm diameter and inter-electrode spacing of 200μm. Spontaneous action potentials (spikes) were recorded in 10 min epochs at 2 to 3 days from DIV13 until DIV20 (where DIV stands for days *in vitro*) in culture medium at a temperature of 37˚C. Spikes were detected online using MC Rack (Multi Channel Systems) and offline analysis were performed using MC Rack (Multi Channel Systems) and Neuroexplorer (Nex Technologies, Littleton, MA). Spike

detection was performed using a threshold of 5 degrees standard deviation from the

baseline.

Chapter Four

Chapter IV

Conducting Polymer Polypyrrole: Synthesis and Characterization

4.1 Chapter Overview

This chapter presents results and discussions of electropolymerization of the electron-cation transducer films of the conducting polymer polypyrrole on different substrates. First, indium tin oxide coated glass substrates were used in order to be able to visually assess the biocompatibility of the electrogenerated polypyrrole for different biological tissues. Then electropolymerization was performed on titanium nitride microelectrodes in order to assess the ability of the polypyrrole polymer to record nerve activities from neural populations, *in vitro*. The chapter then presents physico- and electro- chemical characterizations of polypyrrole. Then it presents a study on the electrochemical impedance measurements for titanium nitride microelectrodes with or without polypyrrole conducting polymer coating. The aim of this study is the synthesis and characterization of conducting polymer polypyrrole for possible neural interface applications.

4.2 Electrochemical Synthesis (Electropolymerization)

Conducting polymers can be synthesized either chemically or electrochemically. However, electrochemical polymerization (or electropolymerization) is an easy, fast and effective method for conducting polymer synthesis (Otero *et al* 2010, Conzuelo *et al* 2010). Electropolymerization is the method used for the synthesis of conducting polymer films, for research purposes, and it is able to functionalize the synthesized film' surface. It was first discovered, by Diaz *et al* in 1979, that electrochemical methods are perfect for the electropolymerization of conducting polymers (Diaz *et al* 1979, Kanazawa *et al* 1979). Electropolymerization works by imposing an anodic potential to pass through the monomeric solution together with a dopant material in an electrochemical cell. Then, the monomer starts to oxidize depositing the corresponding polymer on the surface of the working electrode. In the following, the electropolymerization of conducting polymer polypyrrole is presented.

4.2.1 Electropolymerization on ITO Substrates

Polypyrrole (pPy) synthesis was performed at room temperature using the electropolymerization method, as explained in section (3.4) in the method's chapter. Starting from an aqueous solution of pyrrole monomer together with the counterions doping salt poly(sodium 4-styrenesulfonate) (NaPSS), films of polypyrrole doped with NaPSS (pPy/PSS) were electrogenerated. For the working electrode on which the polymer was electrogenerated, an indium tin oxide coated glass (ITO) substrates were first employed. Electropolymerization was performed by applying a constant potential of 750 mV for 200 seconds. The counter electrode was a stainless steel plate. Electropolymerization process initiates by monomeric oxidation that leads to polymer

deposition on the working electrode. Figure (4-1) shows the anodic

chronoamperometric (current-time) response during the polymer growth. The graph

shows a smooth chronoamperometric response which results in a homogeneous and

smooth polymer film. The amount of the material deposited on the electrode was

controlled by the total charge Q consumed during the deposition. The value of the

charge consumed is automatically displayed by the software during

electropolymerization. However, this value corresponds to the area under the current-

time curve and can be obtained offline by the mathematical integration of the

chronoamperometric response curve. The charge consumed was calculated from various

responses and the mean value was about 180 mC for the 200 s time period.
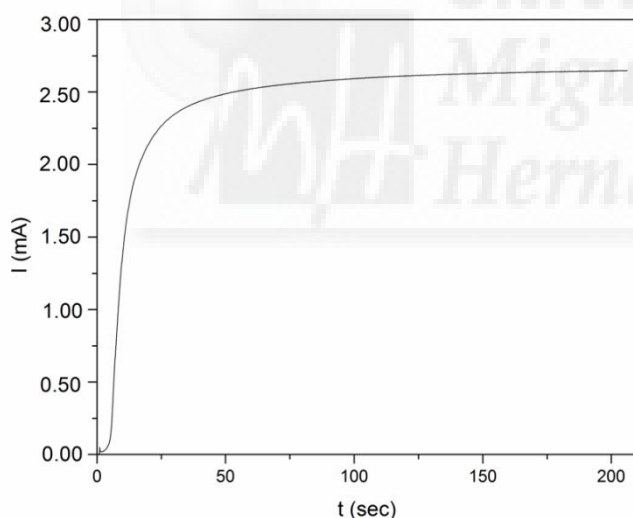
Figure (4-1): Chronoamperometric response during electrogeneration of pPy/PSS films, in 0.1M pyrrole and 0.05M NaPSS aqueous solutions. Submitting an ITO electrode for 200 seconds. Graph represents current in (mA) vs. time in seconds.

4.2.2 Electropolymerization on TiN Microelectrodes

The second working electrode that was employed was titanium nitride (TiN) microelectrode stated in multielectrode array (MEA) plate. As explained in chapter three, each TiN microelectrode has a geometrical size of 30 microns and inter-electrode spacing of 200 micron. These micro-dimensions resulted in a quite sophisticated polymerization process due to working in a micrometer scale and the lack of visualizing the electrode while polymerization. However, the polymerization procedure was quite similar to the one employed with ITO substrates except for the polymerization time and the electrochemical cell. For polymerization on TiN, the MEA plate itself was used as the electrochemical cell and the electrical connections were performed via special plate (from multichannel systems). The counter electrode was a platinum plate. The amount of deposited polypyrrole was also controlled by means of the charge consumed. The chronoamperometric response is shown in figure (4-2). The charge consumed was calculated to be varying from 150 to 400 µC depending on the electrode position in the MEA plate. However, in order to have the same polymer amount on all treated microelectrodes, the studied microelectrodes were connected in parallel and the charge consumed was calculated to be about 250 µC.
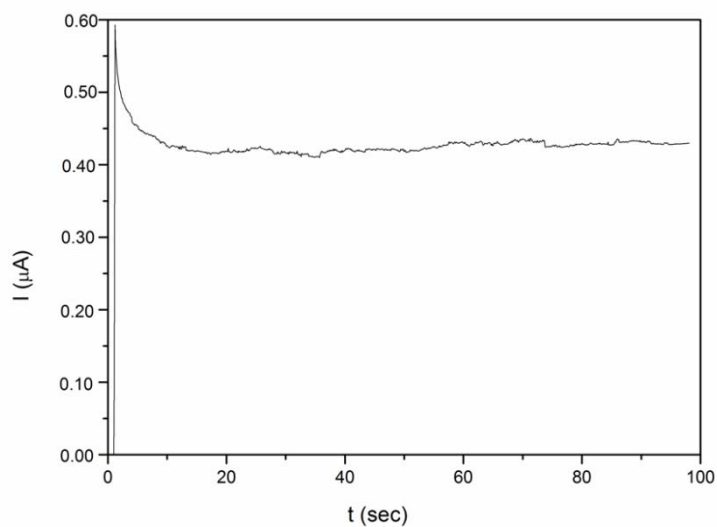
Figure (4-2): Chronoamperometric response during electrogeneration of pPy/PSS films, in 0.1M pyrrole and 0.05M NaPSS aqueous solutions. Submitting a TiN microelectrode for 100 seconds. Graph represents current in µA vs. time in seconds.

4.3 Physical Characterization of the Electrogenerated Film

4.3.1 Film Thickness Assessment on ITO Substrates

Film thickness is an important parameter that affects surface roughness and dopant stability (Fonner *et al* 2008). It is related to other film properties by equation (4-1), which was used to calculate the film thickness. For the assessment of film thickness, following steps were performed. Once electrogenerated, the pPy/PSS conducting polymer film was rinsed thoroughly with deionized water in order to remove any non-polymerized residuals. Then the mass of the film was obtained by weight difference of the ITO electrode before and after coating. The film mass was calculated to be 2 mg. This value is then sued for the calculation of the film thickness. Thickness calculation was performed using the data of the electrode coated surface area a, which was calculated to be 4.37 cm^2, the deposited polymer mass m and the pPy/PSS density ρ. The value of the polymer density was used from the literature (Qi and Pickup 1997, Lei *et al* 1992), that was reported to be $\rho = 1.44 \pm 0.05$ gcm^{-3}. Then the following equation was used:

$$d(cm) = \frac{m(g)}{\rho(gcm^{-3}) * a(cm^2)} \qquad \text{(Equation 4-1)}$$

Substituting the values of mass, density, and area in this equation, the film thickness, d, was calculated to be 3.18 ± 0.10 μm.

4.3.2 Physical Topography

Scanning electron microscopy (SEM) measurements were performed on the polymer films. Film topographic assessment was performed in the high vacuum mode at a typical voltage of 20 kV. For pPy/PSS film on ITO substrates, the material is distributed as a uniform and homogeneous film on the electrode, figure (4-3).
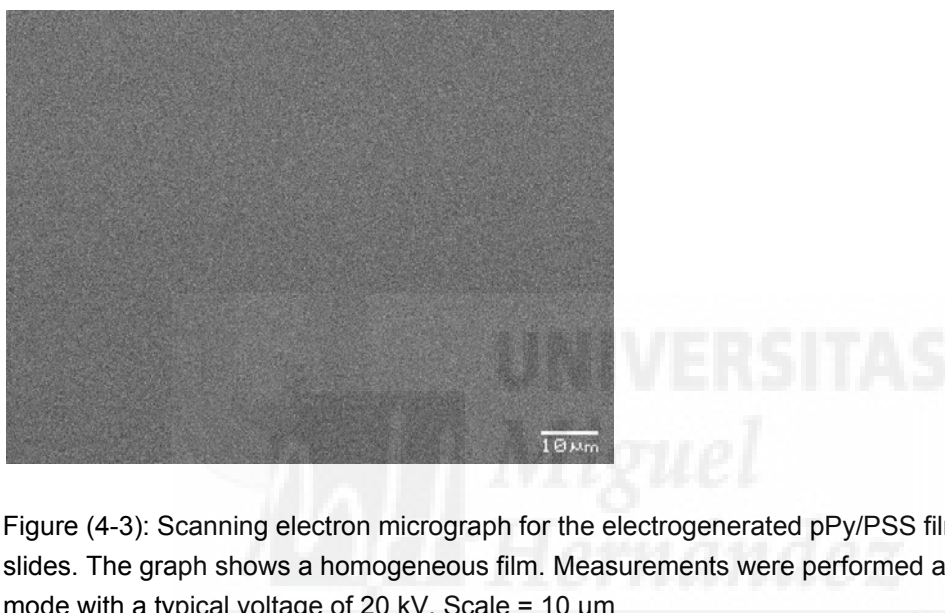
Figure (4-3): Scanning electron micrograph for the electrogenerated pPy/PSS film on ITO slides. The graph shows a homogeneous film. Measurements were performed at high vacuum mode with a typical voltage of 20 kV. Scale = 10 μm

For the pPy/PSS film deposited on TiN microelectrodes in MEA plate the film shown to be a bit rough than the one for ITO. This could be argued to the small geometrical size of the microelectrode. Actually this result was expected from the chronoamperometric response curve. However, as will be seen later in chapter 5, this affected neither the cell growth nor the recording quality. Figure (4-4) shows the SEM micrograph for: (A) two TiN microelectrodes one coated and one bare, for comparison, and (B) a closer shot for the polymer coated microelectrode.
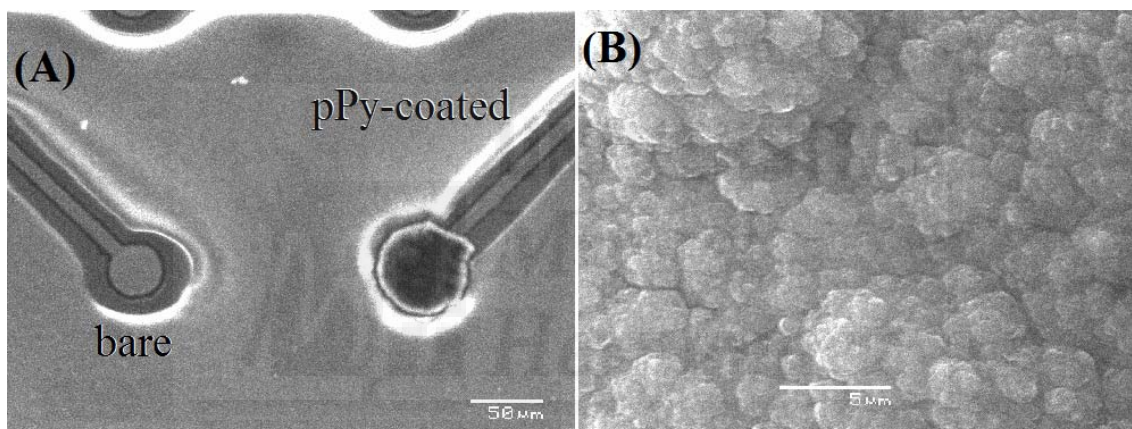
Figure (4-4): Scanning electron micrograph for the electrogenerated pPy/PSS film on TiN microelectrodes. Measurements were performed at high vacuum mode with a typical voltage of 20 kV.

(A) Represents two microelectrodes, in the MEA plate, one bare and one polymer coated. Scale = 50 μm
(B) Represents magnified shot for the polymer coated microelectrode, labeled pPy-coated in (A). Scale = 5 μm

4.4 Electrochemical Characterization of the pPy/PSS Film Electroactivity

After electropolymerization, every ITO substrate coated with an electrogenerated pPy/PSS film was used as the working electrode (WE) in 0.1M NaCl or 0.2M KCl aqueous solution. There, they were submitted to 5 consecutive potential cycles between -0.75 V as cathodic potential limit and $+0.75$ V as anodic potential limit, at a scan rate of 0.05V/s. After two consecutive cycles a stationary voltammogrametric response, figure (4-5), was attained. During the anodic potential sweep from -0.75 to 0.75 V positive currents flow the polymer promoting its oxidation and expelling the charge balancing cations towards the solution, as shown in the reaction (4-1).

$$\left[\left(Pol^0\right)\left(MA^-\right)_n\left(C^+\right)_n\right]_s \rightleftharpoons \left[\left(Pol^{n+}\right)\left(MA^-\right)_n\right]_s + n\left(C^+\right)_{aq} + n\left(e^-\right)_{metal}$$

Neutral chains　　　　　　Oxidized chains

Reaction (4-1)

Where, *s* stands for solid and *aq* stands for aqueous. The rightwards arrow over the leftwards arrow indicate a reversible Oxidation/Reduction process. MA^- represents any macroscopic anion (here, NaPSS) trapped inside the conducting polymer during polymerization. C^+ represents a cation (here, Na^+ or K^+) required to balance the charge of the macro-anion trapped inside the reduced polypyrrole film. These results are discussed in accordance to (Conzuelo *et al* 2010).

During the cathodic potential sweep from $+0.75$ to -0.75 V negative currents flow through the WE promoting the polymer reduction: Electrons are injected into the film, positive charges on pPy chains are eliminated and the cations penetrate into the film from the solution to compensate the negative charges on the negative PSS^- chains.

To avoid the polymer degradation by over-oxidation, the electroactivity of the film was characterized within the water potential window. That prevents hydrogen and oxygen evolution together, which can result in strong bioincompatible pH variations. The system becomes an electron/cation transducer (as shown in reaction 4-1) allowing the flow of charge carriers (bearing electrical and chemical information) between electronic systems and electrolytes. Therefore, it allows the flow of charge carriers between electronic systems and cells cultured on the polymer. Working inside the water potential window avoids bio-incompatibility of large pH variations produced by water hydrolysis.

This cyclic voltammetry study shows the voltage range where the oxidation/reduction reactions, redox processes, take place on the pPy/PSS polymer. It also provides a surface fictionalization mechanism for the polymeric system and converts it into an electron/cation transducer. It converts the oxidized (pPy^{n+}/PSS^{n-}) polymer into its reduced $pPy/PSS^{n-}(K^{+})_{n}$ or $pPy/PSS^{n-}(Na^{+})_{n}$ forms. However, these three forms of the polymeric system, the oxidized one, the reduced saturated with K^{+} ions and the reduced saturated with Na^{+} ions, are used as support surface for biological tissues.
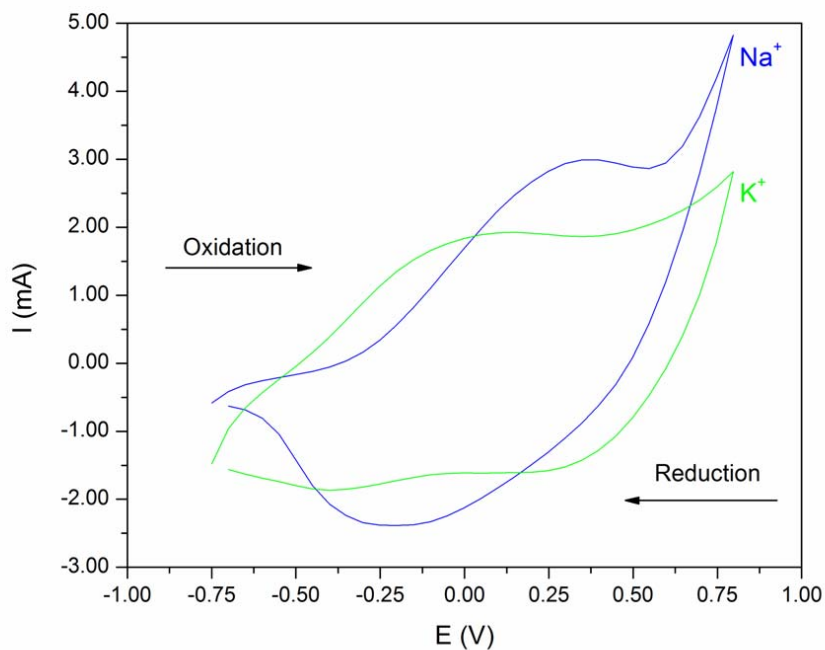
Figure (4-5): Stationary voltammogrametric response from the electrogenerated pPy/PSS film between −0.75 and 0.75 V at scan rate of 50 mVs^{-1} in 0.1M NaCl or 0.2M KCl aqueous solution. Positive currents indicate oxidation reactions, negative currents indicate reduction reactions.

4.5 Electrochemical Impedance Measurements

Electrical impedance of neural electrodes is a crucial parameter that affects the electrode performance. However, electrochemical impedance spectroscopy (EIS) provides a fast and easy technique able to characterize the electrical impedance of different conductors. This section presents the results of EIS performed on two types of microelectrodes, TiN bare and pPy/PSS coated microelectrodes in MEA. The oxidized polymer form pPy/PSS was deposited on labelled TiN microelectrodes of the MEA plate randomly selected. To check for the electrical characteristics of the polymer coated microelectrodes, electrochemical impedance measurement was performed. Figure (4-6) shows results from the impedance measurements in the frequency range from 100 Hz to 100 kHz from both TiN bare and pPy/PSS coated microelectrodes. Experiments were performed in a 2 ml of the standard PBS solution.

By analyzing the results, it was found that the presence of conducting polymer film results in a decrease of the coated microelectrode impedance when compared to that of the uncoated TiN microelectrodes. At the biological relevant frequency of 1 kHz a decrease of the material impedance from 148.6kΩ (in case of bare metal microelectrode) to 24.8kΩ (in case of polymer coated microelectrode) was observed. The difference was 124 ± 3kΩ which is almost 83% of the initial value in case of uncoated metal. These results are in agreement with the ones by Harris *et al*. They reported that the polypyrrole coated electrodes showed an increased charge density and lower impedance values at 1kHz (Harris *et al* 2013).

This decrease in the impedance of the polymer coated microelectrode is attributed to the fact that the polypyrrole coating functionalized the surface chemistry of

the electrode, meaning that higher geometrical surface area and fast electron/ion transfer

(Otero *et al* 2010, Guimard *et al* 2007). This surface functionalization works out so the

polymeric coating is an electron/cation transducer. The electron/cation transduction

causes the conduction mechanism to be faster and more effective in terms of charge

transfer. Accordingly, the conductivity of the metal/polymer/electrolyte system was

higher, and the impedance is then less.
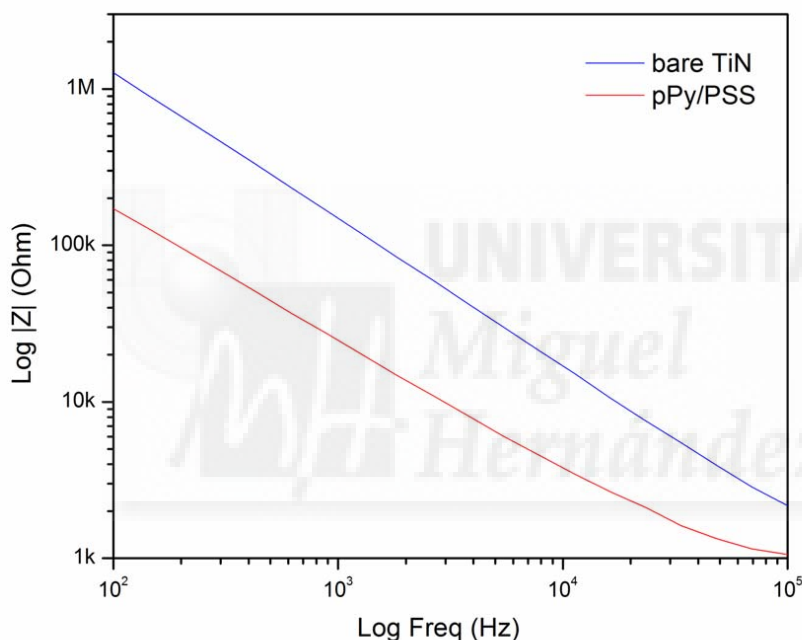
Figure (4-6): Impedance measurements performed at different frequencies from TiN microelectrodes (coated with pPy/PSS or uncoated) in MEA arrays. The experiment was performed in 2 ml of the standard PBS solution. Impedance magnitude (Ohm) is plotted logarithmically vs. frequency (Hz). The result shows lower impedance of the polymer coated (red line) with respect to that of the bare TiN (blue line) microelectrodes in the full frequency range from 100 Hz to 100 kHz.

4.6 Conclusions

Polypyrrole conducting polymers were electrochemically deposited onto two different surfaces. Electrogeneration can produce oxidized material (pPy^{n+}/PSS^{n-}) or cation saturated (reduced material) with K^+ ions ($pPy/PSS^{n-}(K^+)_n$) or with Na^+ ions ($pPy/PSS^{n-}(Na^+)_n$). Electrochemical cyclic voltammetry studies of polypyrrole polymer surface showed that the polymer is stable in the working range and can perform its redox mechanisms inside the safe water window. Physical characterization of polypyrrole showed that electropolymerization of the polymer resulted in homogeneous film surface. Electrochemical impedance spectroscopy (EIS) measurements showed that polypyrrole films present a chemically surface functionalized material that is capable of electron/cation exchange. EIS showed lower electrical impedance of the value $24.8k\Omega$ in case of the polymer coated electrodes than the bare electrode of the value$148.6k\Omega$, which favors the use of the polymer to record from neural populations, as will be shown in the next chapter.

Chapter Five

Chapter V

In Vitro Assessment of pPy/PSS Biocompatibility and Recording of Neural Activity

5.1 Chapter Overview

In the previous chapter, electropolymerization of conducting polymer pPy/PSS was presented and physico-chemical studies on the polymer surface were performed. This chapter presents *in vitro* assays on the biocompatibility of polypyrrole polymer and the potential for electrode/tissue interface modifications. As explained in the previous chapter, three different forms of the pPy/PSS are studied. Here, the biocompatibility of these three forms is assessed for different biological tissues. First, human neuroblastoma cells are cultured on the oxidized pPy^{n+}/PSS^{n-} or the reduced, $pPy/PSS^{n-}(Na^+)_n$ or $pPy/PSS^{n-}(K^+)_n$, forms. Then, cultures from hippocampal neuron cells and glial cells are assessed on the three materials. The chapter ends by presenting an *in vitro* assessment on the potential of conducting polymer polypyrrole as electrophysiological probe to detect bioelectric signals from neural activities.

5.2 Neuroblastoma Cells Biocompatibility

Following the procedure explained in chapter three for neuroblastoma culturing, neuroblastoma (NB) cells were cultured on the surface of pPy/PSS coated ITO substrates. Cellular division and polymer biocompatibility were monitored and assessed by means of optical and fluorescence microscopy.

5.2.1 Optical Microscopy

The division of neuroblastoma cells was followed by optical microscopy. Figure (5-1) shows neuroblastoma cultures on pPy/PSS oxidized films. Images were taken at different times after plating, ranging from day 2 *in vitro* (day *in vitro* DIV) labelled DIV2 and 5, 7, 9, 12, 14 and 15 days (ahead DIV2, DIV5, DIV7, DIV9, DIV12, DIV14 and DIV15, respectively). Images were taken from the same electrode site each time, so images can be used for the comparison of NB cellular division. Neuroblastoma cells were also cultured on the reduced pPy/PSS (Na^+ or K^+) materials and the results shown in figure (5-3). NB cellular division was continuously monitored until confluence was reached on the day 15 *in vitro* (DIV15).
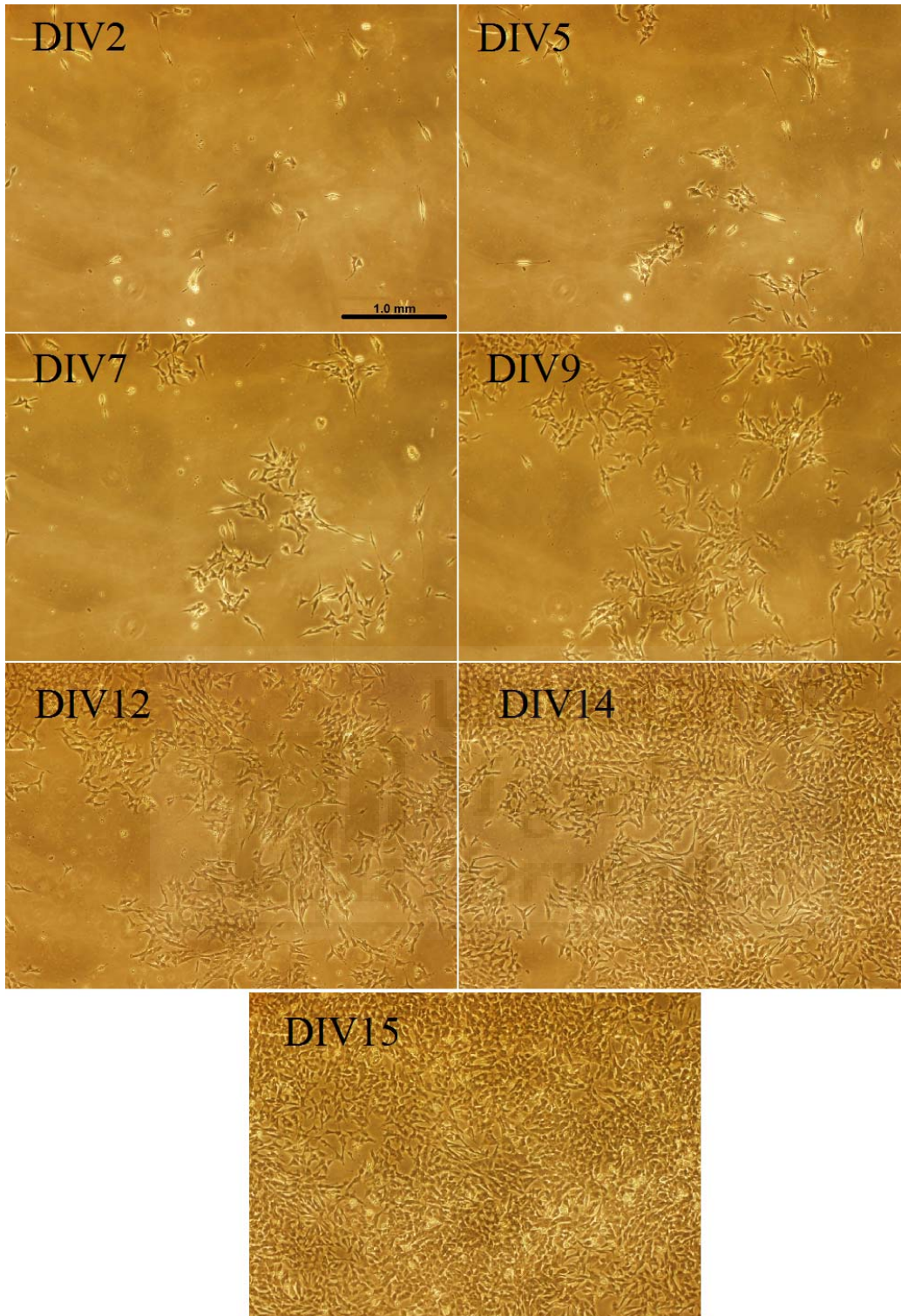
Figure (5-1): Neuroblastoma cell growth on conducting polymer surfaces.

Images following neuroblastoma cellular division on the oxidized pPy/PSS film until confluence was reached (images were taken from the same area which was localized with markers on the culture plate); DIV2, 5, 7, 9, 12, 14 and 15 correspond to the different days in vitro (DIV).

Scale = 1mm.

The cellular growth function was calculated using these images by counting the cells for each development day in each image. Cellular counting was performed by means of the cell-counting Plug-in for the public domain java image processing software imageJ (Rasband 2012, Abràmoff *et al* 2004). For data processing, each image was divided into 20 equal squares and the number of cells was counted in each one obtaining the mean value. The growth function of NB cells was found to be a logistic function behaviour in which the cell division starts exponentially until it reaches saturation when cells reach confluence, as shown in figure (5-2).
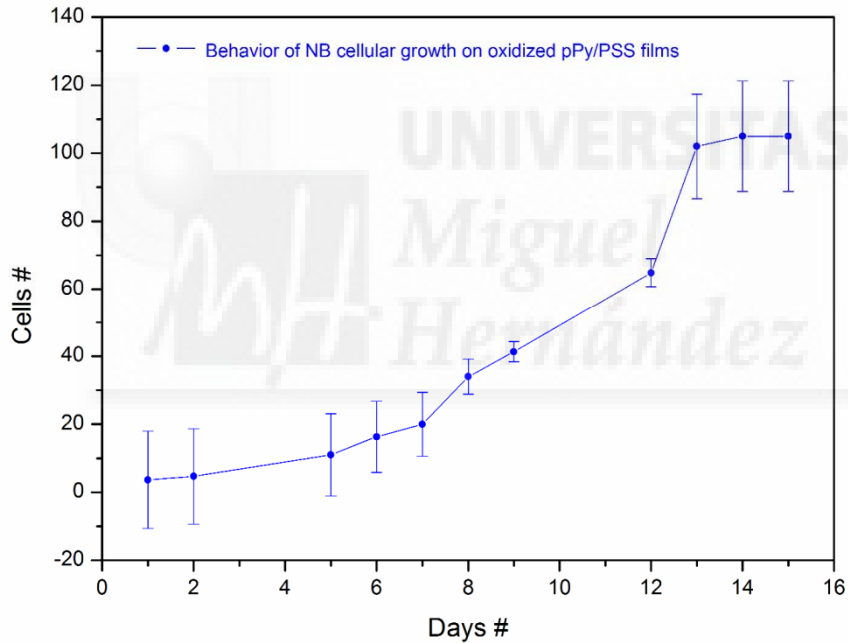
Figure (5-2): Behaviour of neuroblastoma cellular growth on oxidized form of pPy/PSS conducting polymer surfaces. The growth function is found to be a logistic function behaviour in which cellular division starts exponentially until it reaches saturation when cells reach confluence.
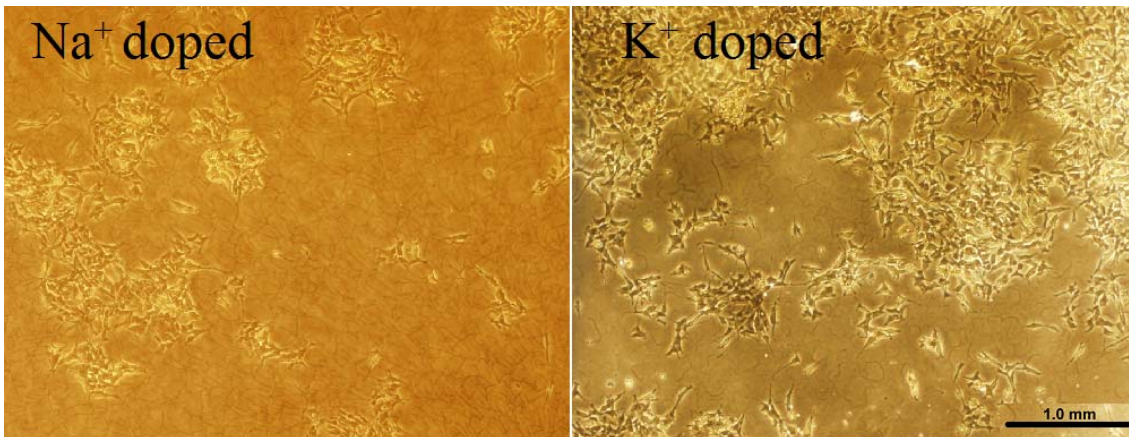
Figure (5-3): Neuroblastoma cell growth on conducting polymer surfaces.

Images following neuroblastoma cells division on the reduced pPy/PSS film, saturated with Na^+ ions (left image) or K^+ ions (right image). The graph shows images on DIV9.

Scale = 1mm.
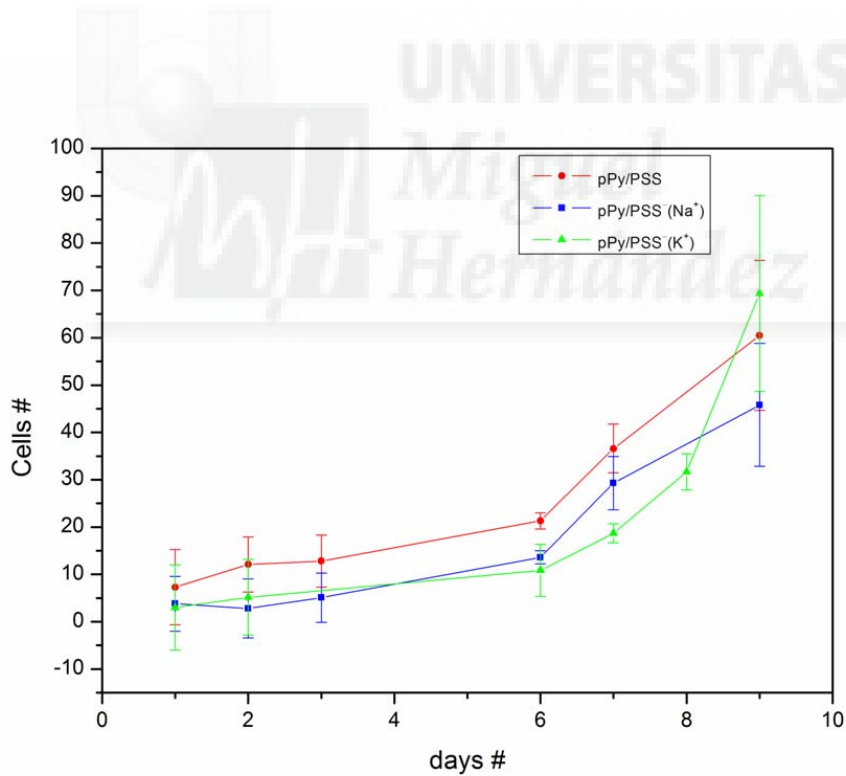
Figure (5-4): Comparison of neuroblastoma cell proliferation on the different studied pPy/PSS films. Oxidized (pPy^{n+}/PSS^{n-}) or reduced $pPy/PSS^{n-}(K^+)_n$ or $pPy/PSS^{n-}(Na^+)_n$ materials. Cellular division was plotted as number of cells vs. days *in vitro*. As seen the three polymer forms show almost the same behaviour of good biocompatibility with some preference to the oxidized form (pPy^{n+}/PSS^{n-}).

Having all the data of cellular growth, for NB on oxidized or reduced (Na^+ or K^+) films, the division of NB cells cultured on oxidized pPy/PSS films was compared to that on the reduced films. Reduced films are those which had been doped with sodium or potassium ions. The graph of cell division in figure (5-4) shows that the cells divide slightly faster on the surface of oxidized films in comparison to the pPy/PSS films doped with sodium ions or potassium ions.

Taking into account the different chemical nature of oxidized and reduced materials, a different biocompatibility could be expected from each one. In this way three different materials were obtained by stopping the potential sweep, during potential cycling, at the anodic potential limit (oxidized material, pPy^{n+}/PSS^{n-}) or by stopping the potential sweep at the cathodic potential limit in sodium or potassium salt solutions [$pPy/PSS^{n-}(Na^+)_n$ and $pPy/PSS^{n-}(K^+)_n$], respectively. However, these results indicate that both oxidized pPy^{n+}/PSS^{n-} and reduced, $pPy/PSS^{n-}(Na^+)_n$ or $pPy/PSS^{n-}(K^+)_n$, films present good biocompatibility for the proliferation of neuroblastoma cells with a slight preference for oxidized material. This slight difference can be due to the fact that the surface of the oxidized material is free of cations and the surface of the reduced materials is saturated with Na^+ or K^+ ions.

5.2.2 Fluorescence Microscopy

Having the oxidized surface more favourable for cellular growth, and in order to assess the cell health in a different way, fluorescence microscopy was used to image fixed neuroblastoma cells grown on the oxidized polymer coated ITO substrates. Cells were fixed and stained for the nuclear marker DAPI and cytoskeletal marker microtubule associated protein b (MAP2b) on DIV11 a few days before reaching

confluence. These results show a good proliferation of the cells, that means a good biocompatibility of the polymer surface. NB cells proliferate in good health with high compatibility on the studied surfaces, as shown in figure (5-5).

Figure (5-5) shows fluorescence images of neuroblastoma cells for cultures on age of DIV11. Images show healthy neuroblastoma cells grown on polymeric substrates. Cells were fixed and stained using the nuclear stain DAPI (blue coloured nuclei) and the cytoskeleton marker MAP2b (red coloured cytoskeleton). Image on the right of the figure is a merge of both markers.
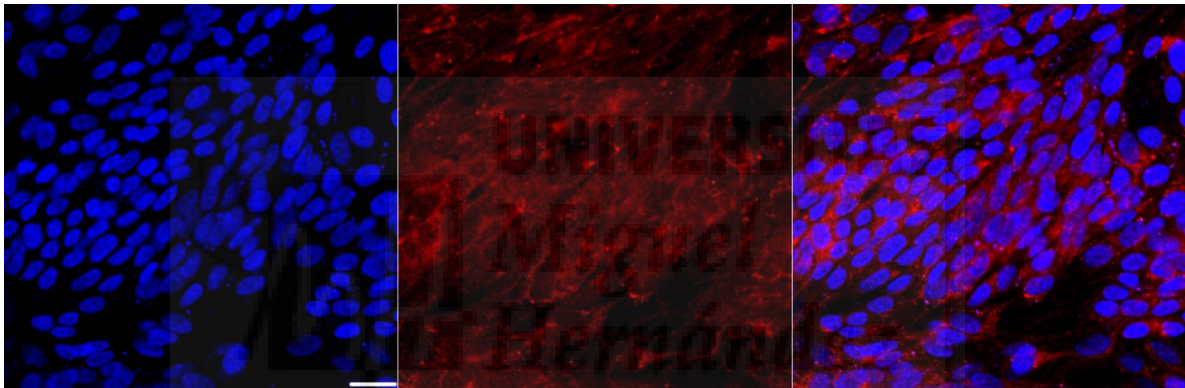
Figure (5-5): Fluorescence images of neuroblastoma cellular nucleus for cultures on DIV11.

Images show healthy neuroblastoma cells grown on polymeric substrates. Cells were fixed and stained using the nuclear stain DAPI (left) and the cytoskeleton marker MAP2b (middle). Right image is a merge of both markers.

Scale = 100 microns.

5.3 Hippocampal Neural Cells Biocompatibility

Since the proliferation of neuroblastoma cells is compatible with the polymer films, a more demanding post mitotic neural tissue was cultured. Embryonic hippocampal neurons were chosen. Having the neuroblastoma cell growth more compatible with the oxidized polymer films, then, hippocampal neurons were cultured on the oxidized materials. By using the oxidized material to culture hippocampal neurons the cells were grown on the oxidized material either without or with application of chronically electrical stimulation using biphasic potential waves. The stimulation was initiated after two days of growth, on DIV2, using consecutive biphasic, anodic first, potential pulses, as introduced in section 2.5 and shown schematically in figure (5-6).
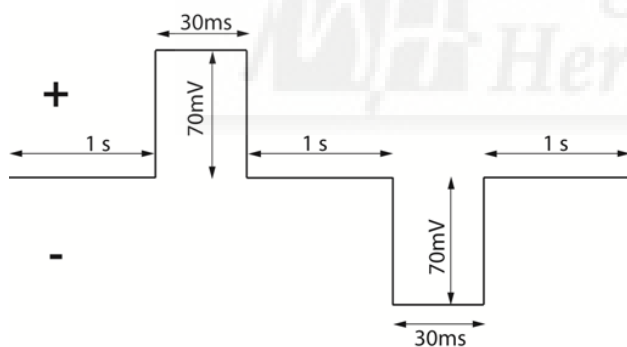
Figure (5-6): Schematic representation (potential vs. time) of the biphasic (anodic first) pulse used for *in vitro* stimulation of neuronal cultures on pPy/PSS. The pulse amplitude was of 70 mV, the phase interval was 30 ms and inter-phase interval was 1s.

5.3.1 Optical Microscopy

Cultures were followed at developmental day 2 and 13 time points by optical microscopy. Having neurons moving and growing continuously with fast variations of cellular morphology, then cell counting is not possible because it is not possible to follow neurons in the same site in the culture, unlike the case of NB cells. Therefore, optical images were not taken every day and just two of them at DIV 2 and 13 were taken, regardless of the site, just to check the cellular health. Optical images show a neat neural structure with cellular bodies and processes interconnected in an amazing network. Figure (5-7) shows two images for neural culture, images were taken on DIV2 and 13. Images show healthy hippocampal neurons grown on the oxidized pPy/PSS conducting polymer film.
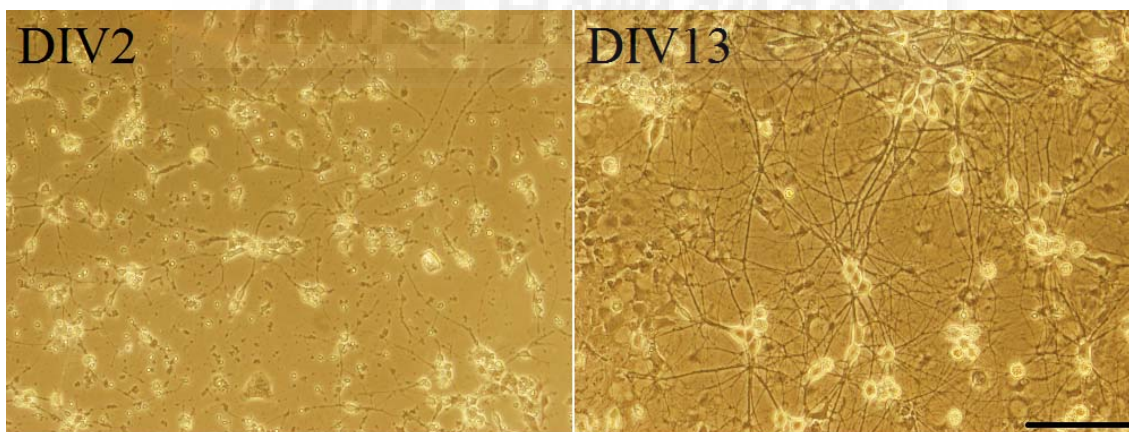
Figure (5-7): Images show healthy hippocampal neurons grown on the oxidized pPy/PSS films. The left image is taken on DIV2 and the right images on DIV13 for the same culture plate.

Scale = 100 micron

5.3.2 Fluorescence Microscopy

Cultures of hippocampal neurons were imaged by fluorescence microscopy. Cultures were fixed and stained with MAP2b for distinct dendritic processes (red coloured process in figure (5-8)) as well as with neurofilament cytoskeleton marker for marking axons (green coloured process in figure (5-8)). Figure (5-8) shows the fluorescence images for fixed and stained hippocampal cultures on DIV 13. Figure (5-8-A) shows three different neighbour zones for the non-stimulated developed DIV13 hippocampal neural culture. Images for the chronically stimulated culture are shown in figure (5-8-B). In case of chronic electrical stimulation, images were taken in three neighbour zones and show that the chronically applied stimulus did not affect the neural growth.

Our results of optical and Fluorescence microscopy demonstrate that conducting polymer polypyrrole is a great surface for cellular attachment. However, cell attachment to conducting polymers has been shown to be improved by the addition of fibronectins fragments (Cui *et al* 2001), laminin peptides (Green *et al* 2010) and neurotrophic factors (Thompson *et al* 2006, 2010).
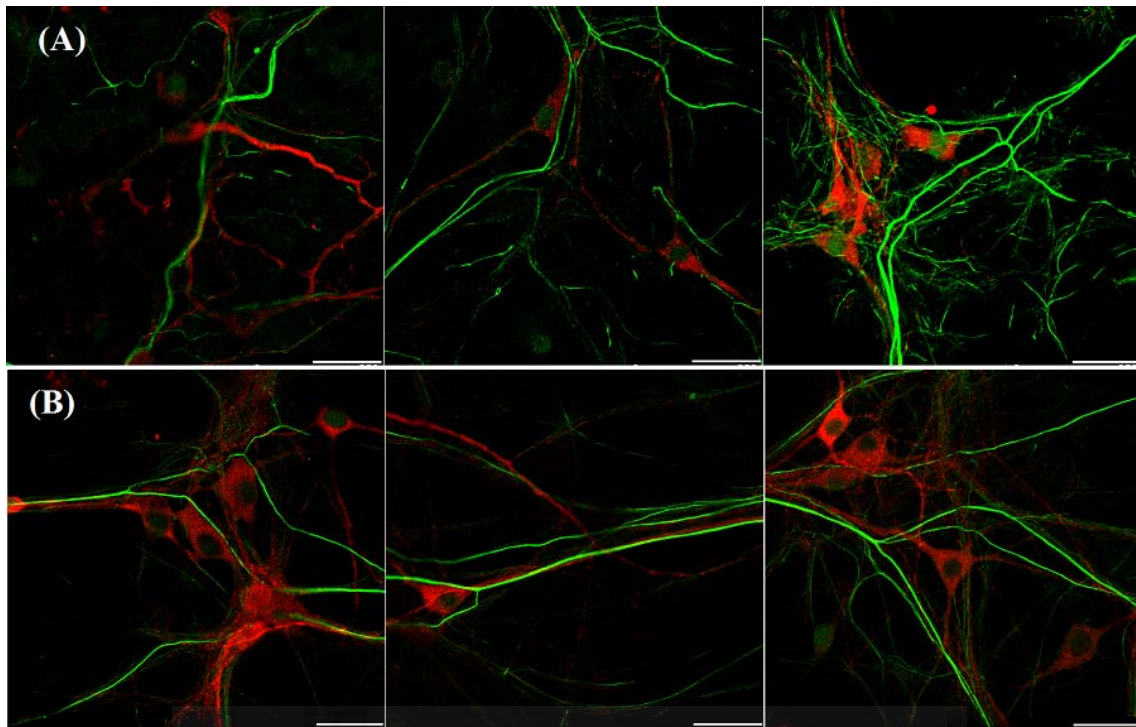
Figure (5-8): Fluorescence microscopy for hippocampal neurons grown on oxidized pPy/PSS films. In the images: The red color marks the cytoskeleton and the dendritic arborizations. The green color marks the axonal processes. Fluorescence imaging is a further assessment for cellular health of the cells grown on polypyrrole surfaces.

(A) Images from three neighbor zones for none stimulated culture.
(B) Images from three neighbor zone in chronically electric field stimulated cultures.

Scale = 100 microns.

5.4 Neuroglial Cells Biocompatibility

Hippocampal neurons' health is dependent on a layer of supportive glial cells which take part in supplying nutrients and oxygen, destroy pathogens and remove apoptotic neurons as well as take part in modulating neurotransmission and plasticity (Auld and Robitaille 2003). Figure (5-9) shows glial cells, cultured on the oxidized polymer films, fixed and stained with the glial marker GFAP on DIV28. The images show a good biocompatibility and proliferation. Results prove that mature glial cells have demonstrated a good adherence to the polymer films. The extending intricate processes onto the surface indicate good biocompatibility between glial cells and the polymeric substrate.
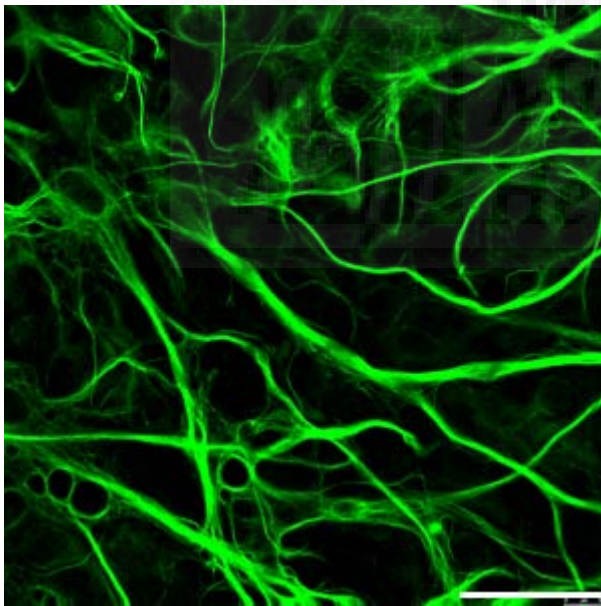
Figure (5-9): Mature glial cells on oxidized film. GFAP staining for neuroglial cells on DIV 28 grown on oxidized pPy/PPS

Scale = 100 microns.

5.5 Bioelectric Signals Recording using pPy/PSS Microelectrodes

In the previous sections, the biocompatibility of conducting polymer polypyrrole pPy/PSS was assessed favorably. Next step was to assess the potential of polypyrrole as neural probe for recording bioelectric signals, or nerve activity, from neural populations. For that purpose, multielectrode arrays were used. Microelectrodes in the multielectrode arrays (MEA) are widely used for *in vitro* recording and stimulation of nerve activity from neural populations (Thiébaud *et al* 1999, Morin *et al* 2005, Johnstone *et al* 2010, Quintero *et al* 2011, Charkhkar *et al* 2012). Hence, electropolymerization of pPy/PSS on randomly selected TiN microelectrodes was performed as explained in section (4.3).

5.5.1 Neural Activity Recording

The MEA plates, which contain polymer modified and bare microelectrodes, were used to culture primary hippocampal neurons. On the developmental day 13, on DIV13, the spontaneous activities of the neuronal populations were recorded. The activity was followed in 10 minutes epochs every 2 or 3 days, until day 20 of culture, by choosing different combinations. Here, we recorded from cells on DIV13 until 20 when synaptogenesis is beginning to plateau and synapses are beginning to refine and mature (Kay *et al* 2011). In all recording days the recording microelectrodes were always the same. All the MEA microelectrodes are labeled for polymer coated and uncoated microelectrodes. Recorded neural activity is known as spikes. Threshold detection for spikes was taken at 5 standard degrees of deviation from the baseline (Lewicki 1998).

5.5.2 Offline Classifications of Neural Activity

Offline classification for sorting different spike populations was performed using the Neural Sorter software which has been custom modified (Sierra and Sanchez 2011). Figure (5-10) shows neural activity spikes recorded from one selected microelectrode for both TiN bare or polymer-modified. In both cases activity was detected, then offline spike sorting was performed. This revealed that both type of microelectrodes were registering activity from two or more different neurons. Figure (5-10: A - D) illustrates examples from coated and uncoated electrode recordings at various developmental time points from DIV 13 to DIV 20. The figures show spike sorting of activity recorded from the same bare (left) and polymer modified (right) microelectrodes. Spikes belonging to distinct neurons are color coded. As seen in figure (5-10: A-C), the bare microelectrode detected spikes from only two different neurons (color coded red and green). While polymer modified microelectrode was able to detect spikes from three different neurons (colored, red, green and blue). This increased number of detected neurons can be due to the higher geometrical surface area of the modified microelectrode due to the presence of the polymer. It also can be due to the lower electrical impedance of the polymeric electrode. It also can be due to the fact that as the cells are more developed the detected signal is higher which reflects the longevity of the polymer surface that doesn't evoke any signal loose due to the time course. These results demonstrate that the recording quality of polymer coated microelectrodes is comparable to, and even better than, that of bare microelectrodes sufficient to make out distinct spike populations.
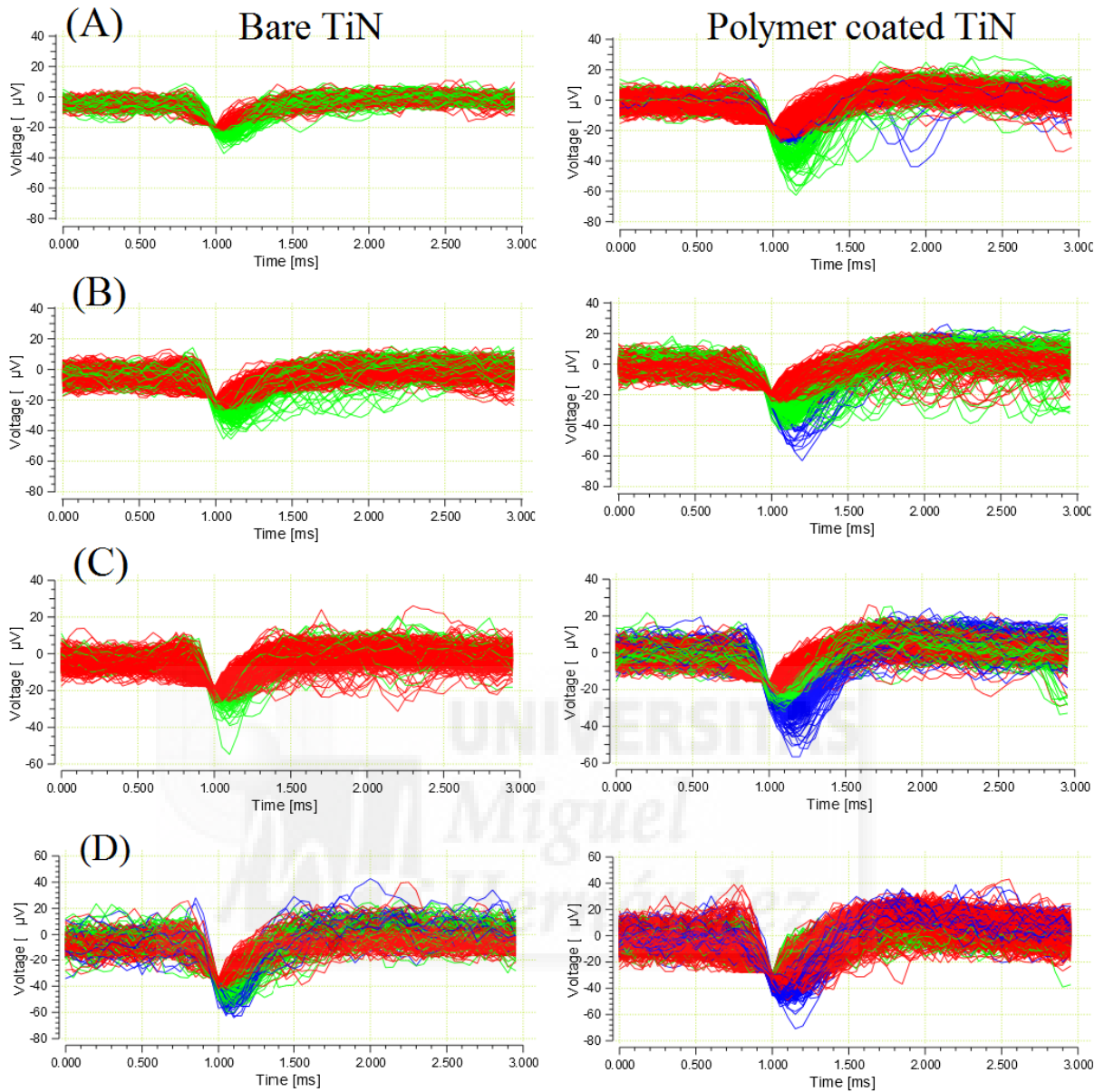
Figure (5-10): Spike sorting of activity recorded from the same (over different developmental days), bare (left) and polypyrrole coated (right), TiN microelectrodes recorded on DIV 13 (A), 15 (B), 17 (C) and 20 (D).

Spikes belonging to distinct neurons are color coded. Amplitude of spikes denoted in μV is plotted vs. time in ms.

Quantitatively speaking, in case of polypyrrole coated microelectrodes the detected signal amplitude value was higher than the case of bare microelectrodes. Table (5-1) represents the values of the signal width in both polypyrrole coated and uncoated microelectrodes, in each developmental day. The data presented in table (5-1) are the mean value for three different experiments obtained from two different electrodes each time.

DIV #	Signal amplitude (μV) Bare microelectrode	Signal amplitude (μV) Polypyrrole coated microelectrode
13	15	25
15	22	29
17	25	31
20	31	39

Table (5-1): Presents values for the detected signal in both uncoated and polypyrrole coated microelectrodes. Column 1 represents the number of days *in vitro* (DIV #), column 2 the signal amplitude in (μV) in case of uncoated microelectrode and column 3 the signal amplitude in (μV) in case of polypyrrole coated microelectrode.

These results demonstrate that the use of polymer coatings on neural interfacing electrodes does not interfere with recording of electrical activity and serves as promising alternatives to the issues faced by metal based electrodes during chronic recording and stimulations in neuroprosthetic devices. In addition, and based on our cyclic voltammetry results presented in section (4-4), the polymer can be used to store and release anti-inflammatory drugs such as dexamethasone (Thompson *et al* 2006). Moreover, conducting polymers can be doped with a variety of ions, biomolecules and neuromodulators which can be released upon electrical stimulation (Wadhwa *et al* 2006, George *et al* 2006). This property will undoubtedly have profound implications on how the polymer will be applied in biomedical interfaces. In essence, the coatings of metal electrodes can be customized to facilitate different experimental needs.

5.6 Conclusions

The electrochemically synthesized conducting polymer polypyrrole (pPy/PSS), both oxidized and reduced forms, has shown great biocompatibility for human neuroblastoma cells as well as for primary cultures of hippocampal neurons and neuroglial cells. Biocompatibility was assessed to be good even under the application of chronic stimulation on cells while growth. The pPy/PSS was deposited on randomly selected titanium nitride (TiN) microelectrodes on multielectrode array MEA plates. As shown in the previous chapter, impedance spectroscopy analysis obtained from the MEA microelectrodes showed lower values of the impedance, over the full frequency range, from coated microelectrodes compared with those obtained from uncoated (standard) microelectrodes. In this chapter, both coated and uncoated microelectrodes are good sensors of the spontaneous electrical activity of developed neuronal cultures. We can easily distinguish clearly distinct spike populations at each developmental time point in both bare (standard) and modified (polypyrrole coated) microelectrodes (Fig. 5-10).

Chapter Six

Chapter VI

Digital Holographic Microscopy:

A New Paradigm for Matter Probing and Biological Imaging

6.1 Chapter Overview

Light probing of matter is the most sensitive and gentle method that allows imaging accuracy, with high resolution, down to nanometric scale. This chapter presents a new paradigm for matter probing using light: Digital Holographic Microscopy (DHM). The chapter starts with an introduction to optical interferometry. It then introduces the "state of the art" in wave front splitting interferometry called digital holographic microscopy (DHM). Working principle of DHM and the technology associated to it.
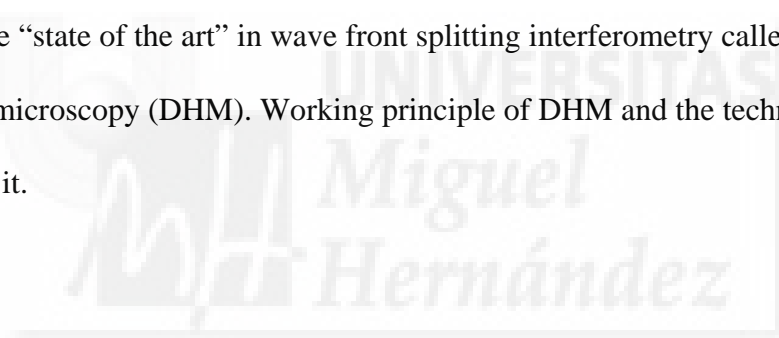
6.2 Optical Interferometry

Optical interferometry is a technique based on employing monochromatic light waves for probing objects. It is based on photoelectric imaging in which light waves transmitted from an object are detected electrically by means of a detector sensitive to light waves (photoelectric detector). In interferometry, fringe pattern (that carries the information about the studied object) is obtained by the constructive interference of two light waves. Light source emits a monochromatic wave that splits by a beam splitter into two light waves. One wave scattered from the object called the object wave (O), constructively interferes with another wave called reference wave (R). Figure (6-1) represents a schematic drawing for the optical configuration of light interferometer.
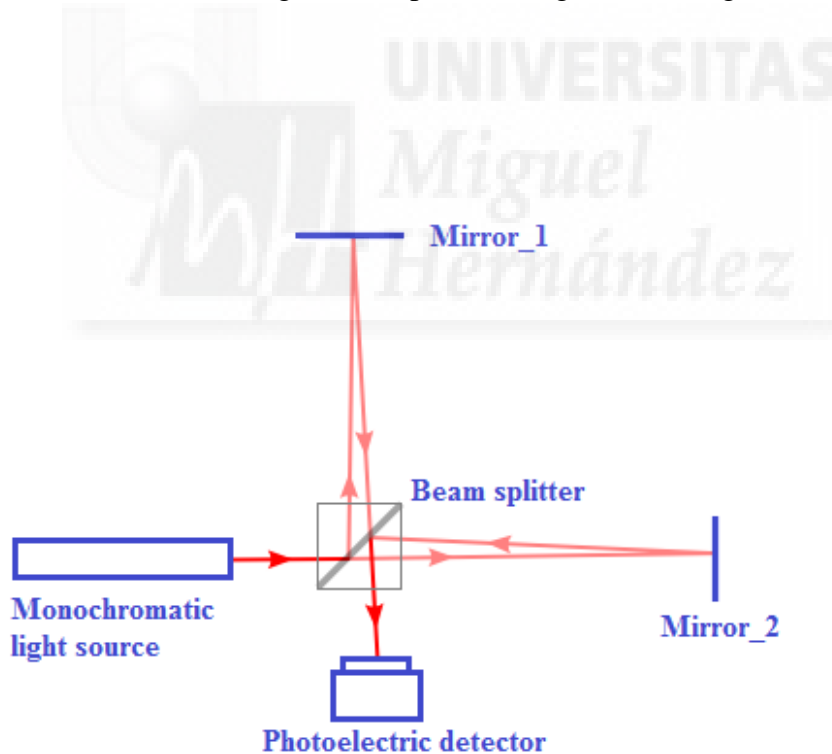
Figure (6-1): Schematic drawing for the basic optical configuration of light interferometry. Light source emits a monochromatic coherent wave that passes through a semi-silvered mirror, or beam splitter, then it reconstructed by a set of two mirrors. The reconstructed wave is detected using special detector.

On the other hand, holographic microscopy is a type of wave-front splitting interferometry. In wave-front splitting interferometry, a beam splitter (or half-silvered mirror) splits a light wave into two waves, one is the reference wave and the other is the object wave that carries all the information of the object under study. The principal mechanism of holographic microscopy is the formation of monochromatic interference fringes between the reference wave and the object wave (Nolte 2011, Hariharan 2010). Holographic microscopy was invented by Gabor in 1948 when he had the idea of correcting and improving image quality in electron microscopy by optical means (Gabor 1948). The word hologram is derived from the Greek word '*holo*' means 'whole' which means the whole information is presented, and is defined as the recorded interference pattern between the scattered beam from the object (object wave) and the reference beam (the coherent background) (Gabor 1972).

Moreover, thanks to technological developments and high performance computational techniques, Gabor holographic microscopy has evolved to digital holographic microscopy (DHM) conserving its fundamental bases and having the amazing advantages of digital processing (Schnars and Jüptner 1994). Digital holographic microscopy is a noninvasive technique, and it offers real time 3D imaging with high resolution in both lateral and vertical directions.

6.3 Working Principle of DHM

The optical configuration of digital holographic microscopy is based on Mach-Zehnder interferometer configuration, figure (6-1). The construction pattern, that carries all the information of the studied object, is detected using a charge-coupled device (CCD) camera and then reordered digitally in a hologram (Marquet *et al* 2005). CCD camera is used in digital imaging and is able to convert light photons into electricity, photoelectric device. The hologram is numerically reconstructed based on the amplitude and phase of the incident light wave (Cuche *et al* 1999c).

DHM allows measuring the phase shift in the wavelength, or optical path-difference length (OPL), originated from the difference in refractive index (RI) between the specimen and the surrounding medium (Depeursinge *et al* 2007). It provides short acquisition time and fast measurement acquisition rate that enables quantitative phase difference mapping and dynamical analysis. It offers 3D real time monitoring of the studied object with high resolution.

Figure (6-2) represents schematic drawing for the optical configuration of a reflection configured digital holographic microscope employed in this study. The configuration is modified from a Mach-Zehnder interferometer (Marquet *et al* 2005).
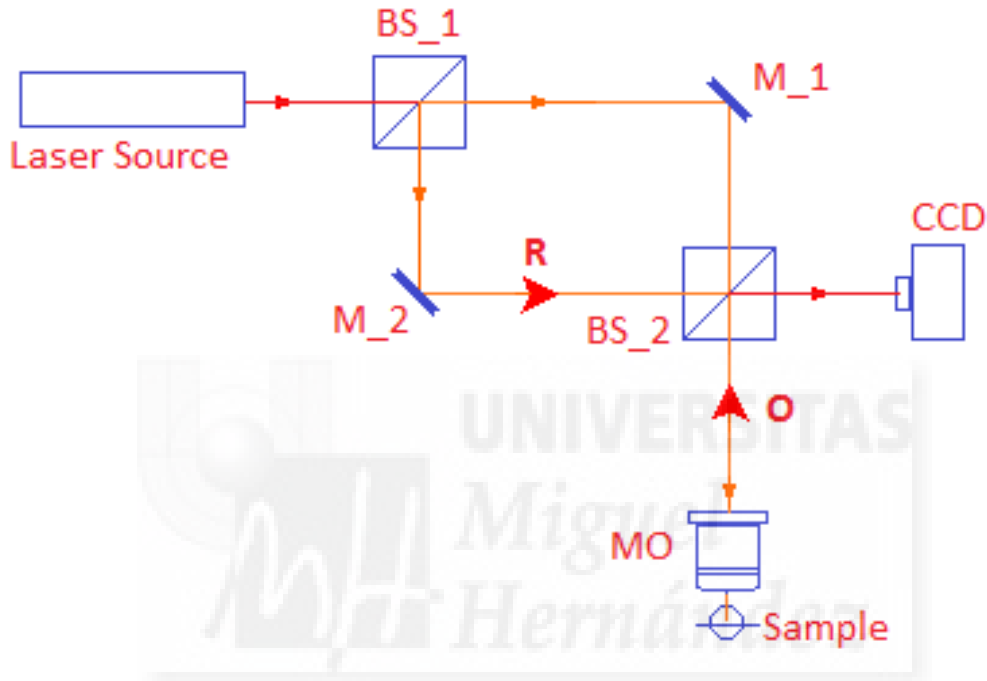
Figure (6-2): Schematic configuration of reflection configured digital holographic microscope. Optical components are: Monochromatic Light (Laser Source), Beam Splitter (BS_1 and BS_2), Mirror (M_1 and M_2), Microscope Objective (MO) and Photoelectric Detector (Charged Coupled Device CCD). Beam splitter BS_1 splits the light wave into reference wave (R) and object wave (O). Object wave carries the information of the sample via the MO. Beam splitter BS_2 reconstructs the two, R and O, waves and the CCD camera records the hologram.

It consists of a laser source that emits a monochromatic light wave through the beam splitter BS_1 that splits the light wave into two waves. One is considered the coherent background reference wave (R) and the other is used via microscope objective (MO) to probe the sample, the object wave (O). The object wave is transmitted back from the sample and is reconstructed together with the reference wave forming the fringe pattern. The fringe pattern is digitally detected by photoelectric detector, CCD. The detected pattern is then numerically reconstructed as a hologram using powerful computer software (Cuche *et al* 1999b). Once recorded, the hologram contains all the data of the sample and can be reconstructed for offline use.

Practically, the phase shift difference or the optical path-length OPL signal provides quantitative information about the physical aspects and dynamical morphologies of the studied object. OPL is proportional to the thickness d of the observed specimen which means that a higher specimen thickness corresponds to a higher phase shift and vice versa (Cuche *et al* 1999a). The phase shift value Φ is related to the optical path length difference (OPL) and can, thus, be expressed as:

$$\Phi = \frac{4\pi}{\lambda} OPL = \frac{4\pi}{\lambda} (n_s - n_m)\, d(x, y) \qquad \text{(a)}$$

since, $$OPL = (n_s - n_m)\, d(x, y) \qquad \text{(b)}$$ (6-1)

then, $$\Phi = \frac{4\pi}{\lambda} (n_s - n_m)\, d(x, y) \qquad \text{(c)}$$

Where, λ is the wavelength of the illuminated light, n_m is the RI of the surrounding medium, n_s is the RI of the specimen and d is the thickness of the specimen at the position (x, y) in the full-field view.

The thickness as a function of the position $d(x, y)$ means that the specimen's physical attributes or morphological changes depend on the focal plane in which the measurements are performed. Digital holographic microscope adjusts its focal plane in relation to the changes in the morphology and dynamics of the studied object.

Thanks to the potential of numerical calculation of digital holographic microscope, morphometric characteristics can easily be calculated. The measured value of optical path length (OPL) and the refractive index (RI) of the studied object n_s and its surrounding medium n_m are related together with the value of the thickness d as (from equation (6-1:b)):

$$d = \frac{OPL}{(n_s - n_m)} \tag{6-2}$$

The digital hologram that contains all the specimen's characteristics is recorded as interference patterns from the constructive interference between the object wave and the coherent background reference wave (Reese *et al* 2009).

6.4 DHM Microscope Information

As shown in figure (6-2), in digital holography a monochromatic light source is employed. In this study, the reflection configured digital holographic microscope (Lyncée tech DHM-DHM R2000) works by illuminating samples with a diode laser source (wavelength $\lambda = 683$ nm) linearly polarized in a modified Mach-Zehnder interferometer with an off-axis geometry configuration. Off-axis geometry means that the reference wave reaches the detection device with a small incidence angle with respect to the propagation direction of the object wave. The microscope objective (MO) magnifies the image of the sample using the scattered wave from the sample (called object wave). The object wave then interferes constructively with the reference wave building the fringes pattern. The photoelectric sensor, called charged coupled device, (CCD) camera records the construction pattern and builds the corresponding 3D digital hologram (called hologram reconstruction). Depending on the numerical aperture (NA) of the microscope objective, the lateral resolution can go down to the nanometer scale (Cuche *et al* 1999b).

6.5 Conclusions

This chapter presented an approach to the "cutting edge technology" in light interferometry, called digital holographic microscopy (DHM). DHM is a non-invasive tool for 3D imaging with high resolution and accuracy down to the nanometric scale. It is based on wave front splitting interferometry and is used for probing different objects. In this thesis, the new technology of DHM is used for microelectrode inspection and for biological imaging. DHM is able to detect the thermoelectric deformations occur in a microelectrode due to the application of external electric stimuli. On the other hand, DHM is also used for imaging of either assemblies of neural populations or single neuron. The next two chapters present experimental results on these two topics.

Chapter Seven

Chapter VII

Digital Holographic Microscopy:

A Study on Microelectrodes (either bare or polypyrrole coated) Response to

Applied Electrical Stimuli

7.1 Chapter Overview

Chapter two presented that artificial stimulation for excited tissue plays a crucial role for neuroprosthetics (Cogan 2008, Kandel *et al* 2000, Rutten 2002). On the other hand, chapters four and five presented studies on the potential of conducting polymers for coating metal based electrodes, for overcoming issues related to biocompatibility and longevity. However, chapter six introduced a new paradigm for materials' inspection and biological imaging: Digital holographic microscopy. This chapter presents studies on the use of digital holographic microscopy for monitoring microelectrodes used for *in vitro* neuroprosthesis research. The study is about detecting the thermoelectric responses, or deformations, of the microelectrode (either bare or polymer coated) to the different applied electrical stimuli. The present study evaluates the potential of conducting polymers to substitute conventional metal based electrodes for neural interfaces.

7.2 Brief Background

In electrochemical systems there are several thermoelectric processes and electrochemical interactions that occur at the site interface between metal electrode and electrolyte solution. A stimulation electrode implanted into neural tissue is considered an electrochemical system, in which neural tissue is the electrolyte solution. One important process that occurs at the site interface, between the electrode and the electrolyte, is called Redox (Reduction/Oxidation) reaction. Redox reactions need to occur in order for a charge to be transferred between electrode and electrolyte solution. The reactions can be generally represented by the equations:

$$C \rightleftharpoons C^{n+} + ne^- \qquad\qquad (7\text{-}1)$$

$$A^{m-} \rightleftharpoons A + me^- \qquad\qquad (7\text{-}2)$$

Where, n is the valence of a cation material C and m is the valence of an anion material A.

In this context, there are two kinds of currents that can cause electron transfer at the electrode/electrolyte site interface: one is Faradic currents and the other is non-Faradic currents. Faradic currents involve direct transfer of electrons via oxidation reactions at one electrode and reduction reactions at the other (or the electrolyte solution). A Faradic current requires continuous mass transfer of reactive species from the bulk of the electrolyte to the electrode surface (and vice versa). This can involve the motion of species brought about by a concentration gradient. Non-Faradic currents involve capacitative transfer of charges across the electrode and the electrolyte solution without electrochemical interactions. Thus in non-Faradic currents, electrons remain at

the electrode surface and increase the charge on the double layer causing capacitative transfer of charges (Wang 2004). Capacitative transfer of charge means that the charge is first collected on one layer (the electrode) of an electrical double layer system and when reaches a specific value it transfers to the other layer (the electrolyte).

Hence, since the conductivity in non-Faradic systems is capacitative, then non-Faradic currents are usually related to a process called local heat generation. This local heat generation is due to charge accumulation at the electrode interface of the double layer system. According to electrochemistry (Bagotsky 2005), in case of metallic electrodes the associated currents are non-Faradic. Then, in this study the currents associated to the bare metallic TiN microelectrodes are non-Faradic type and the ones associated to the polypyrrole coated microelectrodes are Faradic type.

7.2.1 Conducting polymer coated vs. uncoated metallic electrode

In the present study, titanium nitride (TiN) microelectrodes are employed and the surface of the electrode will be either bare metal or polypyrrole (pPy/PSS) conducting polymer coated. By applying an external electric current on either polymer coated or uncoated metallic electrode, there will be two mechanisms of electron injection to the electrolyte (surrounding salt solution). One is non-Faradic current injection and will occur at the bare electrode. The other is Faradic current injection and will occur at the conducting polypyrrole coated electrode. The reason for the association of Faradic currents with the conducting polymer polypyrrole coated surface is the existence of an adequate system, the conducting polymer, for redox reactions to take place.

7.3 Microelectrode Thermoelectric Variations

As presented in chapter two, artificial stimulation for excited tissue plays a crucial role for neuroprosthetics (Cogan 2008, Kandel *et al* 2000, Rutten 2002). However, the charge injection needed to evoke artificial stimulation is usually associated with a variety of electrochemical reactions (Merrill *et al* 2005). Some of these electrochemical reactions can result in damaging the stimulation electrode or the stimulated tissue. Examples can be electrolysis of water in the medium, oxidation or corrosion of electrode metal and oxidation, or reduction, of organic components of the stimulated tissue (Brummer and Turner 1977). Therefore, bioincompatibility can be referred to one of these reactions, especially if the reaction varies the pH of the medium. For the sake of stability and safety, neuroprosthesis electrodes need to be inspected and standardized. This chapter presents studies, using digital holographic microscopy, on titanium nitride (TiN) microelectrodes in MEA. The studies employed uncoated as well as pPy/PSS conducting polymer coated microelectrodes.

7.3.1 Method

According to the procedure explained in chapter six, digital holographic microscopy (DHM) was employed to study the microelectrode thermoelectric variations due to applied electrical stimuli. Using the multichannel stimulation setup together with multielectrode array (MEA), stimuli were applied on microelectrodes. The electric stimuli were applied on the MEA plate containing 2 ml of the standard Phosphate Buffered Saline (PBS) with Ca^{2+} and Mg^{2+} salt solution. PBS solution is added to close the electric circuit with respect to the reference electrode inside the MEA plate.

Stimuli were applied as cathodic/anodic biphasic pulse. The pulse duration was 250 ms with amplitudes of 25, 50, 75 and 100 µA, and the inter-pulse duration of 3s with zero applied stimuli. The stimuli were applied in burst mode up to 10 subsequent phases for each amplitude value. This stimulation criterion was chosen as it was already employed for electrophysiological studies. The 20X microscope objective was focused on the MEA microelectrode array. Here we focus on the two electrodes, polypyrrole coated and uncoated, indicated *pPy/PSS coated* and *uncoated TiN* in figure (7-1).
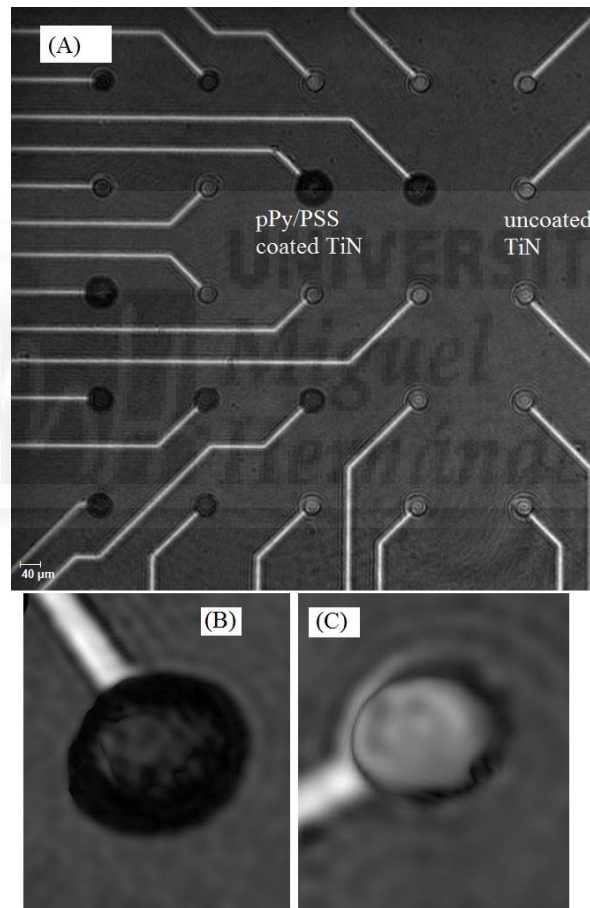
Figure (7-1): (A) Digitally reconstructed phase image that reflects the topography of MEA plate containing TiN microelectrodes. Scale = 40 µm. (B) Magnified shot for pPy/PSS coated TiN and (C) uncoated TiN.

Figure (7-1) shows digitally reconstructed hologram for the superficial phase shift difference of MEA plate containing TiN microelectrodes, one is uncoated and the other is pPy/PSS conducting polymer coated. Colors indicate the height of the topographic objects in the hologram, having the red colored objects the highest and the blue colored objects the lowest.

Holograms were digitally recorded and numerically reconstructed using powerful computer software (Cuche *et al* 1999). Data was analyzed in a plot of axial distance (in µm) on the X axis vs. the optical path length difference OPL (in nm) on the Y axis. Axial distance refers to the variations take place either on the X direction or the Y direction, and OPL corresponds to the changes in the Z direction.

7.4 Results

The following figures represent the different electrode profiles in response to the different applied electrical stimuli values of 0, 25, 50, 75 and 100 µA. Figures from (7-2) to (7-6) represent profile views for uncoated vs. polypyrrole (pPy/PSS) conducting polymer coated TiN microelectrodes. As mentioned previously, the electrode profiles are presented for OPL in (nm) vs. axial distance in (μm). In figures (7-2) to (7-6) the numbers presented on each axis are only for representing the nanometric variations detected in each profile. The numbers on the axis of (A) and (B), in each figure, are not comparable. That is because each one of the studied object has its own confocal plane adjusted by the microscope objective.

7.4.1 Working at no applied stimuli

Figure (7-2) represents the OPL profile for both bare (A) and pPy/PSS polymer coated (B) microelectrodes at no applied stimuli. This profile was taken just after connecting the MEA plate to the pulse generator, while the later was off. These profiles are considered as reference profiles for the subsequent ones with applied electrical stimuli. As the DHM microscope records the interferometric pattern of the object under study. The profiles represented here show the morphological shape of each microelectrode. The negative profile of the uncoated microelectrode, in (7-2: A), is due to the small refractive index of the centre, "well-like" shape, of the electrode with respect to the electrode borders. However, in case of the polypyrrole coated microelectrode, in (7-2: B), this "well-like" was filled with the black polypyrrole resulting in a "mountain-like" shape and higher refractive index that the microelectrode borders.
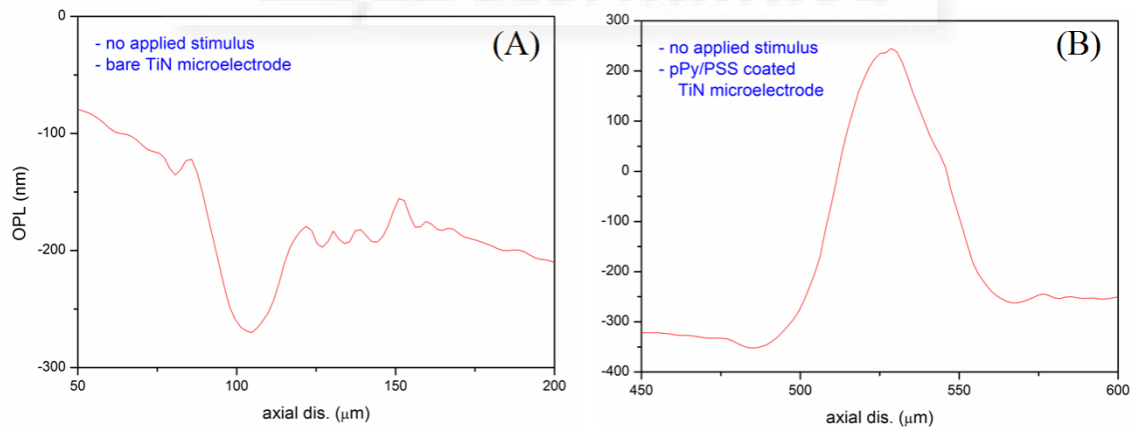
Figure (7-2): Optical path length difference (OPL) vs. axial difference, measured by dual wave length digital holographic microscope; OPL in nm and axial difference in micron. The measurements performed on microelectrode in MEA plate at no applied electric stimuli for:

(A) Bare TiN microelectrode.
(B) Polypyrrole (pPy/PSS) conducting polymer coated microelectrode.

7.4.2 At 100 µA

Consequently, a biphasic (anodic first) pulse was applied during 2ms ON for each phase and 5s inter-phase time OFF. Pulses were applied to the MEA plate microelectrodes, labeled *pPy/PSS coated* and *uncoated TiN* in figure (7-1). As shown in figure (7-3), two different profiles were recorded; one before applying any stimulus, labeled 0 µA (as represented in figure (7-2)), and the other one presented here is the mean value for ten measurement profiles recorded while applying the stimulus of 100 µA. The result shows that in the case of uncoated metal there was a big difference between the profile of the electrode before and after applying the external stimulus. This difference was calculated at the full width at half maximum of each profile peak. The difference of the optical path length (OPL) value was 261 nm in case of uncoated microelectrode and 41 nm in case of polymer coated microelectrode.
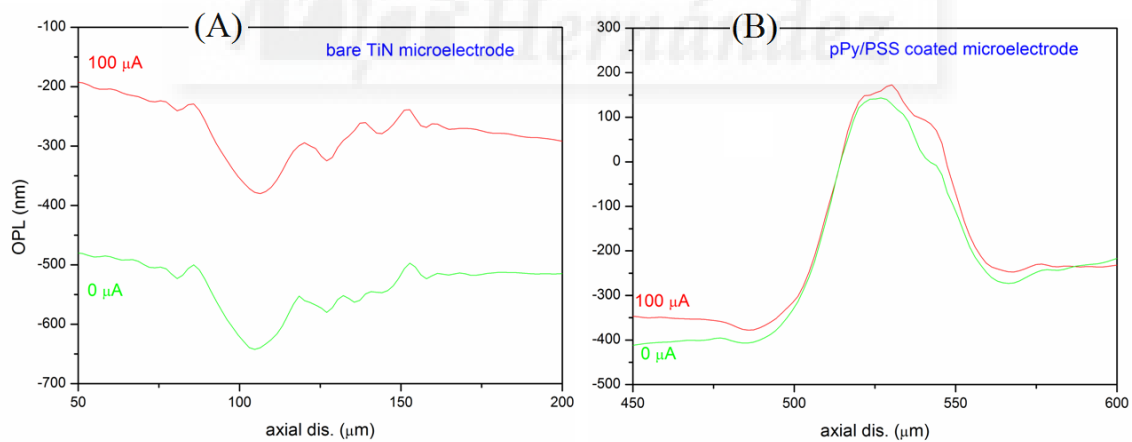
Figure (7-3): Optical path length difference (OPL) vs. axial difference, measured by dual wave length digital holographic microscope; OPL in nm and axial difference in micron. The measurements performed on microelectrode in MEA plate at 100 µA applied electric stimuli for:

(A) Bare TiN microelectrode.
(B) Polypyrrole (pPy/PSS) conducting polymer coated microelectrode.

7.4.3 At 75 µA

After having the results of 100 µA of external stimuli, the system was put at rest for 10 min and then another stimulus value of 75 µA was applied. As shown in figure (7-4), the uncoated microelectrode still suffers variations due to the applied stimulus. There was a difference in the OPL value of 206 nm in case of uncoated metal and 34 nm in case of polymer coated metal. The difference was calculated at the full width at half maximum of each profile peak.
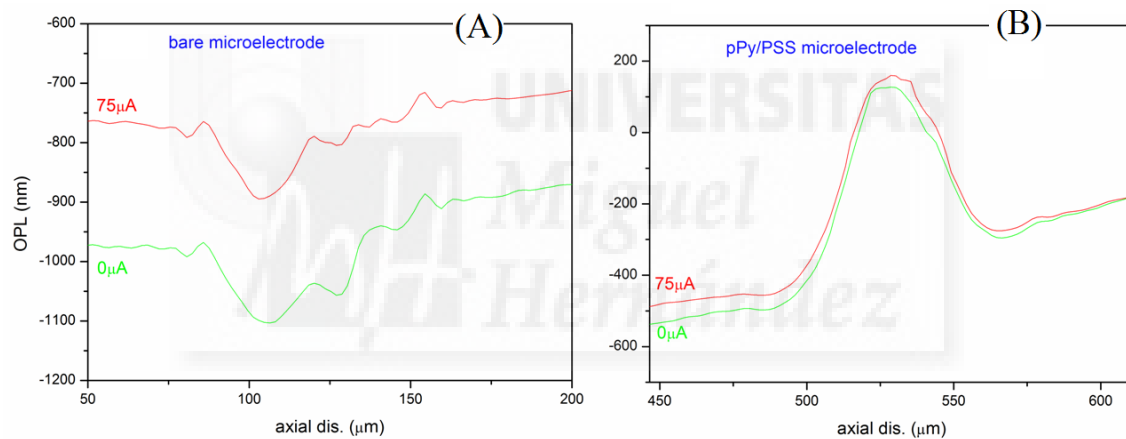
Figure (7-4): Optical path length difference (OPL) vs. axial difference, measured by dual wave length digital holographic microscope; OPL in nm and axial difference in micron. The measurements performed on microelectrode in MEA plate at 75 µA applied electric stimuli for:

(A) Bare TiN microelectrode.
(B) Polypyrrole (pPy/PSS) conducting polymer coated microelectrode.

7.4.4 At stimuli values of 50 and 25 µA

Results for 100 and 75 µA of applied stimuli show that there was a big variation in the microelectrode's profiles in the case of uncoated microelectrode than the coated one. However, in the case of lower stimuli values these variations were not so big. In case of 50 µA shown in figure (7-5) there was a difference in the OPL value of 36 nm in case of uncoated metal and 22 nm in case of polypyrrole coated metal.

In the case of 25 µA of external stimulus, shown in figure (7-6), there was a difference in the OPL value of 26 nm in case of uncoated metal and 10 nm in case of polypyrrole coated metal.

Additionally, figure (7-7) represents a comparison between the behaviour of thermoelectric variations in uncoated metallic microelectrode vs. conducting polymer polypyrrole coated microelectrode. The graph represents the differences in the OPL value in each case Δd on the Y axis vs. the value of the applied stimuli on the X axis. As mentioned previously, the profiles represented for each stimulus value are the mean value of ten different profiles measured for each microelectrode. Therefore, the difference in the OPL value Δd is considered a mean value. It is clear that the behaviour of conducting polymer polypyrrole coated microelectrode is more stable, in terms of thermoelectric variations, to an external applied stimulus than the case of uncoated metallic one.
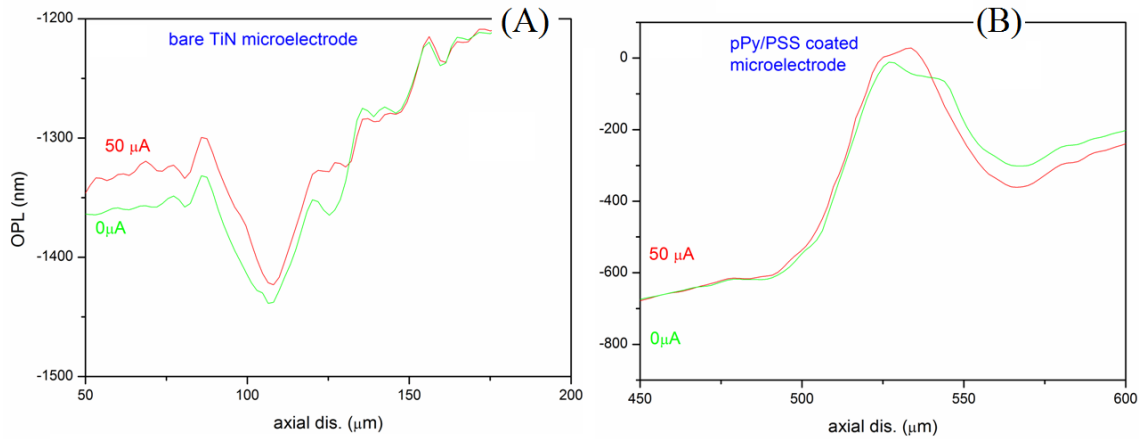
Figure (7-5): Optical path length difference (OPL) vs. axial difference, measured by dual wave length digital holographic microscope; OPL in nm and axial difference in micron. The measurements performed on microelectrode in MEA plate at 50 μA applied electric stimuli for:

(A) Bare TiN microelectrode.
(B) Polypyrrole (pPy/PSS) conducting polymer coated microelectrode.
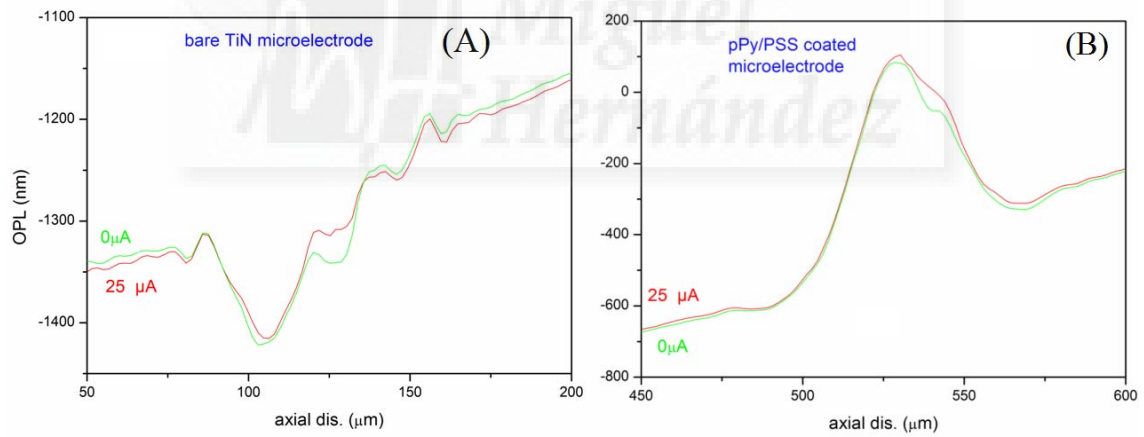
Figure (7-6): Optical path length difference (OPL) vs. axial difference, measured by dual wave length digital holographic microscope; OPL in nm and axial difference in micron. The measurements performed on microelectrode in MEA plate at 25 μA applied electric stimuli for:

(A) Bare TiN microelectrode.
(B) Polypyrrole (pPy/PSS) conducting polymer coated microelectrode.
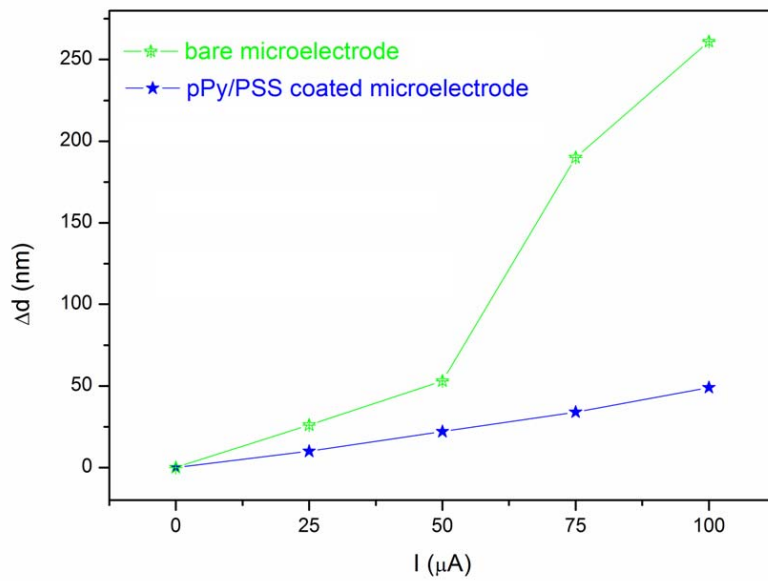
Figure (7-7): Graph represents the change in the OPL vs. the stimulus value. Comparison between the behaviour of polypyrrole coated microelectrode vs. uncoated metallic one under applied stimuli. It is clear that the behaviour of polypyrrole coated microelectrode is more stable, in terms of thermoelectric variations, to an external applied stimulus than the case of uncoated metallic one. The values of Δd correspond to the difference in the OPL and are the mean value as obtained from ten different profile measurements.

7.5 Discussions

Results presented in the previous section are discussed here in light of the background information presented in section (7.2). As planned for this study, the DHM microscope was used for real time detection of the thermoelectric changes and variations take place in microelectrodes due to an external applied stimulus. However, results show that in case of relatively higher stimulus values such as 100 μA (figure (7-3)) and 75 μA (figure (7-4)), the changes occurred in the uncoated metallic microelectrode was obvious. As noted, in case of uncoated metal, the DHM laser detected a change in the microelectrode profile, on applying the stimuli, which is considered as thermoelectric response. In comparison, the case of pPy/PSS conducting polymer this thermoelectric response was less.

In the case of bare metallic electrode, the currents associated are non-Faradic type which means that the local heat generation took place. The detected variation of the microelectrode profile was due to the detection of the heat generated due to the accumulated electronic charges, especially in the case of high current values. This is because the higher is the current value the more charge is accumulated at the electrode surface.

In the case of pPy/PSS conducting polymer coated metal, the situation is different. The associated currents are Faradic type and the redox reactions take place at the interface between the saline solution and the polymeric surface. In redox processes, a charge transfer take place between the negative charges on the electrode surface, electrons, and the cations (or anions) stored in the polymeric film, equations (7-1) and (7-2). Then these cations (or anions), in return, transfer the charge to the anions (or

cations) in the saline solution of the system. Therefore, the electron transfer is involved only to initiate the ionic conductivity between polymeric interface and surrounding saline solution. In this case, the electric current imposes not electrons but ions to leave the charged polymeric surface. Relatively, the charge accumulation in this case is much less than the case of uncoated metal electrode that means the local heat generation is less.

On the other hand, figure (7-7) reflects the thermoelectric behaviour of microelectrode, either polymer coated or bare, with respect to each applied electric stimulus. As shown in the graph, the behaviour of conducting polymer coated microelectrode is relatively more stable and homogeneous than the case of bare metallic one. These results then added to the potential of conducting polymers to substitute conventional metallic electrodes since they show more stability upon the application of electrical stimuli.

The DHM microscope resolution is down to the nanometric scale with a systematic error of 10 nm. Taking into account the experimental error that is calculated by statistical standard deviation of the set of ten measured profiles, the data can be presented. Table (7-1) presents the values of optical path length differences, OPL, for both microelectrodes in response to each applied stimuli.

Stimulus value (μA)	Bare microelectrode OPL (nm)	pPy/PSS conducting polymer coated microelectrodes OPL (nm)
100	261 ±16	41 ±12
75	206 ±15	34 ±11
50	53 ±11	22 ±11
25	26 ±11	10 ±10

Table (7-1): Different values of OPL variations in response to each applied external stimuli of the microelectrode. Column 1 presents the values of the applied stimuli in μA. Column 2 presents the values of OPL for bare metallic microelectrode. Column 3 presents the values of OPL for conducting polymer coated microelectrodes.

Errors: 10 nm systematic and the rest experimental error calculated by statistical standard deviation.

7.6 Theoretical Considerations

These results are supported by the theoretical considerations. From the theoretical point of view, the heat transfer at an interface between solid and liquid phases is governed by the heat transfer coefficient h of each material's phase. Equation (7-3) defines the heat transfer coefficient in terms of heat and temperature:

$$h = \frac{Q}{A \cdot \Delta T} \tag{7-3}$$

Where, h is the heat transfer coefficient in (W/m^2 K), Q is the amount of heat flow in (J/s), A the surface area in (m^2) and ΔT is the temperature difference between solid phase surface and the surrounding fluid area in (K).

Rearranging equation (7-3) to get the definition for temperature difference ΔT:

$$\Delta T = \frac{Q}{A \cdot h} \tag{7-4}$$

Considering equation (7-4) and taking into account that the current applied on both coated and uncoated microelectrodes was the same then the quantity Q is considered the same in both cases. According to Joule's first law, the amount of heat generated Q is proportional to electric current I. That yields the same quantity of heat Q generated by the same electric current in both, polypyrrole coated and bare microelectrode, cases. Considering that the surface area of the polypyrrole coated microelectrode A_{pPy} is higher than the one for the bare microelectrode A_{bare}. On the other hand, the thermal conductivity κ of polypyrrole is 0.2 W/mK (Avloni *et al* 2007) which is almost three times higher than the one for titanium nitride 0.07 W/mK (Pierson 1996).

Taking into account that the heat transfer coefficient h (W/m^{2}K) is related to thermal conductivity κ (W/mK) by the formula $\kappa = h \cdot l$, since l is the length of the conductor. However, having the thermal conductivity value of polypyrrole higher than of titanium nitride, and having the geometrical dimensions of polypyrrole coated microelectrode higher than the one for the titanium nitride microelectrodes. Then the value of heat transfer coefficient of polypyrrole must be higher than of titanium nitride.

Substituting into equation (7-4) with the following parameters:

- Same Q for both cases due to the application of the same electric current.
- Heat transfer coefficient is 3 times higher in case of polypyrrole than in case of bare titanium nitride.
- Geometrical surface area of polypyrrole higher than the one of titanium nitride.

Having the parameters h and A in the denominator, and the same value for the parameter Q in the numerator of the equation, then the higher the denominator the lesser the value of ΔT and vice versa. That means that the temperature difference in the case of conducting polymer polypyrrole is at least three times lesser than the case of bare titanium nitride.

These theoretical considerations are in agreement with the experimental resulted detected by the digital holographic microscope technique.

7.7 Conclusions

In conclusion, the recently invented digital holographic microscopy DHM was employed here to detect the thermoelectric variations that occur in microelectrodes. The DHM technique is a powerful method to detect in real time the variations occur in stimulation microelectrodes due to the applied electric stimuli. The technique can be presented as standardization method to evaluate neural interfaces.

The results show that in case of bare metallic microelectrodes there was a difference of 261 nm of change due to the application of electrical stimuli up to 100 μA. In comparison, in the case of pPy/PSS conducting polymer coated microelectrodes, this difference was only 41 nm of change due to the application of electrical stimuli up to 100 μA. These numbers correspond to the differences in the optical path length detected by digital holographic microscope, and their value lies in showing the detected variations.

The present results, as shown in figure (7-7), reflect the relative instability of the bare metallic microelectrode in comparison to the pPy/PSS conducting polymer coated one. However, the conducting polymer coated microelectrode seems to be more stable to the different applied stimuli and it shows more homogeneous behaviour. This is because the less generated heat (due to the applied electric current) in the case of conducting polymer interfacing than the case of bare metallic interfacing. The use of digital holographic microscopy, to assess the microelectrode behaviour in response to externally applied electric stimuli, can be a powerful method. This study presents evidence and adds value to the potential of conducting polymers to substitute conventional (standard) metallic electrodes for neural interfaces.

Chapter Eight

Chapter VIII

Digital Holographic Microscopy:

Dynamics and Morphometric Studies on Neural Cells

8.1 Chapter Overview

Chapters six and seven reported on the recently discovered powerful imaging technique based on light interferometry, called digital holographic microscopy DHM. DHM was emerged as 3D real time and noninvasive imaging technique. In chapter seven, studies were presented on the power of DHM technique to detect the effect of electric current application on stimulation electrodes. This chapter presents studies on the power of this newly discovered DHM technique to study, in real time, the morphometry of neural cells. *In vitro* assays were performed on live and fixed neural cells.

8.2 A Paradigm Shift in Biological Imaging

Excitable tissues, such as neural and muscular cells, are highly active dynamic structures and are continuously changing and adapting their biophysical and morphological attributes in response to the surrounding environment. Having these dynamical changes and responses affiliated with the cellular functions can provide us with analytical information. This information can be analyzed quantitatively to study the degenerative origin of neural dysfunctions that arise in neural structures and result in neurodegenerative diseases. Visualization and imaging of biological structures can reflect cellular dynamics and morphological changes.

Notwithstanding, biological specimens are transparent entities and they distinguished from their surroundings in terms of structural concentrations and intensity. However, conventional methods for imaging and visualization of living or fixed biological tissues, including neural cells, are based on photochemical dyeing and staining. These techniques are based on the introduction of chemical agents, such as antibodies, for photochemical contrasting.

In confocal microscopy, green fluorescence protein was used as contrast agent to visualize subcellular structures in living cells (Haseloff 1999). Dynamics of the fluorescently stained microglia cells was studied using confocal microscopy (Stence *et al* 2001). Cellular processes and intracellular structures were studied using green fluorescence labeling based light microscopy (Stephens and Allan 2003). However, biological tissue imaging is not just about making images and visualizing structures, more importantly is doing so without bothering the tissue (Pawley 2006). In the case of fluorescence dyeing agents, they can cause photo-conversion due to UV excitations

which results in false data (Jež *et al* 2012) and the technique has become quite sophisticated (Fernández-Suárez and Ting 2008, Lin and Wang 2008). Moreover, problems with antibodies such as lower specificity (Buchwalow *et al* 2011), cross reactivity (cross linking), high background and fixation problems (Ramos-Vara 2005) in addition to time consumption, possible tissue quenching and color attenuation over time.

On the other hand, optical phase contrast microscopy such as Zernicke phase contrast microscopy (Zernike 1942) and Normarski's differential interference contrast microscopy (G. Nomarski 1955) have been used for biological imaging (Mehta and Sheppard 2008). Even so, and due to the fact that biological tissues are transparent entities, these techniques were not able to provide three dimensional quantitative mapping of phase shift induced by the specimen (Cuche *et al* 1999a, Marquet *et al* 2005). Accordingly, interferometric techniques have recently involved intensively in biological imaging research. Interferometric microscopy employs refractive index (RI) of the measured specimen as an intrinsic contrast agent, and phase shift produced by the biological tissue is converted into intensity variations. Optical interferometry was already employed for studying some biophysical attributes of red blood cells (Popescu *et al* 2006). In comparison to fluorescence labeling microscopy, interferometric microscopy was introduced as highly sensitive and specific staining-free microscopy (Min *et al* 2011). For three dimensional analysis, interferometer microscope together with optical diffraction tomography were successfully implemented for 3D mapping of refractive index in living cells (Sung *et al* 2009).

Thanks to its promptness, digital holographic microscopy (DHM) has involved intensively in biological applications for 3D imaging and visualization. DHM is a non-invasive, label free and real time 3D online visualization and mapping method for biological tissues and structures. Its optics is based on Mach-Zehnder interferometer (Marquet *et al* 2005). The image is collected by the microscope objective (MO) and then it is reordered in a hologram via using a charge-coupled device (CCD) camera. The hologram is then numerically reconstructed based on the amplitude and phase of the incident light wave collected by the MO (Cuche *et al* 1999b). DHM allows measuring the phase shift in the wavelength, or optical path-difference length (OPL), originated from the difference in refractive index (RI) between the transparent specimen (biological structures) and the surrounding medium (or tissue) (Depeursinge *et al* 2007). It provides short acquisition time and fast measurement acquisition rate that enables quantitative phase difference mapping and dynamical analysis of living tissues. Preliminary study was employing DHM as a fast method for the early cell death detection (Pavillon *et al* 2012).

8.3 Procedure

A reflection configured digital holographic microscope (explained in chapter six) was employed to detect biophysical characteristics and morphological changes of either fixed or live neural cells in culture. Neural culture was performed for hippocampal extracted neurons as explained in chapter three, in section (3.5.1). Cultures were placed to the XY platform and visualized with a 50X long working distance microscope objective.

Figure (8-1) shows how to obtain the morphological dimensions online from the value of the optical path-length (OPL). As seen in the figure, the green line represents the surface morphology and the shape of a neural cell body. The red and yellow cursors are used to determine the size and the height of the 3D shaped soma.
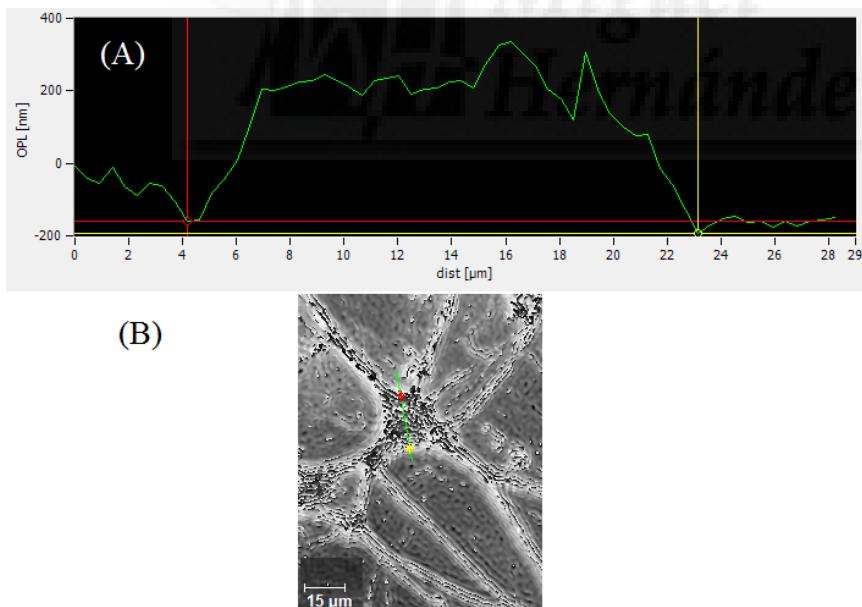
Figure (8-1): (A) Optical path difference length OPL as extracted online from the hologram phase. The green line represents the morphological shape of the studied object (cell body as shown in (B)). The red and the yellow cursors are used to determine the size and the height of the 3D shaped soma.

(B) Shows phase image taken for a neuron cell in culture. As shown the green line and the red and yellow cursors are used to mark the cell body.

8.4 Results and discussions for Fixed Neural Cells

Neural cultures of developmental age of 14 days *in vitro* were fixed on cover slips using 4% paraformaldehyde (PFA) for 20 min. The fixation technique is explained in chapter 3, in section (3.5.3). Cover slip containing fixed neurons was brought to the XY platform of the 50X microscope objective (with numerical aperture NA of 0.75). Holograms were recorded for different cover slips and images were taken in the full field view. Optical path length difference (OPL) was extracted online from the reconstructed holograms and the morphological characteristics of cells were calculated using equation (6-2).

$$d = \frac{OPL}{(n_s - n_m)} \qquad (8\text{-}1)$$

Where d is the height (or width) of the cell under study and n_s and n_m are refractive indices of sample (cell) and medium, respectively.

Figure (8-2) shows the reconstructed hologram recorded from the fixed neurons. Figure (8-3) shows the intensity and phase of the hologram shown in figure (8-2). Both intensity and phase were used for online extraction of the optical path difference length. Applying equation (8-1) and using the OPL signal as extracted from hologram intensity and phase, morphological characteristics of the studied cell can be then obtained. These data was measured from the recorded hologram using the method represented in figure (8-1).
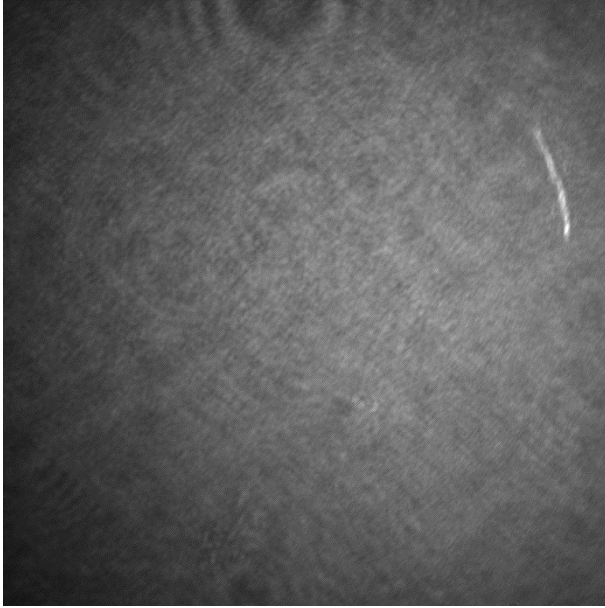
Figure (8-2): Digital hologram as recorded numerically. The hologram contains whole data of all fixed neurons in the field view. The hologram was recorded using a CCD camera and the image was taken using a 50X microscope objective.
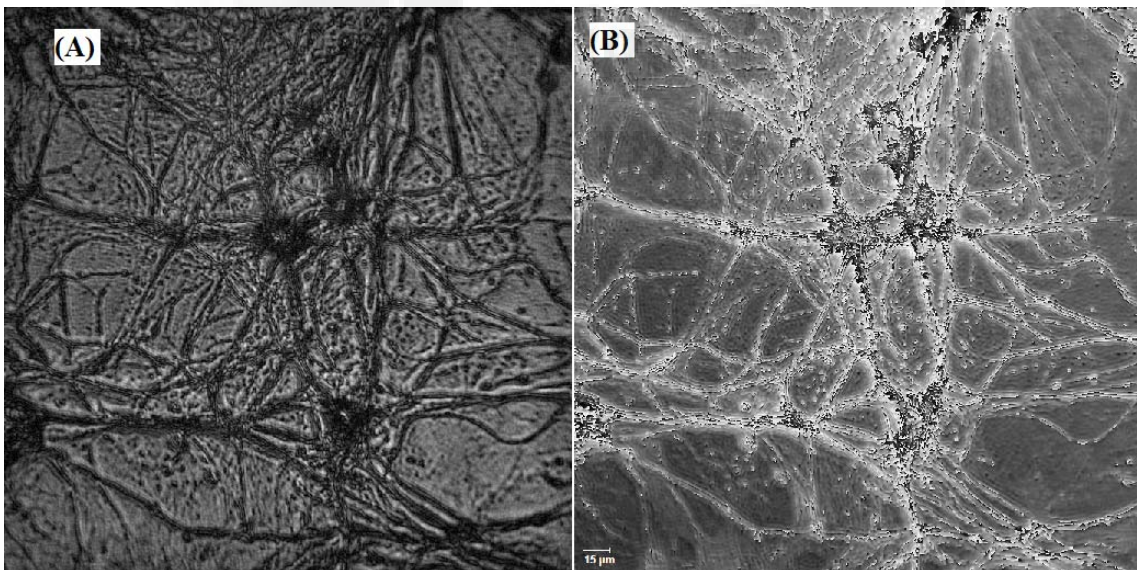
Figure (8-3): Intensity (A) and phase (B) modes of the hologram shown in figure (8-2). The two modes were used for online extraction of the OPL value for different randomly selected neural cell bodies or cellular processes.

Intensity image is the one taken by the microscope objective and recorded by the CCD camera while the phase image is the one that contains all topographic information of the optical path length.

Scale = 15 μm

Figure (8-4) shows the Optical path difference length OPL as can be extracted online (or offline) from the recorded hologram's intensity and phase images. Intensity image represents the interference pattern recorded by the CCD camera, while phase image is the one that contains all topographic information of the optical path length. Cellular dimensions can be then calculated in terms of the OPL. Red markers indicate the positions at the borders of the cell body. The negative phase difference visible on the cell's profile is due to the small refractive index of the membrane than the extracellular medium. However, these values don't affect the dimensions of the studied cell.
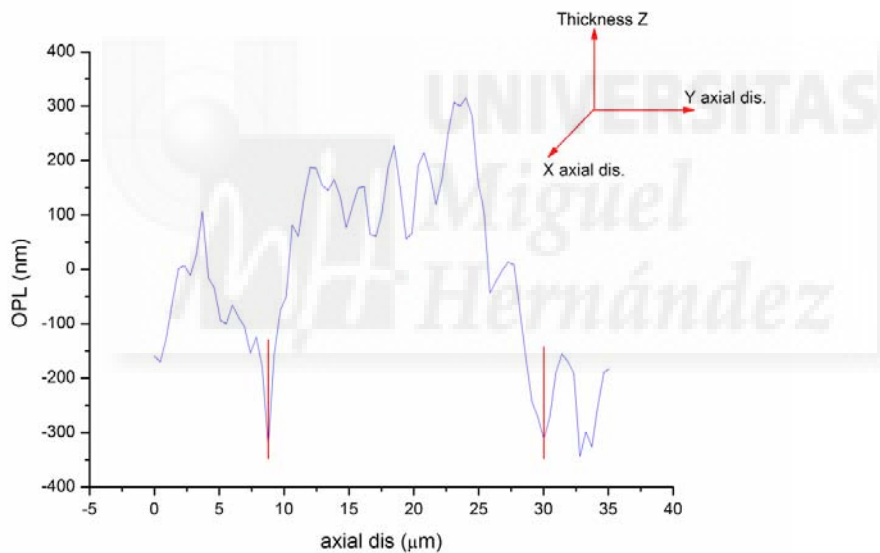
Figure (8-4): Cellular dimensions can be calculated in terms of optical path difference length OPL that be extracted online (or offline) from the recorded hologram. Red markers indicate the positions at the borders of the cell body. The upright panel indicates coordinate system of the measured dimensions, showing X and Y axial distances, and thickness (OPL) on Z axis. The negative phase difference visible on the cell's profile is due to the small refractive index of the membrane than the extracellular medium.

Experiments were repeated three times and the extracted phase (OPL) value was employed in order to calculate the morphometric characteristics of neurons. Numerical results for morphological dimensions are presented in table (8-1). Equation (8-1) relates OPL value to d and RI for medium and sample. Getting RI values of neural cell body n_s= 1.3774 (Farinas and Verkman 1996, Rappaz *et al* 2005, Dunn and Richards-Kortum 1996) and for medium n_m= 1.3410 (Rappaz *et al* 2005) from the literature. Applying in equation (8-1) we will get the data in table (8-1). Values of the cell body thickness were calculated and presented with the standard deviation value calculated from the different experiments.

Cell #	Size (µm)	Phase (OPL)	Thickness (µm)
1	21.10	458.72	12.60 ± 0.05
2	18.02	455.44	12.51 ± 0.09
3	17.12	451.06	12.40 ± 0.04
4	16.16	493.27	13.55 ± 0.07
5	18.26	407.11	11.20 ± 0.02

Table (8-1): Presents values for morphological dimensions of cellular bodies from some randomly selected neurons. Column 1 represents the cell number, column 2 the cell size in µm, column 3 represents values of the phase (OPL) and column 4 represents values of the cell body thickness in µm. Data in column 4 are obtained by applying equation (8-1) on column 3 and using values of RI of both medium and cell.

8.5 Results and discussions for live neural cells

As presented in the previous section, digital holographic microscopy technique was able to give analytical information about the cellular dimension in fixed neural cultures. This section employs the DHM technique to visualize and image live neural cells in cultures. The section presents some images, either intensity and phase or 3D reconstructed hologram, on some selected neurons in cultures. The 3D images reflect the dynamic activity of the live cells and the power of DHM to monitor the shape adaptation of neural cells.

In this study, neural cultures of developmental age of 15 days *in vitro* were employed. Petri dishes containing neural cultures were brought to the XY platform of the 50X microscope objective. The microscope objective magnifies the specimens and collects the object wave that is then detected by the CCD camera. The holograms were reconstructed numerically and saved for data processing.

Figure (8-5) shows images selected for two different developed neural cultures at 15 days of age. In each culture, image (A) shows the intensity of the reconstructed hologram contains about six cellular bodies with a network of interconnected cellular processes. Image (B) represents colored image of the phase shift as induced on the transmitted wave arises from the difference in refractive index between the neural cell and the surrounding medium. Even in same cellular body, the phase shift is induced on the transmitted wave arises from the difference in refractive index between the cellular membrane and its organelles. The arrows indicate the cellular bodies of the neurons under study. The colors indicate the different topographical characteristics of the cellular networks. The red color is the highest and the dark blue is lowest site.
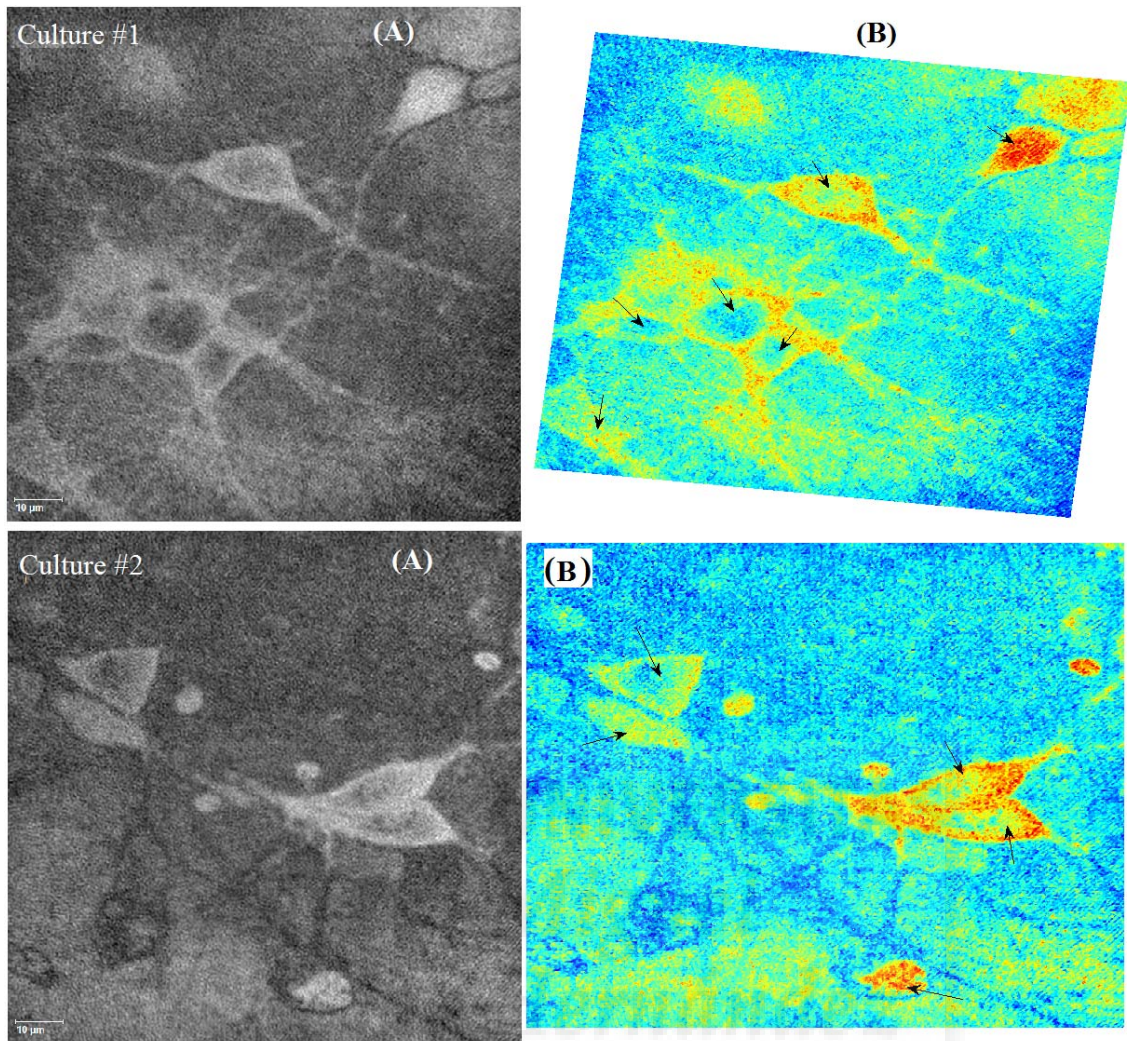
Figure (8-5): Two sets of neural cells in live cultures (culture #1 and culture #2) as imaged by digital holographic microscopy.

Image (A) shows the intensity of the reconstructed hologram. Images were taken by 50X MO from a two weeks age neural cultures. Scale = 10 μm.

Image (B) shows the phase shift as induced on the transmitted wave arises from the difference in refractive index between the neural cell and the surrounding medium.
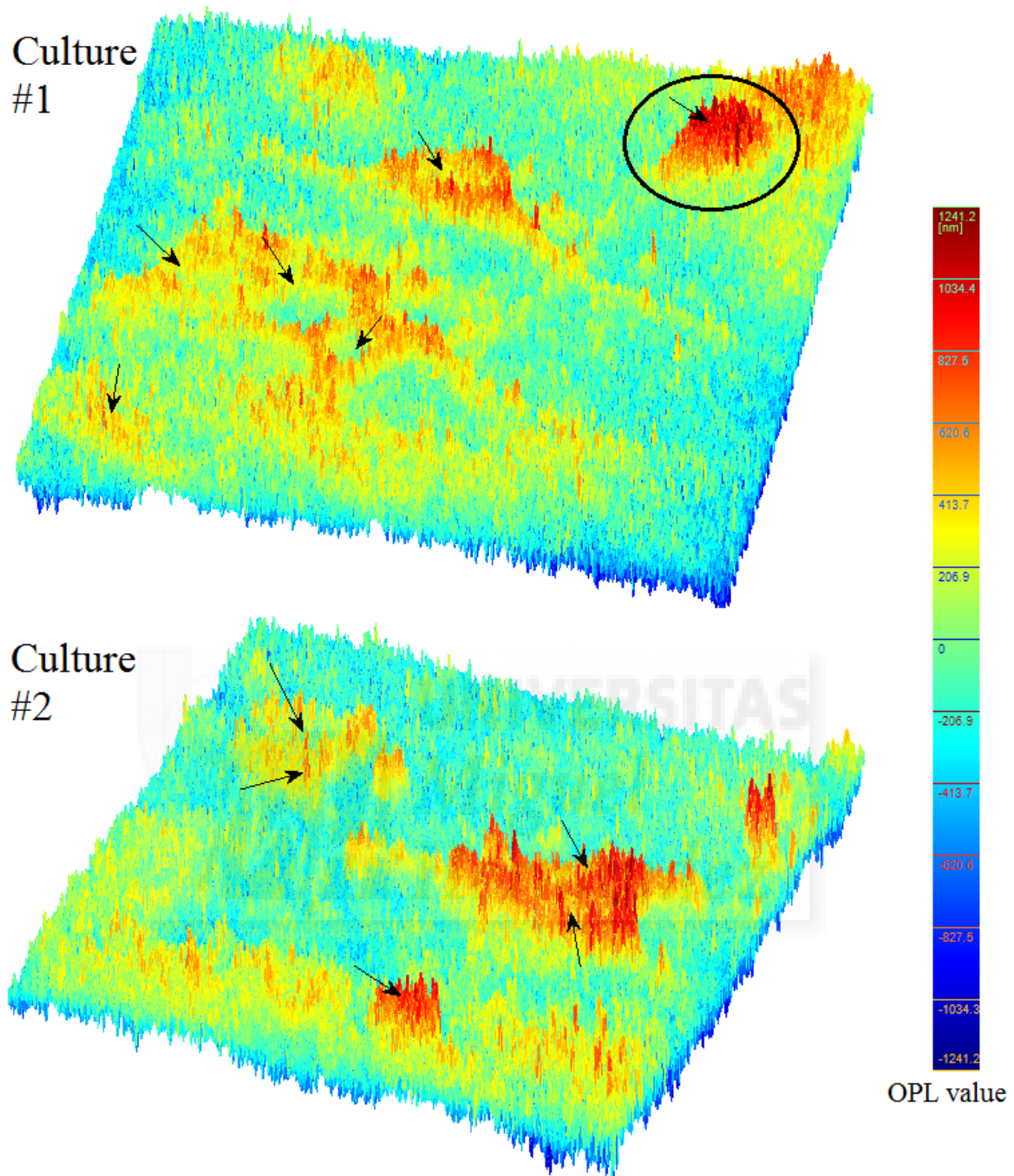
Figure (8-6): 3D image for the hologram intensity represented (for both culture #1 and #2) in figure (8-5)-A. Arrows indicate the active cellular bodies that changing their size and shape continuously while the cell is active. Colors indicate the different topographical characteristics of the cellular networks. Color bar represents the corresponding OPL value, in nm, for each color. One needs to bear in mind that the OPL value must be compensated with the value of the RI of both sample and medium in order to obtain the real dimensions of the cell depth, as in the case of fixed neuron data in table (8-1). The neuron surrounded by a black circle is represented in figure (8-7).

Figure (8-6) shows three dimensional image of the same hologram (for both cultures #1 and #2) represented in figure (8-5). Arrows indicate the cellular bodies of the studied neurons. As shown, the activity of the neurons is represented by the different colors indicated by the arrows.

After presenting the power of digital holographic microscopy to detect and image the cellular dynamics and activity, the following two figures will represent morphometric characterization of active neural cells.

Figure (8-7) shows a graphical representation for both Y axial distance (upper panel) and X axial distance (lower panel) on the X axis vs. the optical path length difference (OPL) on the Y axis.
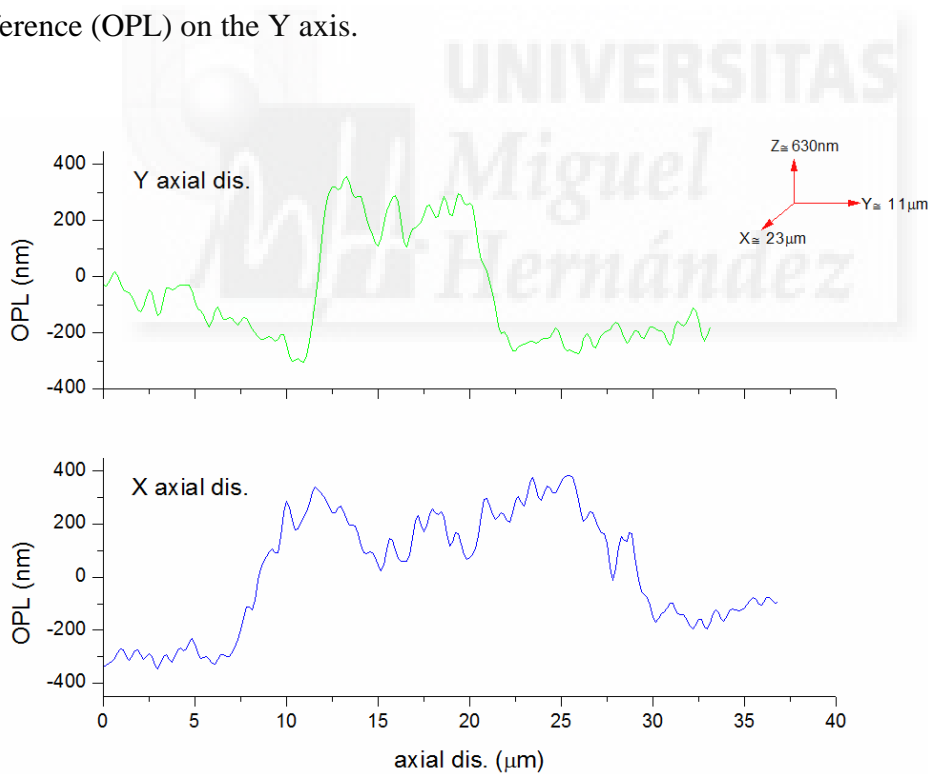
Figure (8-7): A graphical representation for both Y axial distance (upper panel) and X axial distance (lower panel) on the X axis vs. the optical path length difference (OPL) on the Y axis. The graph represents the cellular body of the neural cell surrounded by a black circle in culture#1 image in figure (8-6). The shape of the profile line reflects the cellular dynamics, since the soma is continuously moving.

X axial distance might represent the length of the cellular body of the studied

cell and Y axial distance might represent the width of it. The right side of the upper

panel represents the three dimensions of the studied cell body. As shown, the OPL (on Z

axis) of the cell body is about 630 nm, applying in equation (8-1) by this OPL value and

the values of the RI previously mentioned we will get the thickness of the cell body

$d =17.31 \mu m$. The length X is about 23 µm and the width Y is about 11 µm.

Figure (8-8) graph for axial distance vs. OPL of an active neural cell body. The

three different shapes (blue, green and red) represent three different situations of the

same cellular body. These three positions were taken from the same neural cell in same

hologram at three different times separated by fractions of a minute. The numbers on

the Y axis are just to show the changes in the cellular position while its activity. This

change in the position means that the cellular body swells and shrinks while its activity.
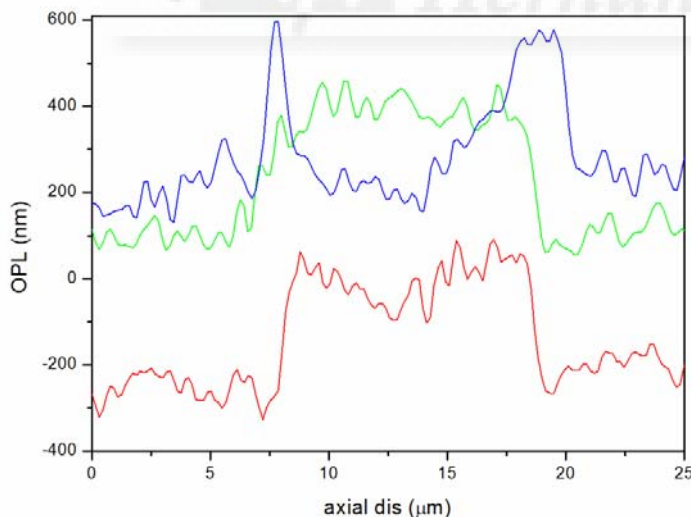
Figure (8-8): Graphical representation for axial distance vs. OPL of an active neural cell body. The three different shapes (blue, green and red) represent three different situations of the same cellular body. Here one cannot consider a baseline since the DHM microscope adapts its focal plane based on the object. These profiles are dependent on the refractive index values in each focal plane.

Figure (8-9) represents a magnified shot for the cellular body of a neuron. The magnified soma shot is presented in 3D graph on which X and Y axial distances are presented on X and Y axes respectively and the depth (or thickness) of the soma (or any other process) is presented on Z axis. It is worth noting that this magnification can be done for any part of the neuron, soma, axon or dendrites. The morphometric characterization is done experimentally by simply measuring the corresponding dimension. Unlike images taken by conventional microscopy techniques, such as confocal microscope, the neuron shown in figure (8-9) has a relatively rough surface. This roughness is due to the nanometer scale, in which the image is taken, comparing to the micrometer scale in case of conventional microscopy. Moreover, the negative phase shown on the Z axis is due to the movements that take place in the cell body. These movements and variations are represented clearly in figure (8-8) by the blue line. The blue line, together with the red and green ones, reflects the dynamics of the cell body that can be assured by topography shown in figure (8-9).
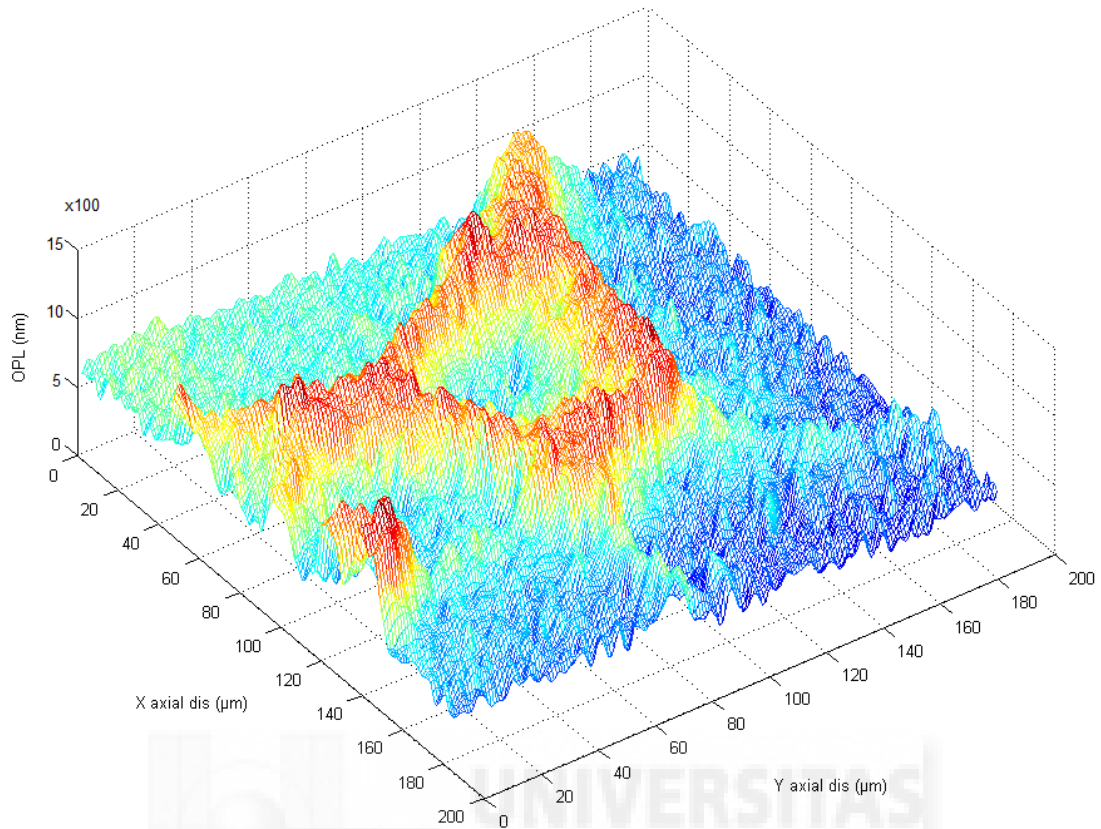
Figure (8-9): Representation for a magnified cellular body of a neuron of developmental age of 15 days. The graph is 3D represents X and Y axial distances in (μm) on X and Y axes respectively, and the OPL value in (nm) on Z axis. The OPL value is related to the cellular depth by substituting in equation (8-1).

8.6 Conclusions and Future Work

This chapter reported on the power of digital holographic microscopy (DHM) as a paradigm shift in biological imaging. DHM was able to present quantitative analysis on the morphometry of fixed neural cells. It was also able to detect and represent the activity of live neural cells in developed cultures. Although the studies reported in this chapter are still preliminary, but they opened the door to a new imaging technique in biological sciences. It is known that visualization and imaging of biological structures can reflect their dynamical and morphological changes. The emersion of digital holographic microscopy in the field of neuroscience could be of great value. It is capable of providing information that can be analyzed quantitatively to study the degenerative origin of neural dysfunctions that arise in neural structures and result in neurodegenerative diseases.

Despite the youthfulness of digital holographic microscopy in the field of biological imaging and especially in neuroscience, it could be of great interest for physiological and electrophysiological studies. It also could be of great importance in the field of pharmacological research since it could provide quantitative imaging of drug molecules inside biological tissues. However, our main focus for the future research would have two main branches. One would be the use of digital holographic microscopy as an electrophysiological technique, which means that the detection of bioelectric activity of neural cells through dynamics imaging of their activity. The other one would be the monitoring, and control, of drug delivery inside cellular bodies and membranes. This could be of great importance in the pharmacological industries.

Chapter Nine

Chapter IX

Thesis Conclusions

1. The electrochemically synthesized conductive polymer polypyrrole, both oxidized and reduced forms, is able to improve the biocompatibility and the electrochemical properties of neural electrodes.

2. Polypyrrole conductive polymer is capable of electron/cation exchange allowing faster charge transfer than metal-based electrodes. Our results show that polypyrrole coated electrodes have good biocompatibility and have several potential advantages over standard electrodes like lower noise characteristics and therefore higher signal to noise ratio, lower impedance and higher charge capacity.

3. The flexibility of polypyrrole and its performance in electrophysiological applications has the potential to improve the neural interfaces. Our results suggest that polypyrrole based electrodes can be successfully used for electrical stimulation and also to record single and multi-unit activity.

4. Digital holographic microscopy is a powerful tool able to provide quantitative analysis of neural electrodes. Our results demonstrated that polypyrrole-coated microelectrodes are more stable, in terms of thermoelectric variations, than standard electrodes.

5. Digital holographic microscopy (DHM) is an interferometric imaging technique that allows getting quantitative images of neural cells. This technique measures the phase shift induced on the transmitted wave by the observed cells and provides 3D real time measurements of cell dynamics. Our results show that the

activity and morphology of neuron cells can be studied noninvasively by simple

analysis of the phase optical signal detected by DHM.

Chapter Ten

Capítulo X

Desarrollo de Nuevos Polímeros Conductores y Estudios Microscópicos para

Mejorar las Interfaces Neurales

(Resumen de la Tesis Doctoral)

10.1   Visión de Conjunto

Este capítulo presenta un resumen del trabajo presentado en esta memoria de Tesis Doctoral, la cual está compuesta de nueve capítulos. El primero de ellos es una introducción en la que se presenta la motivación, los objetivos del trabajo y la estructura de la Tesis. El segundo capítulo expone los antecedentes científicos de los trabajos presentados en la Tesis. El tercer capítulo presenta los materiales, métodos, técnicas y aparatos utilizados en el desarrollo del trabajo de la Tesis. Los capítulos cuatro, cinco, seis, siete y ocho reflejan los resultados experimentales del presente trabajo. El capítulo nueve resume las conclusiones y los objetivos logrados. El décimo capítulo es un resumen en español de los anteriores capítulos. Y en último lugar se encuentra la bibliografía citada en el trabajo.

10.2 Resumen de la Tesis

Los accidentes que causan daños en el sistema nervioso y las enfermedades neurodegenerativas suelen tener consecuencias graves. Una de las principales razones es que la regeneración de las células nerviosas y el restablecimiento de las conexiones sinápticas adecuadas no son posibles en la mayor parte de casos. Otra razón es que las neuronas muertas no pueden ser reemplazadas con nuevas neuronas. En este contexto, los recientes avances tecnológicos en el campo de las neurociencias y la neuroingeniería junto con el desarrollo y fabricación de nuevos sistemas de microelectrodos con dimensiones cada vez más similares a las neuronas con las que pretenden interaccionar, están permitiendo que estos microdispositivos puedan ser considerados como una alternativa real para la recuperación parcial de algunas enfermedades y degeneraciones del sistema nervioso (Marin and Fernández 2010, Normann *et al* 1999, Ranck 1975, (Hochberg *et al* 2006). Sin embargo no debemos olvidar que la inserción de cualquier tipo de electrodo en el tejido nervioso es siempre un procedimiento traumático. Así cuando se introduce un electrodo en el parénquima cerebral, se produce inicialmente un cierto daño mecánico, que ocasiona una reacción inflamatoria aguda que puede transformarse en una respuesta inflamatoria crónica que se caracteriza por proliferación de astrocitos y activación de células microgliales en la proximidad de los electrodos, que llegan a quedan rodeados de una capa que contiene abundante colágeno y células gigantes multinucleadas (Marin and Fernández 2010; Seymour and Kipke 2007). Esta reacción puede llegar a comprometer seriamente la utilidad y aplicación de estos microelectrodos, por lo que uno de los objetivos de la presente investigación ha sido ensayar diversos recubrimientos, basados en polímeros conductores, con el fin de

mejorar su biocompatibilidad a largo plazo gracias a sus características fisicoquímicas, biológicas, y eléctricas (Otero 2009, Martinez and Otero 2013, Fonner *et al* 2008).

Por otro lado, la tecnología ha avanzado mucho en el contexto de los equipos de la microscopía y esta permitiendo hacer observaciones en vivo que eran impensables hace pocos años. Una de las técnicas más avanzadas en este contexto es la microscopía holográfica digital (DHM). La DHM permite analizar de una manera cuantitativa los mecanismos, la dinámica, y las actividades de los tejidos biológicos. A diferencia de las técnicas fotoquímicas, la microscopía holográfica digital no necesita marcadores fluorescentes, ni anticuerpos y es capaz de hacer imágenes 3D en tiempo real (Gabor 1948, 1972, Marquet *et al* 2005).

En esta Tesis Doctoral se han desarrollado nuevos recubrimientos para mejorar la biocompatibilidad y las características electroquímicas de microelectrodos destinados a interaccionar con poblaciones de células nerviosas. Los efectos de los diferentes recubrimientos han sido estudiados en soluciones salinas e "in vitro". Nuestros resultados han permitido desarrollar nuevos recubrimientos, basados en polímeros conductores, que permiten mejorar las características físico-químicas de los electrodos convencionales, y mejorar su relación señal/ruido. Estos resultados se presentan en los capítulos cuatro y cinco de la Tesis.

Por otro lado, se han realizado estudios, usando técnicas de microscopía holográfica digital, para estudiar el efecto termoeléctrico de los estímulos eléctricos sobre los propios microelectrodos. Para estos estudios se han empleado electrodos estándar de nitruro de titanio y electrodos recubiertos de polipirrol. Gracias a la

utilización de la DHM, ha sido posible demostrar la mayor estabilidad del polímero al aplicar una corriente eléctrica.

También se ha usado la DHM para caracterizar la morfología y la dinámica de las neuronas *in vitro*. Los resultados de estos estudios se presentan en los capítulos seis, siete y ocho de esta Tesis Doctoral.

En el futuro esperamos ser capaces de utilizar la DHM para desarrollar modelos y patrones de las actividades neuronales. Ello nos permitirá correlacionar la dinámica celular con los cambios físicos que ocurren a nivel de las células. Además esperamos ser capaces de visualizar en tiempo real los cambios que se producen en las células nerviosas como consecuencia de la estimulación eléctrica.

Bibliography

Bibliography

Abràmoff, M.D., Magalhaes, P.J., Ram, S. J. (2004). Image processing with ImageJ. *Biophotonics International*, *11*(7), 36 – 42.

Archibald, N., Miller, N., & Rochester, L. (2013). Neurorehabilitation in Parkinson disease. *Handbook of clinical neurology / edited by P.J. Vinken and G.W. Bruyn*, *110*, 435–42.

Auld, D. S., & Robitaille, R. (2003). Glial Cells and Neurotransmission : An Inclusive View of Synaptic Function Glial cells throughout the nervous system are closely. *Neuron*, *40*, 389–400.

Avloni, J., Florio, L., Henn, A. R., & Sparavigna, A. (2007). Thermal electric effects and heat generation in polypyrrole coated PET fabrics. arXiv preprint arXiv:0706.3697.

Bagotsky, V. S. (2005). *Fundamentals of Electrochemistry*. Wiley.

Bates, G. P. (2005). History of genetic disease: the molecular genetics of Huntington disease - a history. *Nature reviews. Genetics*, *6*(10), 766–73.

Benabid, A. L., Costecalde, T., Torres, N., Moro, C., Aksenova, T., Eliseyev, A., Charvet, G., et al. (2011). Deep brain stimulation: BCI at large, where are we going to? *Progress in brain research*, *194*, 71–82.

Biran, R., Martin, D. C., Tresco, P. A., C Martin, D., & A Tresco, P. (2005). Neuronal cell loss accompanies the brain tissue response to chronically implanted silicon microelectrode arrays. *Experimental neurology*, *195*(1), 115–26.

Bolto, B., McNeill, R., & Weiss, D. (1963). Electronic Conduction in Polymers. III. Electronic Properties of Polypyrrole. *Australian Journal of Chemistry*, *16*(6), 1090.

Bower, D. I. (2002). *An introduction to polymer physics*. Cambridge University Press.

Bredas, J. L., & Street, G. B. (1985). Polarons, bipolarons, and solitons in conducting polymers. *Accounts of Chemical Research*, *18*(10), 309–315.

Brindley, G. S., & Lewin, W. S. (1968). The sensations produced by electrical stimulation of the visual cortex. *The Journal of physiology*, *196*(2), 479–93.

Brindley, G. S., Polkey, C. E., Rushton, D. N., & Cardozo, L. (1986). Sacral anterior root stimulators for bladder control in paraplegia: the first 50 cases. *Journal of neurology, neurosurgery, and psychiatry*, *49*(10), 1104–14.

Brown, R. C., Lockwood, A. H., & Sonawane, B. R. (2005). Neurodegenerative Diseases: An Overview of Environmental Risk Factors. *Environmental Health Perspectives*, *113*(9), 1250–1256.

Brummer, S. B., & Turner, M. J. (1977). Electrochemical considerations for safe electrical stimulation of the nervous system with platinum electrodes. *IEEE transactions on bio-medical engineering*, *24*(1), 59–63.

Buchwalow, I., Samoilova, V., Boecker, W., & Tiemann, M. (2011). Non-specific binding of antibodies in immunohistochemistry: fallacies and facts. *Scientific Reports*, *1*(August), 1–6.

Busskamp, V., Duebel, J., Balya, D., Fradot, M., Viney, T. J., Siegert, S., Groner, A. C., et al. (2010). Genetic reactivation of cone photoreceptors restores visual responses in retinitis pigmentosa. *Science (New York, N.Y.)*, *329*(5990), 413–7.

Calderón, E., Guimerà, A., Los, P., Mouroux, A., & Pitts, N. (2007). Multichannel Handheld Hard-tissue Bio-impedance Meter with Bluetooth Link. In H. Scharfetter & R. Merwa (Eds.), *13th International Conference on Electrical Bioimpedance and the 8th Conference on Electrical Impedance Tomography SE - 65* (Vol. 17, pp. 244–247). Springer Berlin Heidelberg.

Cha, K., Horch, K., & Normann, R. A. (1992). Simulation of a phosphene-based visual field: visual acuity in a pixelized vision system. *Annals of biomedical engineering*, *20*(4), 439–49.

Chang, B. S., & Lowenstein, D. H. (2003). Epilepsy. *The New England journal of medicine*, *349*(13), 1257–66.

Charkhkar, H., Knaack, G. L., Gnade, B. E., Keefer, E. W., & Pancrazio, J. J. (2012). Development and demonstration of a disposable low-cost microelectrode array for cultured neuronal network recording. *Sensors and Actuators B: Chemical*, *161*(1), 655–660.

Cogan, S. F. (2008). Neural stimulation and recording electrodes. *Annual review of biomedical engineering*, *10*, 275–309.

Cohen, E. D. (2007). Prosthetic interfaces with the visual system: biological issues. *Journal of Neural Engineering*, *4*(2), R14–R31.

Conzuelo, L. V., Arias-Pardilla, J., Cauich-Rodríguez, J. V, Smit, M. A., & Otero, T. F. (2010). Sensing and tactile artificial muscles from reactive materials. *Sensors (Basel, Switzerland)*, *10*(4), 2638–74.

Cruccu, G., Aziz, T. Z., Garcia-Larrea, L., Hansson, P., Jensen, T. S., Lefaucheur, J.-P., Simpson, B. A., et al. (2007). EFNS guidelines on neurostimulation therapy for neuropathic pain. *European journal of neurology : the official journal of the European Federation of Neurological Societies*, *14*(9), 952–70.

Crumrine, P. K. (2001). Degenerative disorders of the central nervous system. *Pediatrics in review / American Academy of Pediatrics*, *22*(11), 370–9.

Cuche, E, Marquet, P., & Depeursinge, C. (1999). Simultaneous amplitude-contrast and quantitative phase-contrast microscopy by numerical reconstruction of Fresnel off-axis holograms. *Applied Optics*, *38*(34), 6994–7001.

Cuche, Etienne, Bevilacqua, F., & Depeursinge, C. (1999). Digital holography for quantitative phase-contrast imaging. *Optics Letters*, *24*(5), 291.

Cuche, Etienne, Marquet, P., & Depeursinge, C. (1999). Simultaneous amplitude-contrast and quantitative phase-contrast microscopy by numerical reconstruction of Fresnel off-axis holograms. *Applied Optics*, *38*(34), 6994.

Cui, X., Lee, V. A., Raphael, Y., Wiler, J. A., Hetke, J. F., Anderson, D. J., & Martin, D. C. (2001). Surface modification of neural recording electrodes with conducting polymer/biomolecule blends. *Journal of Biomedical Materials Research*, *56*(2), 261–272.

Cybulski, G. R., Penn, R. D., & Jaeger, R. J. (1984). Lower extremity functional neuromuscular stimulation in cases of spinal cord injury. *Neurosurgery*, *15*(1), 132–46.

Delgado, J M R. (1969). *Physical control of the mind: Toward a psychocivilized society* (Vol. 41). Harpercollins.

Delgado, José M. R. (1966). Aggressive Behavior Evoked by Radio Stimulation in Monkey Colonies. *Integrative and Comparative Biology*, *6*(4), 669–681.

De-Paula, V. J., Radanovic, M., Diniz, B. S., & Forlenza, O. V. (2012). Alzheimer's disease. *Sub-cellular biochemistry*, *65*, 329–52. doi:10.1007/978-94-007-5416-4_14

Depeursinge, C., Colomb, T., Emery, Y., Kühn, J., Charrière, F., Rappaz, B., & Marquet, P. (2007). Digital holographic microscopy applied to life sciences. *Conference Proceedings of the International Conference of IEEE Engineering in Medicine and Biology Society*, *2007*(4), 6244–6247.

Diaz, A. F., Kanazawa, K. K., & Gardini, G. P. (1979). Electrochemical polymerization of pyrrole. *Journal of the Chemical Society, Chemical Communications*, *0*(14), 635–636.

Dobelle, W. H., & Mladejovsky, M. G. (1974). Phosphenes produced by electrical stimulation of human occipital cortex, and their application to the development of a prosthesis for the blind. *The Journal of physiology*, *243*(2), 553–76.

Dunn, A., & Richards-Kortum, R. (1996). Three-dimensional computation of light scattering from cells. Selected Topics in Quantum Electronics, IEEE Journal of, 2(4), 898–905.

Edgerton, B. J., House, W. F., & Hitselberger, W. (1982). Hearing by cochlear nucleus stimulation in humans. *The Annals of otology, rhinology & laryngology. Supplement*, *91*(2 Pt 3), 117–24.

Farinas, J., & Verkman, A. S. (1996). Cell volume and plasma membrane osmotic water permeability in epithelial cell layers measured by interferometry. Biophysical Journal, 71(6), 3511–3522.

Fernández-Suárez, M., & Ting, A. Y. (2008). Fluorescent probes for super-resolution imaging in living cells. *Nature Reviews Molecular Cell Biology*, *9*(12), 929–43.

Ferrari, S., Di Iorio, E., Barbaro, V., Ponzin, D., Sorrentino, F. S., & Parmeggiani, F. (2011). Retinitis pigmentosa: genes and disease mechanisms. *Current genomics*, *12*(4), 238–49.

Ferreira, H. G., & Marshall, M. W. (1985). *The biophysical basis of excitability*. Cambridge University Press.

Finnerup, N. B., Otto, M., McQuay, H. J., Jensen, T. S., & Sindrup, S. H. (2005). Algorithm for neuropathic pain treatment: an evidence based proposal. *Pain*, *118*(3), 289–305.

Fisher, R. S., Van Emde Boas, W., Blume, W., Elger, C., Genton, P., Lee, P., & Engel, J. (2005). Epileptic seizures and epilepsy: definitions proposed by the International League Against Epilepsy (ILAE) and the International Bureau for Epilepsy (IBE). *Epilepsia*, *46*(4), 470–2.

Fonner, J. M., Forciniti, L., Nguyen, H., Byrne, J. D., Kou, Y.-F., Syeda-Nawaz, J., & Schmidt, C. E. (2008). Biocompatibility implications of polypyrrole synthesis techniques. *Biomedical materials (Bristol, England)*, *3*(3), 034124.

Foulds, N. C., & Lowe, C. R. (1986). Enzyme entrapment in electrically conducting polymers. Immobilisation of glucose oxidase in polypyrrole and its application in amperometric glucose sensors. *Journal of the Chemical Society, Faraday Transactions 1*, *82*(4), 1259.

Fulzele P. M. & Dorle, A. K., S. V. . S. (2003). Study of the biodegradation and in vivo biocompatibility of novel biomaterials. *Eur J Pharm Sci*, *20*(1), 53–61.

G. Nomarski. (1955). [Differential microinterferometer using polarized light]. *Journal de Physique et le Radium*, *16*, 9S – 11S.

Gabor, D. (1948). A new microscopic principle. *Nature*, *161*(4098), 777.

Gabor, D. (1972). Holography, 1948-1971. *Proceedings of the IEEE*, 1948–1971.

Galvani, L. (1791). De viribus electricitatis in motu musculari commentarius. *Bononiensi Sci. Artium Inst. Acad*, *7*, 363–418.

George, P. M., LaVan, D. a., Burdick, J. a., Chen, C.-Y., Liang, E., & Langer, R. (2006). Electrically Controlled Drug Delivery from Biotin-Doped Conductive Polypyrrole. *Advanced Materials*, *18*(5), 577–581.

Glenn, W. W. L., & Phelps, M. L. (1985). Diaphragm Pacing by Electrical Stimulation of the Phrenic Nerve. *Neurosurgery*, *17*(6).

Green, R. a, Lovell, N. H., & Poole-Warren, L. a. (2010). Impact of co-incorporating laminin peptide dopants and neurotrophic growth factors on conducting polymer properties. *Acta biomaterialia*, *6*(1), 63–71.

Guimard, N. K., Gomez, N., & Schmidt, C. E. (2007). Conducting polymers in biomedical engineering. *Progress in Polymer Science*, *32*(8-9), 876–921.

Guimerà, A., Gabriel, G., Parramon, D., Calderón, E., & Villa, R. (2009). Portable 4 Wire Bioimpedance Meter with Bluetooth Link. In O. Dössel & W. Schlegel (Eds.), *World Congress on Medical Physics and Biomedical Engineering, September 7 - 12, 2009, Munich, Germany SE - 241* (Vol. 25/7, pp. 868–871). Springer Berlin Heidelberg.

Hariharan, P. (2010). *Basics of Interferometry*. Elsevier Science.

Harris, A. R., Morgan, S. J., Chen, J., Kapsa, R. M. I., Wallace, G. G., & Paolini, A. G. (2013). Conducting polymer coated neural recording electrodes. *Journal of Neural Engineering*, *10*(1), 16004.

Harrison, W. A. (1970). *Solid State Theory*. Dover Publications.

Haseloff, J. (1999). GFP variants for multispectral imaging of living cells. *Methods in cell biology*, *58*, 139–51.

Heeger, A. J. (2001). Semiconducting and metallic polymers: the fourth generation of polymeric materials (Nobel lecture). *Angewandte Chemie International Edition*, *40*(14), 2591–2611.

Heiduschka, P., & Thanos, S. (1998). Implantable bioelectronic interfaces for lost nerve functions. *Progress in Neurobiology*, *55*(5), 433–461.

Henze, D. A., Borhegyi, Z., Csicsvari, J., Mamiya, A., Harris, K. D., & Buzsáki, G. (2000). Intracellular features predicted by extracellular recordings in the hippocampus in vivo. *Journal of neurophysiology*, *84*(1), 390–400.

Hochberg, L. R., Serruya, M. D., Friehs, G. M., Mukand, J. A., Saleh, M., Caplan, A. H., Branner, A., et al. (2006). Neuronal ensemble control of prosthetic devices by a human with tetraplegia. *Nature*, *442*(7099), 164–71.

Hodgkin, A. L., & Huxley, A. F. (1952). A quantitative description of membrane current and its application to conduction and excitation in nerve. *J. Physiol. (Lond.)*, *117*, 500–544.

Hodgson, A. J., Gilmore, K., Small, C., Wallace, G. G., MacKenzie, I. L., Aoki, T., & Ogata, N. (1995). Reactive supramolecular assemblies of mucopolysaccharide , polypyrrole and protein as controllable biocomposites for a new generation of " intelligent biomaterials ". *Supramolecular Science*, *1*(2), 77–83.

Jež, M., Bas, T., Veber, M., Košir, A., Dominko, T., Page, R., & Rožman, P. (2012). The hazards of DAPI photoconversion: effects of dye, mounting media and fixative, and how to minimize the problem. *Histochemistry and Cell Biology*, 1–10 LA – English.

Johnstone, A. F. M., Gross, G. W., Weiss, D. G., Schroeder, O. H.-U., Gramowski, A., & Shafer, T. J. (2010). Microelectrode arrays: a physiologically based neurotoxicity testing platform for the 21st century. *NeuroToxicology*, *31*(4), 331–350.

Kanazawa, K. K., Diaz, A. F., Geiss, R. H., Gill, W. D., Kwak, J. F., Logan, J. A., Rabolt, J. F., et al. (1979). "Organic metals": polypyrrole, a stable synthetic "metallic" polymer. *Journal of the Chemical Society, Chemical Communications*, (19), 854.

Kandel, E. R., Schwartz, J. H., & Jessell, T. M. (2000). *Principles of Neural Science*. (E. R. Kandel, J. H. Schwartz, & T. M. Jessell, Eds.)*Neurology* (Vol. 4, p. 1414). McGraw-Hill.

Kay, L., Humphreys, L., Eickholt, B. J., & Burrone, J. (2011). Neuronal activity drives matching of pre- and postsynaptic function during synapse maturation. *Nature Neuroscience*, *14*(6), 688–690.

Kringelbach, M. L., Jenkinson, N., Owen, S. L. F., & Aziz, T. Z. (2007). Translational principles of deep brain stimulation. *Nature reviews. Neuroscience*, *8*(8), 623–35.

Kumar, D., & Sharma, R. C. (1998). Advances in conductive polymers. *European Polymer Journal*, *34*(8), 1053–1060.

Leavitt, B. R., Wellington, C. L., & Hayden, M. R. (1999). Recent insights into the molecular pathogenesis of Huntington disease. *Seminars in neurology*, *19*(4), 385–95.

Lehle, K., Lohn, S., Reinerth, G. G., Schubert, T., Preuner, J. G. J. G., & Birnbaum, D. E. D. E. (2004). Cytological evaluation of the tissue-implant reaction associated with subcutaneous implantation of polymers coated with titaniumcarboxonitride in vivo. *Biomaterials*, *25*(24), 5457–66.

Lei, J., Cai, Z., & Martin, C. R. (1992). Effect of reagent concentrations used to synthesize polypyrrole on the chemical characteristics and optical and electronic properties of the resulting polymer. *Synthetic Metals*, *46*(1), 53–69.

Lewicki, M. S. (1998). A review of methods for spike sorting: the detection and classification of neural action potentials. *Network: Computation in Neural Systems*, *9*(4), R53–R78.

Li, Y., & Mogul, D. J. (2007). Electrical control of epileptic seizures. *Journal of Clinical Neurophysiology*, *24*(2), 197–204.

Lin, M. Z., & Wang, L. (2008). Selective labeling of proteins with chemical probes in living cells. *Physiology Bethesda Md*, *23*(3), 131–141.

Liu, X., McCreery, D. B., Carter, R. R., Bullara, L. A., Yuen, T. G., & Agnew, W. F. (1999). Stability of the interface between neural tissue and chronically implanted intracortical microelectrodes. *IEEE transactions on rehabilitation engineering : a publication of the IEEE Engineering in Medicine and Biology Society*, *7*(3), 315–26.

Lozano, A. M., Dostrovsky, J., Chen, R., & Ashby, P. (2002). Deep brain stimulation for Parkinson's disease: disrupting the disruption. *Lancet neurology*, *1*(4), 225–31.

MacDiarmid, AG. (2001). "Synthetic metals": A novel role for organic polymers (Nobel lecture). *Angewandte Chemie International Edition*.

MacDiarmid, Alan. (2001). Nobel Lecture: "Synthetic metals": A novel role for organic polymers. *Reviews of Modern Physics*, *73*(3), 701–712.

Maillet, C. J., Tyler, R. S., & Jordan, H. N. (1995). Change in the quality of life of adult cochlear implant patients. *The Annals of otology, rhinology & laryngology. Supplement*, *165*, 31–48.

Malmstrom T. G. & Horch, K. W., J. A. . M. (1998). Recording properties and biocompatibility of chronically implanted polymer-based intrafascicular electrodes. *Ann Biomed Eng*, *26*(6), 1055–1064.

Marin, C., & Fernández, E. (2010). Biocompatibility of intracortical microelectrodes: current status and future prospects. *Frontiers in neuroengineering*, *3*, 8.

Marquet, P., Rappaz, B., Magistretti, P. J., Cuche, E., Emery, Y., Colomb, T., & Depeursinge, C. (2005). Digital holographic microscopy: a noninvasive contrast imaging technique allowing quantitative visualization of living cells with subwavelength axial accuracy. *Optics Letters*, *30*(5), 468–70.

Martinez, J. G., & Otero, T. F. (2013). Biomimetic intracellular matrix (ICM) materials, properties and functions. Full integration of actuators and sensors. *Journal of Materials Chemistry B*, *1*(1), 26–38.

Mehta, S. B., & Sheppard, C. J. R. (2008). Partially coherent image formation in differential interference contrast (DIC) microscope. *Optics Express*, *16*(24), 19462–19479.

Merrill, D. R., Bikson, M., & Jefferys, J. G. R. (2005). Electrical stimulation of excitable tissue: design of efficacious and safe protocols. *Journal of neuroscience methods*, *141*(2), 171–98.

Min, W., Freudiger, C. W., Lu, S., & Xie, X. S. (2011). Coherent nonlinear optical imaging: beyond fluorescence microscopy. *Annual Review of Physical Chemistry*, *62*(1), 507–530.

Morin, F. O., Takamura, Y., & Tamiya, E. (2005). Investigating neuronal activity with planar microelectrode arrays: achievements and new perspectives. *Journal of Bioscience and Bioengineering*, *100*(2), 131–143.

Navarro, X., Krueger, T. B., Lago, N., Micera, S., Stieglitz, T., & Dario, P. (2005). A critical review of interfaces with the peripheral nervous system for the control of neuroprostheses and hybrid bionic systems. *Journal of the peripheral nervous system : JPNS*, *10*(3), 229–58.

Nolte, D. D. (2011). *Optical interferometry for biology and medicine*. Springer.

Normann, R A, Maynard, E. M., Rousche, P. J., & Warren, D. J. (1999a). A neural interface for a cortical vision prosthesis. *Vision research*, *39*(15), 2577–87.

Normann, R A, Maynard, E. M., Rousche, P. J., & Warren, D. J. (1999b). A neural interface for a cortical vision prosthesis. *Vision Research*, *39*(15), 2577–2587.

Normann, Richard A. (2007). Technology insight: future neuroprosthetic therapies for disorders of the nervous system. *Nature Clinical Practice Neurology*, *3*(8), 444–452.

Normann, Richard A, Greger, B., Greger, B. A., House, P., Romero, S. F., Pelayo, F., & Fernandez, E. (2009). Toward the development of a cortically based visual neuroprosthesis. *Journal of neural engineering*, *6*(3), 035001.

Otero, T., Marquez, M., & Suarez, I. (2004). Polypyrrole: Diffusion coefficients and degradation by overoxidation. *The Journal of Physical Chemistry B* 108 (39) 15429–15433.

Otero, T.F., Arias-Pardilla, J., & Chermak, E. (2010). Reactive polymer films Polypyrrole oxidation kinetics in aqueous solution. *Synthetic Metals*, *160*(5-6), 425–431.

Otero, Toribio F. (2009). Soft, wet, and reactive polymers. Sensing artificial muscles and conformational energy. *Journal of Materials Chemistry*, *19*(6), 681.

Pavillon, N., Kühn, J., Moratal, C., Jourdain, P., Depeursinge, C., Magistretti, P. J., & Marquet, P. (2012). Early Cell Death Detection with Digital Holographic Microscopy. (J. Najbauer, Ed.)*PLoS ONE*, *7*(1), e30912.

Pawley, J. (2006). *Handbook of biological confocal microscopy*. Springer.

Peckham, P. H. (1987). Functional electrical stimulation: current status and future prospects of applications to the neuromuscular system in spinal cord injury. *Paraplegia*, *25*(3), 279–288.

Pierson, H. O. (1996). Handbook of Refractory Carbides & Nitrides: Properties, Characteristics, Processing and Apps. Elsevier Science.

Polikov, V. S., Tresco, P. A., & Reichert, W. M. (2005). Response of brain tissue to chronically implanted neural electrodes. *Journal of Neuroscience Methods*, *148*(1), 1–18.

Popescu, G., Ikeda, T., Goda, K., Best-Popescu, C. A., Laposata, M., Manley, S., Dasari, R. R., et al. (2006). Optical measurement of cell membrane tension. *Physical Review Letters*, *97*(21), 218101.

Przedborski, S., Vila, M., & Jackson-Lewis, V. (2003). Series Introduction: Neurodegeneration: What is it and where are we? *Journal of Clinical Investigation*, *111*(1), 3–10.

Purves, D., Fitzpatrick, D., Katz, L. C., Lamantia, A. S., McNamara, J. O., Williams, S. M., & Augustine, G. J. (2001). Neuroscience. Sinauer Associates.

Qi, Z., & Pickup, P. G. (1997). Size Control of Polypyrrole Particles. *Chemistry of Materials*, *9*(12), 2934–2939.

Quester, R., Hermanns, B., Klosterhalfen, B., Schröder, R., & Klug, N. (2003). Biocompatibility and healing process of polyester meshes in the brain: in vivo examination in rats. *Biomaterials*, *24*(5), 711–21.

Quintero, J. E., Pomerleau, F., Huettl, P., Johnson, K. W., Offord, J., & Gerhardt, G. a. (2011). Methodology for rapid measures of glutamate release in rat brain slices using ceramic-based microelectrode arrays: basic characterization and drug pharmacology. *Brain research*, *1401*, 1–9.

Ramòn y Cajal, S. (1909). *Histologie du système nerveux de l'homme et des vertébré.* A. Maloine, Paris.

Ramos-Vara, J. A. (2005). Technical aspects of immunohistochemistry. *Veterinary Pathology*, *42*(4), 405–26.

Ranck, J. B. (1975a). Which elements are excited in electrical stimulation of mammalian central nervous system: a review. *Brain research*, *98*(3), 417–40.

Ranck, J. B. (1975b). Which elements are excited in electrical stimulation of mammalian central nervous system: a review. *Brain research*, *98*(3), 417–40.

Rappaz, B., Marquet, P., Cuche, E., Emery, Y., Depeursinge, C., & Magistretti, P. J. (2005). Measurement of the integral refractive index and dynamic cell

morphometry of living cells with digital holographic microscopy. Optics Express, 13(23), 9361.

Rasband, W. S. (2012). ImageJ, U. S. National Institutes of Health, Bethesda, Maryland, USA, 1997-2012.

Reese, B. E., Barnett, R. E., Alaoui-Ismaili, M., Habibi, E., & Mann, C. J. Quantitative analysis of living cells by digital holographic microscopy. , 37831 2009 First Annual ORNL Biomedical Science Engineering Conference 8–11 (2009).

Rich, J. (2001). Degenerative central nervous system (CNS) disease. *Pediatrics in review / American Academy of Pediatrics*, *22*(5), 175–6.

Rutten, W. L. C. (2002). Selective electrical interfaces with the nervous system. *Annual Review of Biomedical Engineering*, *4*(1523-9829 LA - eng PT - Journal Article PT - Review PT - Review, Tutorial), 407–452.

Schmidt, C. E., Shastri, V. R., Vacanti, J. P., & Langer, R. (1997). Stimulation of neurite outgrowth using an electrically conducting polymer. *Proceedings of the National Academy of Sciences of the United States of America*, *94*(17), 8948–8953.

Schmidt, E. M., Bak, M. J., Hambrecht, F. T., Kufta, C. V, O'rourke, D. K., & Vallabhanath, P. (1996). Feasibility of a visual prosthesis for the blind based on intracortical micro stimulation of the visual cortex. *Brain*, *119*(2), 507–522.

Schnars, U., & Jüptner, W. (1994a). Direct recording of holograms by a CCD target and numerical reconstruction. *Applied Optics*, *33*(2), 179–181.

Schnars, U., & Jüptner, W. P. (1994b). Digital recording and reconstruction of holograms in hologram interferometry and shearography. *Applied Optics*, *33*(20), 4373–4377.

Schultz, R. L., & Willey, T. J. (1976). The ultrastructure of the sheath around chronically implanted electrodes in brain. *Journal of neurocytology*, *5*(6), 621–42.

Seymour, J. P., & Kipke, D. R. (2007). Neural probe design for reduced tissue encapsulation in CNS. *Biomaterials*, *28*(25), 3594–607.

Shirakawa, H. (2001). Nobel Lecture: The discovery of polyacetylene film—the dawning of an era of conducting polymers. *Reviews of Modern Physics*, *73*(3), 713–718.

Shirakawa, H., Louis, E. J., MacDiarmid, A. G., Chiang, C. K., & Heeger, A. J. (1977). Synthesis of electrically conducting organic polymers: halogen derivatives of polyacetylene, (CH) x. *Journal of the Chemical Society, Chemical Communications*, (16), 578.

Siegel, A., Roeling, T. A., Gregg, T. R., & Kruk, M. R. (1999). Neuropharmacology of brain-stimulation-evoked aggression. *Neuroscience and biobehavioral reviews*, *23*(3), 359–89.

Sierra, D. ., & Sanchez, C. S. (2011). Neural Sorter: a tool for offline electrophysiological recording analysis. *Free Software*.

Sourkes, T. L. (2009). Chapter 54 The discovery of neurotransmitters, and applications to neurology. In F. B. and D. F. S. B. T.-H. of C. N. Michael J. Aminoff (Ed.), *History of Neurology* (Vol. Volume 95, pp. 869–883). Elsevier.

Spelman, F. A. (1999). The past, present, and future of cochlear prostheses. *IEEE engineering in medicine and biology magazine : the quarterly magazine of the Engineering in Medicine & Biology Society*, *18*(3), 27–33.

Stence, N., Waite, M., & Dailey, M. E. (2001). Dynamics of microglial activation: a confocal time-lapse analysis in hippocampal slices. *Glia*, *33*(3), 256–66.

Stephens, D. J., & Allan, V. J. (2003). Light microscopy techniques for live cell imaging. *Science (New York, N.Y.)*, *300*(5616), 82–6.

Stoney, S. D., Thompson, W. D., & Asanuma, H. (1968). Excitation of pyramidal tract cells by intracortical microstimulation: effective extent of stimulating current. *Journal of neurophysiology*, *31*(5), 659–69.

Sung, Y., Choi, W., Fang-Yen, C., Badizadegan, K., Dasari, R. R., & Feld, M. S. (2009). Optical diffraction tomography for high resolution live cell imaging. *Optics Express*, *17*(1), 266–277.

Surmeier, D. J., & Sulzer, D. (2013). The pathology roadmap in Parkinson disease. *Prion*, *7*(1).

Szarowski, D. H., Andersen, M. D., Retterer, S., Spence, A. J., Isaacson, M., Craighead, H. G., Turner, J. N., et al. (2003). Brain responses to micro-machined silicon devices. *Brain Research*, *983*(1-2), 23–35.

Tehovnik, E. J. (1996). Electrical stimulation of neural tissue to evoke behavioral responses. *Journal of neuroscience methods*, *65*(1), 1–17.

Thiébaud, P., Beuret, C., Koudelka-Hep, M., Bove, M., Martinoia, S., Grattarola, M., Jahnsen, H., et al. (1999). An array of Pt-tip microelectrodes for extracellular monitoring of activity of brain slices. *Biosensors & bioelectronics*, *14*(1), 61–5.

Thompson, B. C., Moulton, S. E., Ding, J., Richardson, R., Cameron, A., O'Leary, S., Wallace, G. G., et al. (2006). Optimising the incorporation and release of a neurotrophic factor using conducting polypyrrole. *Journal of controlled release : official journal of the Controlled Release Society*, *116*(3), 285–94.

Thompson, B. C., Richardson, R. T., Moulton, S. E., Evans, A. J., O'Leary, S., Clark, G. M., & Wallace, G. G. (2010). Conducting polymers, dual neurotrophins and pulsed electrical stimulation--dramatic effects on neurite outgrowth. *Journal of controlled release : official journal of the Controlled Release Society*, *141*(2), 161–7.

Torab, K., Davis, T. S., Warren, D. J., House, P. A., Normann, R. A., & Greger, B. (2011). Multiple factors may influence the performance of a visual prosthesis based on intracortical microstimulation: nonhuman primate behavioural experimentation. *Journal of neural engineering*, *8*(3), 035001.

Turner, J. N., Shain, W., Szarowski, D. H., Andersen, M., Martins, S., Isaacson, M., & Craighead, H. (1999). Cerebral astrocyte response to micromachined silicon implants. *Experimental neurology*, *156*(1), 33–49.

Van den Honert, C., & Stypulkowski, P. H. (1987). Single fiber mapping of spatial excitation patterns in the electrically stimulated auditory nerve. *Hearing Research*, *29*(2–3), 195–206.

Vernitskaya, T. V, & Efimov, O. N. (1997). Polypyrrole: a conducting polymer; its synthesis, properties and applications. *Russian Chemical Reviews*, *66*(5), 443–457.

Volta, A. (1800). On the Electricity Excited by the Mere Contact of Conducting Substances of Different Kinds. In a Letter from Mr. Alexander Volta, FRS Professor of Natural Philosophy in the University of Pavia, to the Rt. Hon. Sir Joseph Banks, Bart. KBPRS. *Philosophical Transactions of the Royal Society of London*, *90*, 403–431.

Wadhwa, R., Lagenaur, C. F., & Cui, X. T. (2006). Electrochemically controlled release of dexamethasone from conducting polymer polypyrrole coated electrode. *Journal of controlled release : official journal of the Controlled Release Society*, *110*(3), 531–41.

Wallace, G. G., Moulton, S. E., & Clark, G. M. (2009). Applied physics. Electrode-cellular interface. *Science*, *324*(5924), 185–186.

Wang, J. (2004). *Analytical Electrochemistry*. Wiley.

Wang, X., Gu, X., Yuan, C., Chen, S., Zhang, P., Zhang, T., Yao, J., et al. (2004). Evaluation of biocompatibility of polypyrrole in vitro and in vivo. *Journal of biomedical materials research. Part A*, *68*(3), 411–22.

Williams, R. L., & Doherty, P. J. (1994). A preliminary assessment of poly(pyrrole) in nerve guide studies. *Journal of Materials Science Materials in Medicine*, *5*(6-7), 429–433.

Wong R. & Ingber, D. E., J. Y. . L. (1994). Electrically conducting polymers can noninvasively control the shape and growth of mammalian cells. *Proc Natl Acad Sci U S A*, *91*(8), 3201–3204.

Wong, J. Y., Langer, R., & Ingber, D. E. (1994). Electrically conducting polymers can noninvasively control the shape and growth of mammalian cells. *Proceedings of the National Academy of Sciences of the United States of America*, *91*(8), 3201–3204.

Zelikin, A. N., Lynn, D. M., Farhadi, J., Martin, I., Shastri, V., & Langer, R. (2002). Erodible conducting polymers for potential biomedical applications. *Angewandte Chemie (International ed. in English)*, *41*(1), 141–4.

Zernike, F. (1942). Phase contrast, a new method for the microscopic observation of transparent objects. *Physica*.